ARO-URI Center for

...TRONIC SYSTEMS RESEARCH

...CAL REPORT

...NLINEAR OPTICAL SYSTEMS

INTERACTING WITH

AMPLITUDE-MODULATED OPTICAL FIELDS

AFPEA
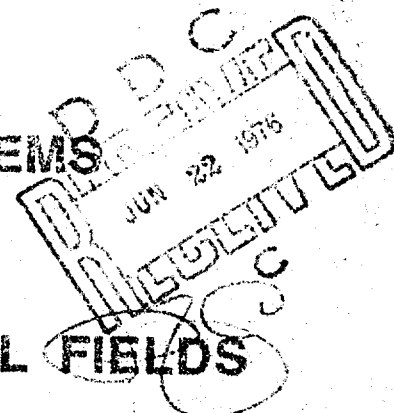
Air Force Packaging Evaluation Agency

Prepared for:

Headquarters

...Research Office Force Logistics Command
DRXRO-IP Library

REPORT DOCUMENTATION PAGE

1. REPORT SECURITY CLASSIFICATION Unclassified	1b. RESTRICTIVE MARKINGS
2. SECURITY CLASSIFICATION AUTHORITY	3. DISTRIBUTION/AVAILABILITY OF REPORT Approved for public release; distribution unlimited.
2. DECLASSIFICATION/DOWNGRADING SCHEDULE	
PERFORMING ORGANIZATION REPORT NUMBER(S)	5. MONITORING ORGANIZATION REPORT NUMBER(S) $ARO\ 24626.155-PH-UIR$

6. NAME OF PERFORMING ORGANIZATION University of Rochester	6b. OFFICE SYMBOL (If applicable)	7a. NAME OF MONITORING ORGANIZATION U. S. Army Research Office
6. ADDRESS (City, State, and ZIP Code) The Institute of Optics Rochester, New York 14627		7b. ADDRESS (City, State, and ZIP Code) P. O. Box 12211 Research Triangle Park, NC 27709-?011

8a. NAME OF FUNDING/SPONSORING ORGANIZATION U. S. Army Research Office	8b. OFFICE SYMBOL (If applicable)	9. PROCUREMENT INSTRUMENT IDENTIFICATION NUMBER $DAAL03-86-K-0173$

8c. ADDRESS (City, State, and ZIP Code) P. O. Box 12211 Research Triangle Park, NC 27709-2211	10. SOURCE OF FUNDING NUMBERS			
	PROGRAM ELEMENT NO.	PROJECT NO.	TASK NO.	WORK UNIT ACCESSION NO

11. TITLE (Include Security Classification)

Nonlinear Optical Systems Interacting With Amplitude-Modulated Optical Fields

12. PERSONAL AUTHOR(S)

Stephen H. Chakmakjian

13a. TYPE OF REPORT Technical	13b. TIME COVERED FROM _____ TO _____	14. DATE OF REPORT (Year, Month, Day) July 1990	15. PAGE COUNT 200

16. SUPPLEMENTARY NOTATION

The view, opinions and/or findings contained in this report are those of the author(s) and should not be construed as an official Department of the Army position, policy, or decision, unless so designated by other documentation.

COSATI CODES			18. SUBJECT TERMS (Continue on reverse if necessary and identify by block number)
FIELD	GROUP	SUB-GROUP	Amplitude modulation; spectroscopy; lasers; parametric resonances

ABSTRACT (Continue on reverse if necessary and identify by block number)

Please see Abstract on Pages v-vi.

20. DISTRIBUTION/AVAILABILITY OF ABSTRACT ☐ UNCLASSIFIED/UNLIMITED ☐ SAME AS RPT. ☐ DTIC USERS	21. ABSTRACT SECURITY CLASSIFICATION Unclassified	
22a. NAME OF RESPONSIBLE INDIVIDUAL Carlos Stroud	22b. TELEPHONE (Include Area Code) 716-275-2598	22c. OFFICE SYMBOL

DD FORM 1473, 84 MAR   83 APR edition may be used until exhausted.   SECURITY CLASSIFICATION OF THIS PAGE
                                All other editions are obsolete.

NONLINEAR OPTICAL SYSTEMS INTERACTING WITH AMPLITUDE-MODULATED OPTICAL FIELDS

by

Stephen H. Chakmakjian

Submitted in Partial Fulfillment

of the

Requirements for the Degree

DOCTOR OF PHILOSOPHY

Supervised by Professor C.R. Stroud, Jr.

The Institute of Optics

University of Rochester

Rochester, New York

1990

CURRICULUM VITAE

The author was born in 1960 in Bridgeport, Connecticut; he spent most of his youth in Trumbull, Connecticut. He attended Fairfield Preparatory High School in Fairfield, Connecticut. From the fall of 1978 until the spring of 1979 he attended the University of Connecticut. In the Winter of 1980 he entered the University of Bridgeport in Bridgeport, Connecticut and graduated magna cum laude in the Spring of 1983 with a Bachelor of Science degree in Physics. While at the University of Bridgeport he was a member of the Physics National Honor Society $\Sigma\Pi\Sigma$ and served as the president of the local chapter of the Society of Physics Students SPS.

In the Fall of 1983 he began graduate study at The Institute of Optics at the University of Rochester. During his graduate career, he conducted research in the fields of modulation spectroscopy and laser instability under the guidance of Professor Carlos R. Stroud, Jr. While at the University of Rochester he was a University Research Initiative fellow. He received his Master of Science degree at The Institute of Optics in January, 1985.

ii

ACKNOWLEDGEMENTS

"No man is an island.." and therefore we are all "standing on the shoulders" of our predecessors. I am glad that my graduate career overlapped with some very knowledgeable predecessors. In particular, I am indebted to Lloyd Hillman for teaching me about closed-loop servo systems and the importance of having a "pole at zero frequency" and for constructing the temperature-stabilized Fabry Perot interferometer. I would also like to thank John Yeazell for teaching me about atomic-beam systems. It is obvious that I have interacted substantially with Karl Koch and Stephanos Papademetriou in the laboratory, and I owe each of them a great deal for sharing with me their scientific knowledge and energy (IFGTBA) in the laboratory. We all owe special thanks to Jonathan Parker for providing us company during after hours research.

Special thanks go to my thesis advisor Dr. Stroud for his guidance and advice throughout my career at Rochester. His insight into theoretical, experimental and writing problems has been a great asset to me. I am appreciative of the freedom he has granted me to pursue my own interests. I would also like to thank him for emphasising the value of a scanning Fabry Perot interferometer.

I would like to thank the members of the 3rd floor research groups for their help and support with many problems. Thanks go to Dr. Boyd and his research group for allowing open access to laboratory and computer equipment used in preparation of this thesis. I cannot possible mention all the people with whom I have interacted, but I would like to thank Mark Beck, Dan Gauthier, Mark Gruneisen, Mark Kramer, Michelle Malcuit, and Ian McMackin for many useful discussions. Also, I am appreciative of the account/bookeeper in the institute

who has helped me through some major acquisitions.

I owe a great deal to my family for their support and love during my graduate career and my entire life. Their support and understanding of my struggles has been a source of great strength for me.

My choice to pursue a graduate degree in optics was made while I was studying in the physics department at the University of Bridgeport. I thank Dr. James Tucci for his guidance and friendship during this time, and I thank him for recommending that I go to Rochester to study optics.

ABSTRACT

This thesis is concerned with the interaction of amplitude-modulated (AM) optical fields with various nonlinear systems. An experimental and theoretical analysis of three distinct nonlinear systems is treated: two-level atoms interacting with a 100% AM field: a four-level laser amplifier with an AM pump intensity: a multimode dye laser with an AM pump intensity.

A 100% AM field is the limiting case of strong modulation in which the energy at the carrier frequency is completely supressed, and only the modulation sidebands remain. The interaction of such an optical field with an ensemble of radiatively broadened two-level atoms (an optically-pumped sodium atomic beam is used) yields a complicated series of parametric resonances when both the Rabi frequency and the modulation frequency are large compared with the atomic-transition linewidth. The time-averaged fluorescence, and therefore, the absorption of energy exhibits parametric-resonant enhancement whenever the modulation frequency is equal to a subharmonic of the Rabi frequency.

Population oscillations in a multilevel laser amplifier are studied using weak amplitude-modulation spectroscopy. Two laser fields are applied to a four level laser amplifier (alexandrite is used as the amplifier). The intensity of the laser tuned to the pump-transition frequency is weakly modulated, while the modulated gain experienced by a second laser, tuned to the inverted transition, is measured. Amplitude-modulation spectroscopy is used to determine the temperature increase due to thermal relaxations within the crystal.

The near-threshold behavior of multimode cw dye lasers with an AM pump intensity is studied for several dye-laser cavity configurations. The intensity of

the argon pump beam is weakly modulated and the modulation spectrum of the laser intensity is studied. Critical slowing down of the response of the laser intensity is observed. The behavior of multimode lasers are compared with the predictions of single-mode four-level laser theory. Also, the modulation spectrum of the fluorescent intensity is studied. The phenomenon of non-adiabatic gain clamping is discussed in relation to the results. Furthermore, the absorption spectrum of the modulation in the intensity of the argon pump beam is studied to complete a modulation-energy-balance analysis.

Table of Contents

List of Figures

PUBLICATIONS

[1] "Modulation Spectroscopy as a Probe of Laser Dynamics", to be published in Coherence and Quantum Optics VI , L. Mandel and E. Wolf editors, (Plenum, N.Y.) with K. Koch, S. Papademetriou, M. Noel, C.R. Stroud, Jr.

[2] "Excited-State Relaxation Dynamics in Continuous-Wave Dye Lasers", to be published in Coherence and Quantum Optics VI , L. Mandel and E. Wolf editors, (Plenum, N.Y.) with K. Koch, S. Papademetriou, C.R. Stroud, Jr.

[3] "Near-Threshold Behavior of Multimode CW Dye Lasers with an Amplitude Modulated Pump", Phys. Rev. A, 40, 1858-1867, (August 15 1989) with S. Papademetriou, K. Koch, C.R. Stroud, Jr.

[4] "Modulation Mixing in a Multimode Dye Laser", Phys. Rev. A, 39, 5744-5750, (May 1989) with K. Koch, S. Papademetriou, C.R. Stroud, Jr.

[5] "Effects of Pump Modulation on a Four-Level Laser Amplifier", published in J. Opt. Soc. Am. B, 6, 1746-1751, (September 1989) with K. Koch, S. Papademetriou, C.R. Stroud, Jr.

[6] "Subharmonic Instabilities in Resonant Interactions with Bichromatic Fields", J. Opt. Soc. Am. B, 6, 58-65, (January 1989), with K. Koch, B. Oliver, C.R. Stroud, Jr.

[7] "Observation of Resonances at Sub-Harmonics of the Rabi-Frequency in the Saturated Absorption of an 100% Amplitude-Modulated Laser", J. Opt.

Soc. Am. B, **5**, 2015-2020, (October 1988), with K. Koch, C.R. Stroud, Jr.

[8] "Multimode Instabilities in CW Dye Lasers", <u>Optical Chaos</u>, J.Chrowstowski, N.B. Abraham, Editors, Proc. SPIE **667**, 47-50 (1986) with K. Koch, L.W. Hillman, C.R. Stroud, Jr.

[9] "Instabilities and Higher-Order States of CW Ring Dye Lasers", <u>Optical Instabilities</u>, R.W. Boyd, M.G. Raymer, L.M. Narducci, Editors, (Cambridge, N.Y. 1986), 274-276 with K. Koch, L.W. Hillman, C.R. Stroud, Jr.

[10] "Multi-Mode Instabilities of Homogeneously Broadened Lasers", <u>Optical Bistability III</u>, (Springer-Verlag, N.Y. 1986) with K. Koch, L.W. Hillman, and C.R. Stroud, Jr.

PRESENTATIONS

[1] "Modulation Spectroscopy as a Probe of Laser Dynamics", presented at International Laser Science V, Palo Alto, California, 1989, with K. Koch, S. Papademetriou, and C.R. Stroud, Jr.

[2] "Near Threshold Behavior of Multimode CW Dye Lasers with an Amplitude Modulated Pump", presented at Coherence and Quantum Optics VI, Rochester, New York, 1989, with S. Papademetriou, K. Koch, M. Noel, and C.R. Stroud, Jr.

[3] "Excited-State Relaxation Dynamics in a Continuous-Wave Dye Laser", presented at Coherence and Quantum Optics VI, Rochester, New York, 1989, with K. Koch, S. Papademetriou, and C.R. Stroud, Jr.

[4] "Homogeneous Hole-Burning in an Inverted System" presented at the annual meeting of the Optical Society of America, Santa Clara, California, 1988, with K. Koch, S. Papademetriou, and C.R. Stroud, Jr.

[5] "Broadband Atomic Response to Incommensurate Modulation Frequencies", presented at the Optical Society of America annual meeting, Rochester, New York, 1987, with K. Koch, L.W. Hillman, and C.R. Stroud, Jr.

[6] "Resonance Fluorescence with Modulated Excitation", presented at the Optical Society of America annual meeting, Rochester, New York, 1987, with K. Koch, L.W. Hillman, and C.R. Stroud, Jr.

[7] "Incoherent Pump Effects in AM Spectroscopy", presented at the Optical

Society of America annual meeting, Rochester, New York, 1987, with K. Koch, L.W. Hillman, and C.R. Stroud, Jr.

[8] "Modulation Mixing in a Dye Laser", presented at the Optical Society of America annual meeting, Rochester, New York, 1987, with K. Koch, L.W. Hillman, and C.R. Stroud, Jr.

[9] "Effects of Detuning on Laser Instabilities", presented at the Optical Society of America annual meeting, Seattle, Washington, October 1986, with K. Koch, L.W. Hillman and C.R. Stroud, Jr.

[10] "Multi-mode Instabilities in CW Dye Lasers", presented at the SPIE meeting on Optical Chaos, Quebec City, Canada, June, 1986, with K. Koch, and C.R. Stroud, Jr.

[11] "Multi-mode Instabilities of Homogeneously Broadened Lasers", presented at the Topical meeting on Optical Bistability III, Tucson, Arizona, December 1985, with K. Koch, and L.W. Hillman, and C.R. Stroud, Jr.

[12] "Multimode Instabilities in Homogeneously Broadened Lasers", presented at the annual meeting of the Optical Society of America, Washington, D.C. 1985, with K. Koch and C.R. Stroud, Jr.

[13] "Instabilities and Higher-Order States of CW Ring Dye Lasers", presented at the Inernational meeting on Instabilities and Dynamics of Lasers and Nonlinear Optical Systems, Rochester, New York, June 1985, with K. Koch, L. W. Hillman, and C.R. Stroud, Jr.

Chapter 1

INTRODUCTION

One of the most effective tools in optical physics is linear spectroscopy. An atomic or molecular system is prepared as a sample and an optical excitation is applied to the sample. Sometimes a narrowband excitation is used and as its frequency is swept an absorption spectrum is obtained. In other cases, the excitation is constant and the spectrum of the scattered radiation is measured. These techniques provide information such as the energy difference between the states, or energy levels, of the system and the bandwidth of the transitions between these levels. The lifetime of the population in these levels can also be determined by rapidly extinguishing the optical excitation and monitoring the decay of the fluorescence from the sample. It is interesting that while the population lifetime can be determined via linear spectroscopic techniques, the very existence of this finite lifetime is the cause of nonlinear saturation of the absorption of light.

These linear techniques involve the interaction of single quanta of optical light with the medium. When the excitation is strong, nonlinear effects begin to

1

appear. For instance, since the population lifetime T_1 is finite, the absorption of radiation by the medium cannot increase linearly with the excitation strength. Eventually, all the population in the medium will be excited to the upper levels and further absorption of the excitation is impossible. Now, if a second resonant field is applied, it will experience decreased absorption since the medium is saturated. The presence of a strong excitation modifies the apparent properties of the medium. This effect is the basis of many nonlinear optical interactions.

Early studies of nonlinear optical interactions involved a single strong field and a weak tunable probe field. Mollow[1] and Haroche[2] used a third-order perturbation theory to predict that when a weak probe field is detuned from a strong resonant field by the Stark-shift or Rabi frequency of the strong field, the probe can experience induced gain even in the absence of a time-averaged population inversion. Ezekiel[3] carried out an experiment using atomic sodium to verify these theoretical results. In this experiment a sodium atomic beam was excited by a strong field supplied by a stabilized dye laser. A second dye laser was used as a weak probe field to probe the gain induced by the strong field. This experiment was perhaps the first two-level atom pump-probe experiment. In a later work Sargent *et al.*[4] described how amplitude modulation could be used to produce a tunable set of probe fields symmetric about a strong saturating optical field. In these works a strong field saturates an optical transition. The strong field is then weakly amplitude modulated. The weak sidebands are used to probe the saturated absorption spectrum of the atomic system. This theoretical work marked the birth of amplitude modulation (AM) spectroscopy.

To better understand the interaction of a modulated optical field with a nonlinear optical system I will treat the simple case of an undamped two-level atom driven by a resonant AM optical field. This type of interaction can be

adequately described by the optical Bloch equations. In the absence of damping and for resonant excitation the Bloch equations reduce to the equation for the in-quadrature dipole moment

$$\dot{v} = \kappa E(t)w, \tag{1.1c}$$

and the equation for the atomic inversion

$$\dot{w} = -\kappa E(t)v, \tag{1.1b}$$

where the dipole coupling constant κ is given by

$$\kappa = 2d/\hbar, \tag{1.2}$$

where d is the dipole-moment matrix element and $\hbar$ is Planck's constant divided by 2π. These equations can be integrated to obtain the solution for the in-quadrature polarization

$$v(t) = -\sin\left[\int_0^t \kappa E(t)dt\right], \tag{1.3a}$$

and the solution for the atomic inversion

$$w(t) = -\cos\left[\int_0^t \kappa E(t)dt\right]. \tag{1.3b}$$

Now, we can represent an arbitrary AM field as

$$E(t) = E_0 + 2E_1\cos(\delta\omega t), \tag{1.4}$$

where E_0 is the dc compnent of the driving field and the amplitude of the modulation sidebands is E_1. When the expression for the modulated field in Eq. (1.4) is substituted into Eqs. (1.3a-b) the response of the system consists of harmonic

overtones of the modulation frequency $\delta\omega$. To demonstrate this principle let us consider the case of 100% amplitude modulation (this is the subject of chapter 2). In this limiting case of strong modulation, the dc component of the field [E_0 in Eq. (1.4)] is zero. The solutions can now be rewritten as

$$v(t) = -sin\left[msin(\delta\omega t)\right], \tag{1.5a}$$

and

$$w(t) = -cos\left[msin(\delta\omega t)\right], \tag{1.5b}$$

where the modulation index m is

$$m = \frac{2\kappa E_1}{\delta\omega}. \tag{1.6}$$

Using some trigonometric and Bessel-function identities Eqs. (1.5a-b) can be rewritten as

$$v(t) = -2\sum_{n=1}^{\infty} J_{2n-1}(m)sin\left[(2n-1)\delta\omega t\right], \tag{1.7a}$$

for the in-quadrature polarization and

$$w(t) = -J_0(m) - 2\sum_{n=1}^{\infty} J_{2n}(m)sin(2n\delta\omega t), \tag{1.7b}$$

for the atomic inversion. It is evident from these solutions that the response of a two-level atom to a 100% AM field consists of harmonic overtones of the modulation frequency $\delta\omega$. This phenomenon typical of interactions of nonlinear systems with modulated optical fields.

In this thesis I apply amplitude modulation spectroscopy to study three distinct types of nonlinear interactions: a two-level atom interacting with 100% amplitude-modulated fields; the interaction of multiple amplitude-modulated driving fields with a multi-level molecular system; the interaction of a dye-laser system with an amplitude-modulated pump intensity. In this chapter I

5

will describe the research contained in each chapter as well as provide a brief background for each project.

In chapter two of this thesis I treat the limiting case of strong modulation interactions: the interaction of a 100% AM field with a two-level atom. The physics behind this work is an extension of the earlier works of Mollow, Haroche, and Ezekiel which I have already discussed. In these works a weak probe field experiences gain in its absorption spectrum as it is detuned in frequency from a strong saturating field by the strong-field Rabi frequency. As long as the probe fields are weak, the physics of this interaction can be adequately described by a third-order perturbation theory. Perhaps the most general self-consistent problem which can be described by a third-order theory is that of four-wave mixing. It is therefore important to mention that Boyd et al.[5] showed that an enhancement in gain occurs in degenerate four-wave mixing when the conjugate beams are detuned from the pump beams by the pump-beam Rabi frequency. These results were later confirmed by Harter et al.[6,7] using two pulsed dye lasers and a sodium cell. In a later work Gruneisen et al.[8] repeated these experiments in a sodium cell using a pair of cw dye lasers. These experiments and the one by Ezekiel[3] confirm the physics of the pump-probe interactions quite well.

This problem can also be described using a modulation formalism. Hillman et al.[9] and Kramer et al.[10] showed that the interaction of strong field and a single sideband with a two-level atomic system can be described as a linear combination of weak AM and frequency modulation (FM). It is also "natural" to describe the interaction in this manner. They show that if an arbitrary linear combination of AM and FM modes are allowed to interact in a self-consistent manner with a two level atomic system the amounts of AM and FM will adjust themselves to a unique ratio depending on the intensity of the strong field and

6

the detuning parameter. Therefore, it is basically correct to describe the pump-probe problem in a modulation formalism.

An obvious extension of these single strong-field experiments are interactions involving two or more strong fields with a two level system. The theoretical predictions of this multiple strong-field interaction are much more complicated than the single strong-field interactions. Not only is there a resonance in the absorption spectrum of the sidebands when they are detuned by the Rabi frequency but there are subharmonic resonances whenever the frequency separation is a submultiple of the Rabi frequency. There have been two noteworthy experiments of this kind. The first experiment by Bonch-Breuvich *et al.*[11] was carried out using Zeeman-split atomic Cadmium. This experiment involved two strong rf fields tuned near resonance. One field was held at a fixed frequency while the other field was tuned in order to obtain an absorption spectrum of the two-field state. A series of subharmonic resonances were observed. The experimental results were quite extraordinary, although the system they used was largely undamped. In a later experiment, Thomann carried out a strong-modulation experiment using atomic sodium and a stabilized dye laser modulated by an electro-optic modulator. In this experiment a modulation depth of 0.65 was obtained. The Rabi resonance and two subharmonic resonances were observed.

In chapter 2 I extend the work in the area of strong-field large modulation depth experiments. We have performed an experiment in atomic sodium using a 100% AM field. The field state is produced from a stabilized dye laser by up-shifting the frequency of a portion of the dye-laser beam using an acousto-optic modulator and recombining the upshifted portion with the unshifted portion. This experiment is, to our knowledge, the first realization of a 100% AM interaction at optical frequencies. The results of the experiment confirm the existence

of subharmonic resonances in this bichromatic interaction. Furthermore, I discuss various techniques of measuring these resonances. I also attempt to shed light on the physics of this interaction by discussing the dynamic trajectories of the atomic variables during such an interaction. Finally, I extend the concept of modulation to include multiple harmonics of the modulation frequency to the limit of an interaction with a mode-locked pulse train with the two-level system.

In chapter 3 we will turn our attention to a multilevel atomic system. I treat the case of a multilevel laser amplifier interacting with multiple driving fields. I show how weak modulation techniques can be used in a signal-limited detection scheme to determine relaxation rates in multilevel systems. This research is an extension of work by Sargent *et al.*[4] and work performed at the Institute of Optics.[6-8] In these works, collisionally broadened saturable absorbing media are studied. In the presence of a weakly modulated saturating field these absorbers reveal a hole in the absorption spectrum of the modulation sidebands at zero modulation frequency. The physics behind this effect is that when the system can follow the modulated excitation it becomes a less efficient absorber of the modulation. Therefore, the measurement of this $1/T_1$ hole in the absorption spectrum of the modulation sidebands is an indication of the ability of the atomic system to undergo population oscillations. These previous works involve a single optical field which is weakly modulated. The obvious extension of these works is to study the propagation of modulation in these multilevel systems when optical fields are present at more than one transition.

In chapter 3 I develop a theory to describe the response of the population in the levels of a canonical four-level laser model to a modulation of either the field tuned to the pump transition of the field tuned to the inverted transition. I derive an expression for the modulated gain experienced by a probe laser tuned

to the inverted transition due to a modulated pump intensity. Although the pump and the probe lasers are incoherent with respect to each other and the transitions which they address are not directly connected, there is an exchange of modulation energy between these fields via population oscillations. I explain how such modulation measurements can be employed in laser-material testing to uncover any slow, hidden decay rates. I outline an experimental test of these predictions which we carried out using alexandrite, pumped by two dye lasers tuned to different transitions within the alexandrite system. After the data is fit using the canonical four-level theory, I also fit the same data using a more detailed energy-level model of the alexandrite system. Using this second model I arrive at an expression for the temperature change within the interaction region of the crystal due to heating by the incomplete conversion of pump photons into spontaneous and stimulated photons at the inverted-transition frequency.

In chapter 4 I apply AM techniques to a laser system operating near the first threshold. This research is an extension of the work in chapter 3; the multilevel system is now within an operating laser. The goal of this final chapter is to develop an understanding of the complex dynamics which govern a laser's behavior near the lasing threshold. In particular, this chapter focuses on the effects of pump fluctuations on the amplitude stability of the laser.

The idea for the research described in chapter 4 came out of recent work describing a delayed bifurcation at the first threshold of a laser.[11-14] As the loss or the gain of a laser is swept through the threshold value very slowly, the laser intensity follows the behavior predicted by the steady-state theory. However, when the sweep rate is increased the turn-on of the laser is delayed past the critical point until the intensity in the cavity can properly build up. This delay in the turn on is a delayed bifurcation. A recent experiment carried out with an

argon-ion laser, by modulating the intracavity loss, confirms these predictions. As the laser is brought back to threshold from the on-state the turn-off of the laser intensity also experiences a delay. The resulting dynamic hysteresis loop increases in area as the sweep rate is increased. The surprising thing about the existence of this slow behavior is that the sweep rate which produces this loop is orders of magnitude slower than the atomic decay rates or the cavity decay rates alone would dictate. This slow behavior in the laser is a manifestation of the effects of critical slowing down.

To better understand these effects, we carried out similar experiments in our own laboratory. Using an acousto-optic modulator we applied a swept pump parameter to one of our home-built dye lasers. We observed the delayed bifurcation in the output power of the dye laser. Furthermore, we monitored the fluorescence emitted from the interaction region of the gain medium. The fluorescent intensity seemed to overshoot the on-state just as the laser intensity did. At this point we decided that our experience with AM spectroscopy would help in studying these dynamics.

Rather than applying a swept pump parameter, we hold the average pump parameter fixed and apply a weak amplitude modulation of the pump intensity. Then, the first-harmonic response of the dye laser intensity and the first-harmonic response of the fluorescent intensity are monitored as a function of modulation frequency using a lock-in amplifier. Our techniques are similar to a previous experiment by Yu et al.[15] in which the power spectrum of the intensity of a dye-laser was monitored at several pump parameters. The transmission of fluctuations from the pump intensity to the dye-laser intensity was found to increase in bandwidth as the pump parameter was increased. Our experiments with an applied modulation allow us the ability to perform in-phase and in-

quadrature detection. Furthermore, we can study the fluorescent intensity since the lock-in detection method offers superior signal-to-noise characteristics.

In chapter 4 I derive an expression for the response of the laser intensity and the excited-state population to a weakly amplitude-modulated pump intensity in a four-level single-mode rate-equation model. In a series of experiments with multimode lasers I demonstrate that this single-mode theory is adequate in describing the behavior of the total intensity of extremely multimode lasers subjected to a weakly modulated pump intensity. In these experiments we used lock-in detection to determine the in-phase and in-quadrature first-harmonic response of the laser intensity and the intensity of the fluorescence emitted from the interaction region of the gain medium of the laser (the fluorescent intensity is directly proportional to the excited-state population). The laser and fluorescent intensities are the two possible output ports of the modulation energy from the laser system. I show that an energy balance is not possible from consideration of these two ports alone. Therefore, we have considered the third port; we measure the absorption of modulation energy from the pump by the atoms in the gain medium of the laser. The modulation in the transmitted pump-beam intensity is monitored as a function of frequency. I show that the spectral response of the population induces a corresponding change in the ability of the atoms in the gain medium to absorb modulation energy from the pump.

The goal of this thesis is to provide an explanation of modulation interactions in various nonlinear optical systems. I present an account of experimental work performed in a variety of systems: two-level atom; multi-level laser amplifier; and finally a laser system. In each of these systems modulation interactions are used to perform a frequency domain measurement of some systematic time-constant or parametric interaction.

11

References

1. B.R. Mollow, "Stimulated emission and absorption near resonance for driven systems," Phys. Rev. A **5**, 2217-2222 (1972).

2. S. Haroche and F. Hartmann, "Theory of saturated absorption line shapes," Phys. Rev. A **6**, 1280-1300 (1972).

3. F.Y. Wu, S. Ezekiel, M. Ducloy, and B.R. Mollow, "Observation of amplification in a strongly driven two-level atomic system at optical frequencies," Phys. Rev. Lett. **38**, 1077-1080 (1977).

4. M. Sargent III, P.E. Toschek, and H.G. Danielmeyer, "Unidirectional saturation spectroscopy, I, theory and short dipole limit," Appl. Phys. **11**, 55-62 (1976).
   M. Sargent III and P.E. Toschek, "Unidirectional saturation spectroscopy, II, general lifetimes, interpretations and analogies," Appl. Phys. **11**, 107-120 (1976).

5. R.W. Boyd, M.G. Raymer, P. Narum, and D.J. Harter, "Four-wave parametric interactions in a strongly driven two-level system," Phys. Rev. A **24**, 411-423 (1981).

6. D.J. Harter, P. Narum, M.G. Raymer, and R.W. Boyd, "Four-wave parametric amplification of Rabi sidebands in sodium," Phys. Rev. Lett. **46**, 1192-1195 (1981).

7. D.J. Harter and R.W. Boyd, "Four-wave mixing enhanced by ac-Stark-split levels in self-trapped filaments of light," Phys. Rev. A **29**, 739-748 (1984).

8. M.T. Gruneisen, K.R. MacDonald, and R.W. Boyd, "Induced gain and modified absorption of a weak probe beam," J. Opt. Soc. Am. B **5**, 123-129 (1988).

9. L.W. Hillman, R.W. Boyd, and C.R. Stroud, Jr., "Natural modes for the analysis of optical bistability and laser instability," Opt. Lett. **7**, 426-428 (1982).

10. M.A. Kramer, R.W. Boyd, L.W. Hillman, and C.R. Stroud, Jr., J. Opt. Soc. Am. B **2**, "The propagation of modulated optical fields through saturable absorbing media: a general theory of modulation spectroscopy," 1444-1455 (1985).

11. A.M. Bonch-Breuvich, T.A. Vartanyan, and N.A. Chigir, "Subradiative structure in the absorption spectrum of a two-level system in a biharmonic radiation field," Sov. Phys. JETP **50**, 901-906 (1979).

12. P. Thomann, "Optical resonances in strong modulated laser beam," J. Phys. B **13**, 1111-1124 (1980).

13. R.E. Silverans, G. Borghs, P. De Bisschop, and M. Van Hove, "Phase effects in bichromatic field interactions with two-level atom," Phys. Rev. Lett. **55**, 1070-1073 (1985).

14. P. Thomann, "Optical parametric resonances," J. Phys. B **9**, 2411-2419 (1976).

15. L.W. Hillman, "Interaction of modulated optical fields with saturable media and its application to laser instability," University of Rochester, Ph.D. Thesis (1984).

8. M.S. Malcuit, R.W. Boyd, L.W. Hillman, J. Krasinski, and C.R. Stroud, Jr., "Saturation and inverse-saturation absorption line shapes in alexandrite," J. Opt. Soc. Am. B **1**, 73-75 (1984).

9. T. Ogawa and E. Hanamura, "Dynamical properties of the multi-mode laser with modulated inversion," Opt. Commun. **61**, 49-54 (1987). item T.Ogawa and E. Hanamura, "Numerical analysis of multimode laser with modulated inversion," Appl. Phys. B **43**, 139-153 (1987).

10. T. Ogawa, "Quasiperiodic instability and chaos in the bad-cavity laser with modulated inversion: numerical analysis of a Toda oscillator system," Phys. Rev. A **37**, 4286-4302 (1988).

11. P. Mandel and T. Erneux, "Laser Lorenz equations with a time-dependent parameter," Phys. Rev. Lett. **53**, 1818-1820 (1984).
P. Mandel and T. Erneux, "Nonlinear control in optical bistability," IEEE J. Quantum Electron. **QE-21**, 1352-1355 (1985).

12. G. Broggi, A. Colombo, L.A. Lugiato, and P. Mandel, "Influence of white noise on delayed bifurcations," Phys. Rev. A **33**, 3635-3637 (1986).

13. M. San Miguel and M.C. Torrent, "First passage time distribution for delayed laser threshold instability," J. Phys. (Paris) **49**, 149-151 (1988).
M.C. Torrent and M. San Miguel, "Stochastic-dynamics characterization of delayed laser threshold instability with swept control parameter," Phys. Rev. A **38**, 245-251 (1988).

14. W. Scharpf, M. Squicciarini, D. Bromley, C. Green, J.R. Tredicce, and
L.M. Narducci, "Experimental observation of a delayed bifurcation at the
threshold of an argon laser," Opt. Commun. **63**, 344 (1987).

15. A.W. Yu, G.P. Agrawal, and R. Roy, "Noise propagation from pump to
secondary lasers," Opt. Lett. **12**, 806-808 (1987).

Chapter 2

A 100% AMPLITUDE MODULATED LASER BEAM
INTERACTING WITH A TWO LEVEL ATOM

A. Introduction

The subject of this chapter is the interaction of a 100% amplitude-modulated
(AM) optical field with a two-level atomic system. A 100% AM field is the limit-
ing case of strong modulation in which all the energy at the carrier frequency has
been displaced in the modulation process into the modulation sidebands. The
field consists only of the modulation sidebands which are separated by twice the
modulation frequency. In this chapter I describe an experimental and theoretical
study of this problem. In the experiment, a sodium atomic beam is prepared as
the atomic medium, and a frequency-stabilized dye-laser is used as the source
of optical radiation.

The work discussed in this chapter is an extension of earlier work involving
a two-level atom resonantly driven by a single strong field with one or more
tunable probe fields. In the earliest of this work Mollow[1] and Haroche[2] each
used a third-order perturbation theory to predict that when a weak probe field

14

is detuned from a strong resonant field by the Stark-shift or Rabi frequency of the strong field, the probe field can experience induced gain even in the absence of a time-averaged inversion. Wu *et al.*[3] performed an experiment to verify these predictions. An intense laser beam from the output of a frequency-stabilized dye laser was used to excite two-level atoms prepared in a sodium atomic beam while a second laser beam was used to probe the modified absorption spectrum. The experimental results were in good agreement with the theoretical predictions for this problem. In a later experiment, Gruneisen *et al.*[4] performed a similar experiment involving a sodium vapor cell and two stabilized dye lasers. In this experiment the effect of varying the collisional dephasing rate was studied.

As long as the probe fields are weak, the physics of the interaction can be adequately treated by a third-order perturbation theory. Perhaps the most general self-consistent problem which can be accurately described by a third-order theory is that of four-wave mixing. It is therefore important to mention that Boyd *et al.*[5] showed that an enhancement in gain occurs in nearly degenerate four-wave mixing when the conjugate beams are detuned from the pump beam by the pump-beam Rabi frequency. These results were later confirmed in experiments by Harter *et al.*[6,7] using a pulsed dye laser incident on a sodium cell.

These pump-probe problems can also be described using a modulation formalism. Hillman *et al.*[8] and Kramer *et al.*[9] showed that the interaction of a strong field and a single sideband with a two-level atomic system can be described as a linear combination of weak AM and frequency modulation (FM). It is also "natural" to describe the interaction in this manner. They show that if an arbitrary linear combination of AM and FM modes are allowed to interact in a self-consistent manner with a two-level atomic system the amounts of AM

and FM will adjust themselves to a unique ratio depending on the intensity of the strong field and the detuning parameter. Therefore, it is basically correct to describe the pump-probe problem in a modulation formalism.

In contrast to these studies of weak modulation interactions, some researchers have focused on interactions in which the modulation amplitudes applied to the resonant driving fields are large.[10-21] In these interactions the modulation sidebands alter the atomic dynamics substantially from the single field dynamic behavior. Although the treatment of strong-modulation interactions is by no means complete, there has been experimental work in this area.[10,12,16] These strong-modulation experiments yield different results from those seen in weak-modulation experiments. The atomic variables exhibit resonant behavior when the modulation frequency is approximately equal to the Rabi frequency or any subharmonic of the Rabi frequency. Bonch-Breuvich et al.[10] performed the earliest such experiment with two strong rf fields tuned to a Zeeman resonance in cadmium. One rf field was held at a constant frequency while the frequency of the other field was tuned about the resonance to obtain an absorption spectrum. The absorption spectrum of the rf field exhibited several subharmonic resonances. This experiment is extremely relevant to the present work; however, a distinct difference exists in that spontaneous emission effects are insignificant in the rf regime. Thomann[12] performed a three-field experiment at the sodium D_2 line resonance. The field was produced by strongly modulating the intensity of a laser beam; the Rabi frequency was varied while the modulation frequency was held fixed. A sinusoidally varying rf voltage was supplied to the electro-optic modulator. This rf modulation signal was chopped at an audio frequency and the fluorescence signal was analyzed using a lock-in amplifier. In this way the collected signal was equal to the difference between the response of the atoms

to single-frequency excitation and the response of the atoms to the modulated excitation. The data revealed the subharmonic resouances as predicted by the theory. However, the fluorescent intensity decreased at each resonance in contrast to the two-field experiment in which the fluorescent intensity increases at the resonances.

The field of laser instabilities has brought renewed interest to these modulation problems since the interaction of modulated fields with atomic media has been related to various laser instabilities.[21-27] Feldman and Feld[21] show that a single-mode standing-wave laser field interacting with a Doppler broadened gain medium is similar to the 100% AM problem. The standing-wave bidirectionally propagating field is resonant with two symmetrically detuned velocity groups, resulting in a bichromatic excitation. Under these circumstances the gain medium will experience resonances in its laser spectrum due to the subharmonic Rabi resonances.

It has been observed that lasers can become unstable to self-modulation caused by the ac Stark effect. Perhaps the earliest predicted laser instability due to a Stark-frequency or Rabi frequency modulation was predicted by Risken et al.[22] A single-mode laser was predicted to become unstable when the Rabi frequency reached a threshold value depending on the laser's characteristic relaxation rate. Instabilities of this type have been observed in far-infrared (FIR) lasers. Harrison et al.[23] show that due to the Stark-splitting of the upper lasing level by the pumping laser, an FIR laser becomes unstable to single mode operation. Although the interaction with the pump and the secondary laser in the FIR laser instability is a bit different from the situation treated by Risken and Nummedal, the physics behind these instabilities is similar.

Another multichromatic laser instability has been observed in a series of

experiments at the University of Rochester.[24-27] Hillman *et al.*[24] found that when the pump power of a dye laser is increased beyond 1.5 times or so above the threshold amount, the spectrum of the dye-laser becomes unstable for single frequency operation. The spectrum of the dye laser laser bifurcates into two frequency components. This instability illustrates the significance of multifrequency interactions in laser systems.

With the renewed interest in these strong modulation interactions has come new approaches to understanding the physics. Silverans *et al.*[16] performed an experimental study of strong modulation for short interaction times. The phase of the modulation is a critical parameter in such interactions. These results were theoretically analyzed by Eberly *et al.*[17] Agarwal showed that the subharmonic resonances appear in the Raman effect[18] and that generation of squeezed states of the phase of the electromagnetic field is possible in multiwave mixing at subharmonic Rabi resonances.[19] Recently, Ruyten[20] has studied the behavior of the various harmonic components of the atomic response to a 100% AM optical excitation.

In this chapter I describe our contribution to the research in this area. I describe an experimental and theoretical study we performed to understand the interaction of a 100% AM optical excitation with an ensemble of homogeneously broadened two-level atoms. I will present a brief theoretical treatment of the problem and describe some numerical calculations we performed to understand the behavior of the atomic variables in such an interaction. Furthermore, I will present a comparison between the interaction of a sinusoidally amplitude-modulated field and a pulsed amplitude-modulated field with two-level atoms.

B. Theoretical review

The response of an atomic system can be characterized, in part, by the rate at which it absorbs, or scatters, energy from a resonant laser beam. I employ a calculation developed by Hillman *et al.*[25] to calculate the rate of absorption from the optical Bloch equation

$$\dot{u} = -u/T_2 - \Delta v, \tag{2.1a}$$

$$\dot{v} = \Delta u - v/T_2 + \kappa E(t)w, \tag{2.1b}$$

$$\dot{w} = -(w+1)/T_1 - \kappa E(t)v, \tag{2.1c}$$

where u and v are the in-phase and in-quadrature dipole moments, respectively, and w is the atomic inversion. The detuning is Δ and $1/T_2$ and $1/T_1$ are the polarization and population decay rates, respectively. The dipole-moment coupling constant κ is given by

$$\kappa = 2d/\hbar, \tag{2.2}$$

where d is the dipole-moment matrix element and $\hbar$ is Planck's constant divided by 2π. We are interested in the response of an atom to a 100% AM excitation. In this case the electric field amplitude can be written as

$$E(t) = 2E_1 \cos(\delta\omega t), \tag{2.3}$$

where $\delta\omega$ is the modulation frequency and the amplitude of each component of the electric field is E_1.

According to Floquet's theorem, the stationary-state response of the atomic variables can be expanded in a Fourier series of the modulation frequency $\delta\omega$. The in-phase and in-quadrature components of the atomic polarization and the atomic inversion can be written as

$$u(t) = \sum_{n=-\infty}^{\infty} u_n \exp(in\delta\omega t), \tag{2.4a}$$

$$v(t) = \sum_{n=-\infty}^{\infty} v_n \exp(in\delta\omega t), \tag{2.4b}$$

$$w(t) = \sum_{n=-\infty}^{\infty} w_n \exp(in\delta\omega t), \tag{2.4c}$$

respectively. The nth-harmonic components of the in-phase and in-quadrature dipole moments and of the atomic inversion are denoted by u_n, v_n, and w_n respectively. When we substitute the expansions given in Eqs. (2.4a-2.4c) into the Bloch equations, Eqs. (2.1a-2.1c), we get a set of recurrence relations for the harmonic components of the atomic variables

$$(1 + in\delta\omega T_2)u_n = -\Delta T_2 v_n, \tag{2.5a}$$

$$(1 + in\delta\omega T_2)v_n = \Delta T_2 u_n + \kappa E_1 T_2 (w_{n+1} + w_{n-1}), \tag{2.5b}$$

$$(1 + in\delta\omega T_1)w_n = -\kappa E_1 T_1 (v_{n+1} + v_{n-1}) + \delta_{n,0} w_{eq}. \tag{2.5c}$$

The recurrence relations for the in-phase and in-quadrature dipole moments [Eqs. (2.5a-2.5b)] can be combined to yield a single recurrence relation

$$\left[1 + in\delta\omega T_2 + \frac{(\Delta T_2)^2}{1 + in\delta\omega T_2}\right] v_n = \kappa E_1 T_2 (w_{n+1} + w_{n-1}), \tag{2.6}$$

Now we can combine the information in Eq. (2.5c) and Eq. (2.6) to yield the ratio of the first-harmonic component of the in-quadrature dipole moment to the zeroth-harmonic (time-averaged) component of the inversion in the form of a continued fraction:

$$\frac{v_1}{w_0} = \cfrac{1}{B_1 + \cfrac{I_1}{B_2 + \cfrac{I_1}{B_3 + \cfrac{I_1}{B_4 + \dots}}}}, \tag{2.7}$$

where the single-field intensity is

$$I_1 = (\kappa E_1)^2 T_1 T_2, \tag{2.8}$$

and the coefficients denoted by B_n are

$$B_n = 1 + in\delta\omega T_2 + \frac{(\Delta T_2)^2}{1 + in\delta\omega T_2}, \qquad (2.9a)$$

for odd n and

$$B_n = 1 + in\delta\omega T_1, \qquad (2.9b)$$

for even n. Note, that the single-field intensity is naturally expressed in dimensionless form in Eq. (2.7). I will use the dimensionless intensity as well as the dimensionless modulation frequency, $\delta\omega T_2$, and the dimensionless detuning, ΔT_2, throughout.

We can solve for the time-averaged component of the atomic inversion, w_0, in terms of the continued fraction and then write the excited-state population as

$$\rho_e = \frac{I_1 \mathrm{Re}\{v_1/w_c\}}{1 + 2I_1 \mathrm{Re}\{v_1/w_0\}}. \qquad (2.10)$$

We are ultimately interested in the absorption of the AM field. The average rate at which a two-level atom scatters light in the form of resonance fluorescence is equal to the time-averaged absorption. The fluorescent emission rate is proportional to the excited-state population. Consequently, for the case of a 100% AM excitation of a two-level atom, the rate of absorption of energy is proportional to the time-averaged component of the excited-state population. Therefore, we can measure the time-averaged absorption of modulation energy and the excited-state atomic population by monitoring the time-averaged fluorescent intensity.

I have plotted the excited-state population given by Eq. (2.10) in Figs. 2.1(a) and 2.1(b). In Fig. 2.1(a) I plot the time-averaged excited-state population for a fixed Rabi frequency as a function of the modulation frequency,

$\delta\omega T_2$. This curve is quite complicated, and it shows several resonances in the absorption spectrum of the fields. To understand these peaks it is helpful to solve the problem on resonance in the absence of damping as I did in chapter 1 in Eqs. (1.7a-1.7b). In this case we obtain an analytic solution in which the time-averaged response of the population inversion is equal to $-J_0(2\kappa E_1/\delta\omega)$. When we numerically pick off the position of each peak from Fig. 2.1(a) we find that the peaks occur whenever the factor $J_0(2\kappa E_1/\delta\omega)$ is equal to zero. The outermost peaks in Fig. 2.1(a) correspond to the first zero of J_0. The next peaks, at smaller values of $\delta\omega T_2$, correspond to the second zero of J_0 and are the first subharmonic resonances. In the limit of large arguments, x, the zeros of $J_0(x)$ become equally spaced versus x. It is in this limit that the resonances are best described as subharmonic resonances.

In Fig. 2.1(b) the time-averaged population of the excited-state is plotted versus the time-averaged dimensionless intensity $2(\kappa E_1)^2 T_1 T_2$ for a fixed modulation frequency of three atomic linewidths ($\delta\omega T_2 = 3$). This is the form of our raw data. The resonances appear as enhancements in the absorption embedded in the usual single-field saturation curve. As the intensity is increased from zero, we approach the first-order resonance. The second resonance, occuring at higher intensity, is the first subharmonic resonance. The order of the subharmonic resonances increases as we look to higher dimensionless intensities. These resonances occur only when the interaction is strong, meaning the Rabi frequency, κE_1, exceeds the natural linewidth of the transition and the modulation depth is large as is the case of a 100% amplitude modulation.

C. The Dynamic behavior of the atomic variables

The dynamic behavior of the atomic variables also reflects the subharmonic
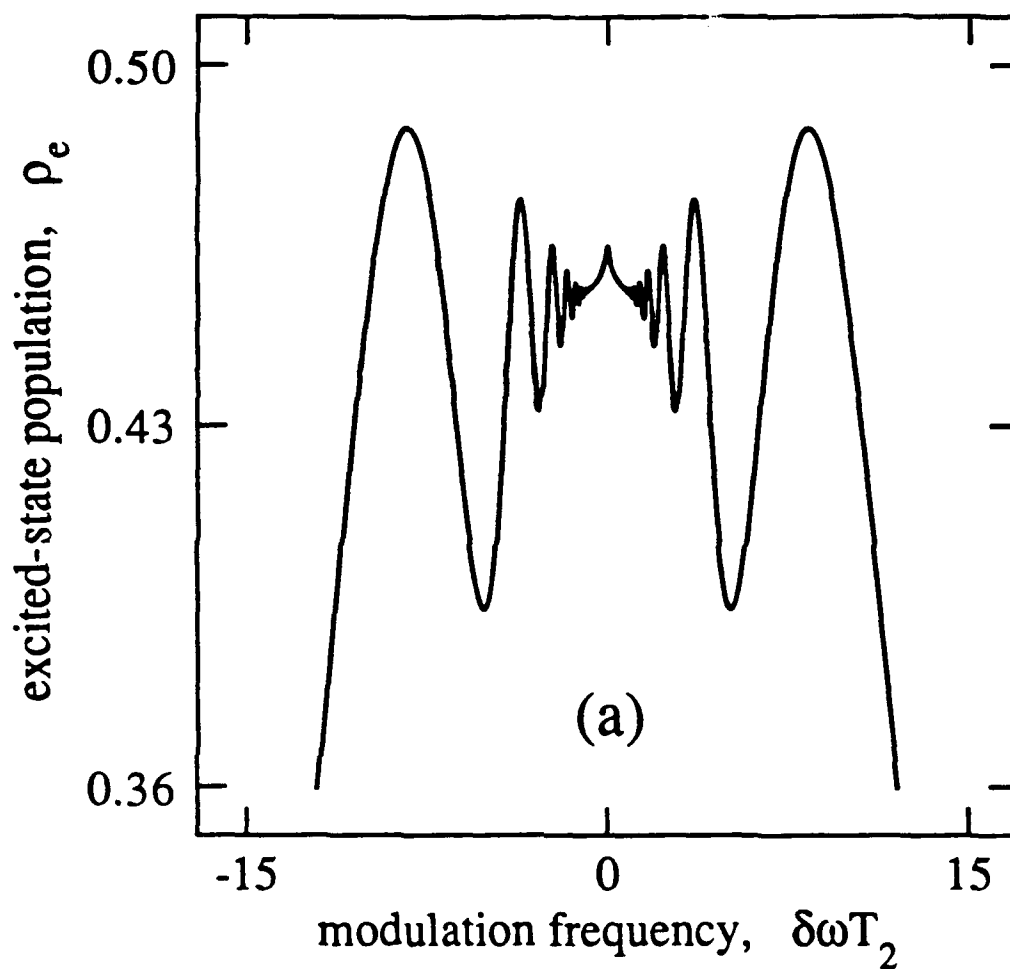
Fig. 2.1(a) Time-averaged excited-state population as a function of the modulation frequency, $\delta\omega T_2$. The dimensionless Rabi frequency is held fixed at $\kappa E_1 T_2 = 10$. and the dimensionless modulation frequency $\delta\omega T_2$ is varied to observe the subharmonic resonances. The detuning is zero, $\Delta T_2 = 0$.
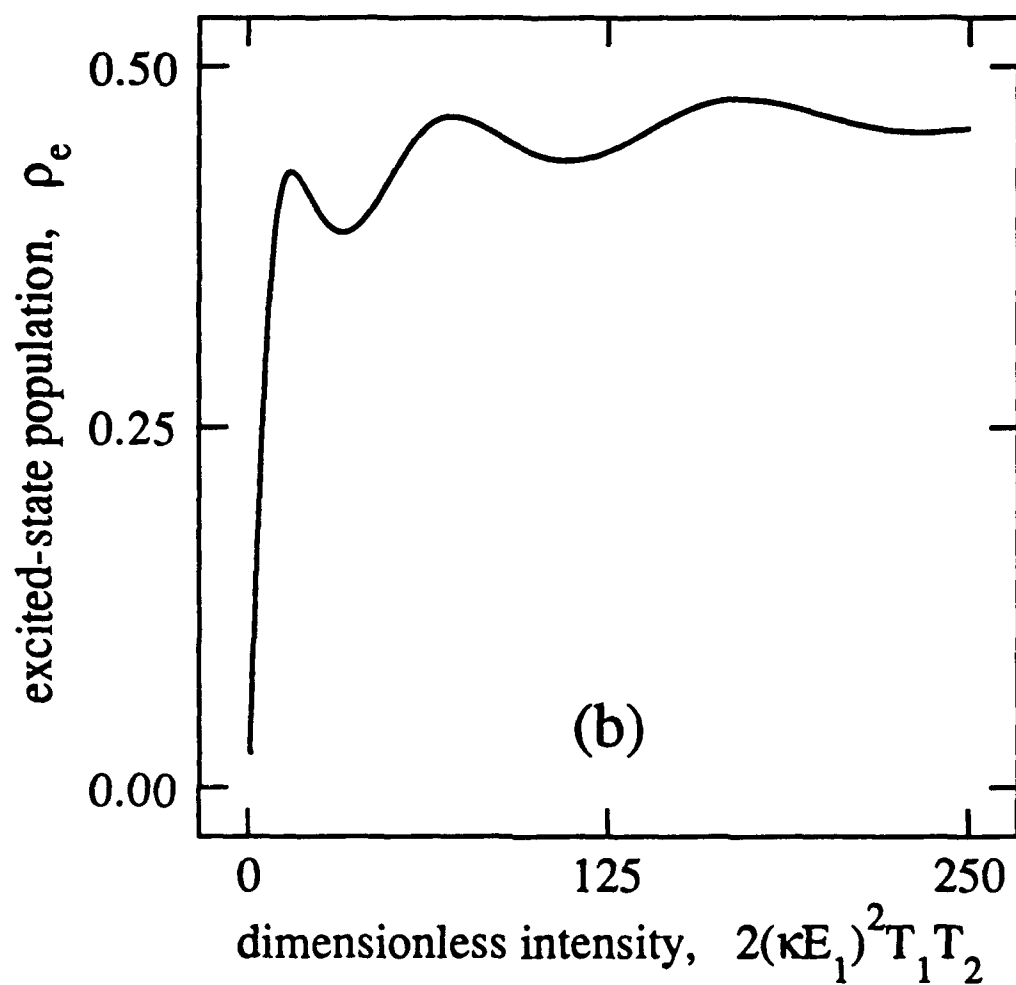
Fig. 2.1(b) Time-averaged excited-state population as a function of intensity. The dimensionless modulation frequency is held fixed at $\delta\omega T_2 = 3$. and the time-averaged dimensionless intensity $2(\kappa E_1)^2 T_1 T_2$ is varied to observe the resonances. The detuning is zero, $\Delta T_2 = 0$.

resonant behavior of the 100% AM interaction. In Figs. 2.2(a-d), I show the phase plots formed by the in-quadrature atomic polarization and the atomic inversion at each of the first four resonances (on-resonance excitation is used for the phase plots so that only the in-quadrature polarization is driven). Each curve in Fig. 2.2 shows the trajectory followed by the atomic variables for a complete period of the modulation. Figure 2.2(a) shows the period-one behavior that occurs at the first resonance. Figure 2.2(b) shows that a second cycle in the trajectory occurs at the second resonance, which is the first subharmonic resonance. Figures 2.2(c) and 2.2(d) show the behavior at the third and fourth resonances, respectively. We can compare this system to an oscillator being driven every nth cycle of its natural frequency. The oscillator can be driven effectively by the fundamental frequency or by any subharmonic of the fundamental. This subharmonic driving is effective because the system responds at higher harmonics of the driving frequency when the driving force is large enough to induce a nonlinearity.

In Fig. 2.3(a-d) I have plotted the dynamic behavior of the atomic variables at each of the first four anti-resonances (minima of the fluorescence-versus-intensity response). The parameters corresponding to the local minima in Fig. 2.1(b) are used to construct these figures. The sequence of the behavior of the atomic variables can be constructed for increasing intensity as follows: Figs. 2.2(a) - 2.3(a) - 2.2(b) - 2.3(b) - 2.2(c) - 2.3(c) - 2.2(d) - 2.3(d). The atomic trajectory closes in on itself as the excitation strength increases. This behavior is analogous to the behavior of a pair of vortices in the wake of a boat as they turn inward toward one another.

The dynamic behavior depicted in the phase plots can be further examined by calculating a histogram of this periodic behavior. The phase plots are recal-
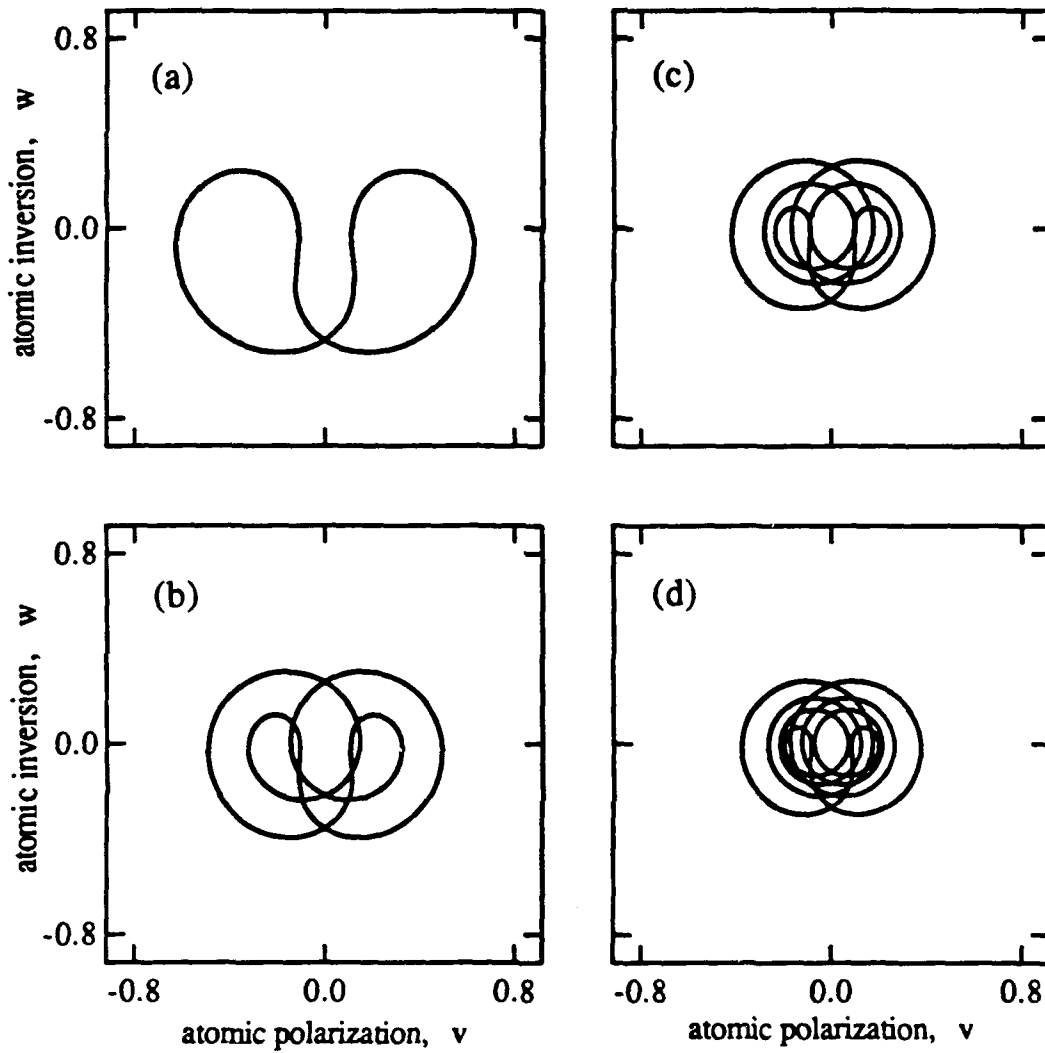
Fig. 2.2 Trajectories of the atomic inversion and the in-quadrature polarization. I plot the atomic inversion versus the atomic polarization at the first four resonances. The modulation frequency is $\delta\omega T_2 = 3$. In (a) the Rabi frequency corresponds to the first resonance. In (b)-(d) the behavior at the first three subharmonic resonances are shown. The Rabi frequencies used in these figures are: (a) $\kappa E_1 T_2 = 3.9$; (b) $\kappa E_1 T_2 = 8.43$; (c) $\kappa E_1 T_2 = 13.1$; (d) $\kappa E_1 T_2 = 17.8$. The detuning for all figures is zero, $\Delta T_2 = 0$.
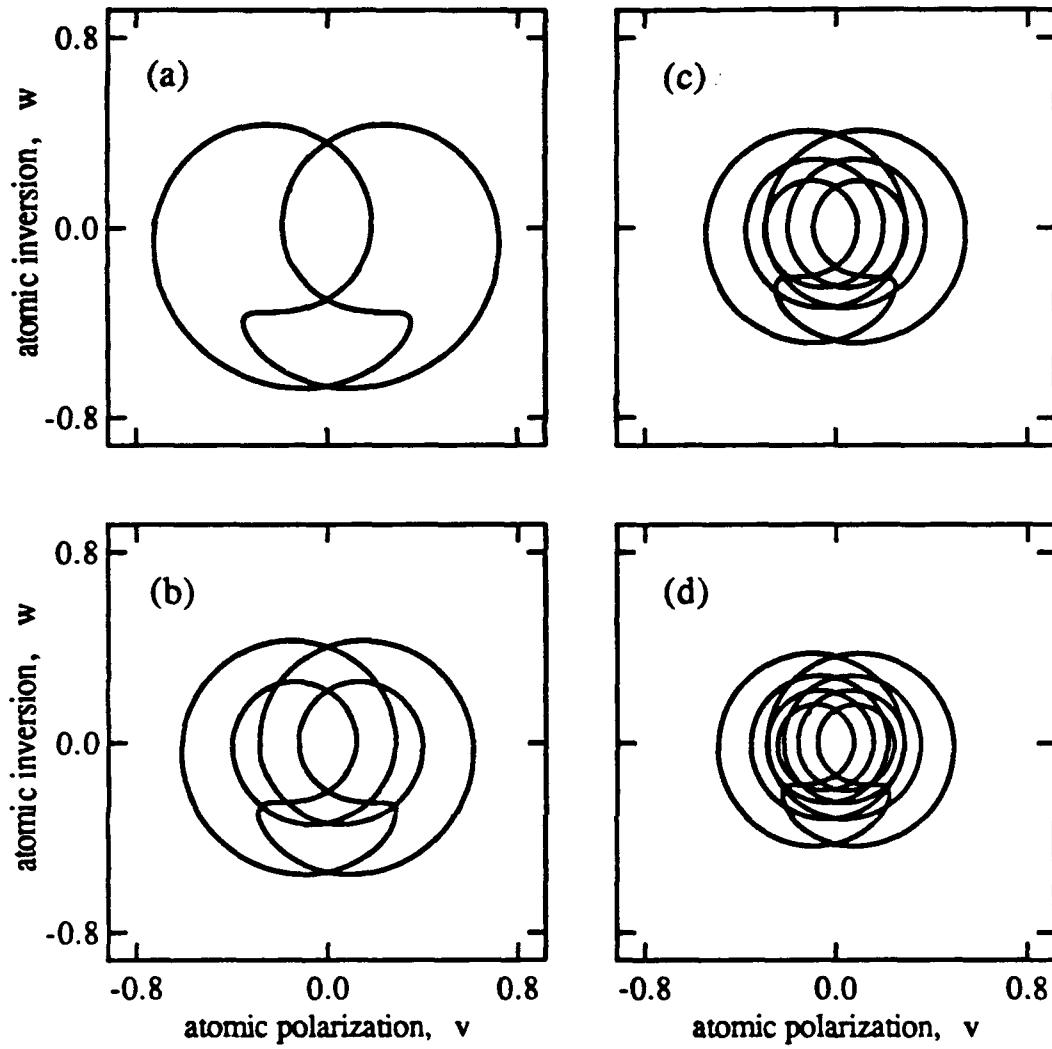
Fig. 2.3 Trajectories of the atomic inversion and the in-quadrature polarization. I plot the atomic inversion versus the atomic polarization at the first four anti-resonances. The modulation frequency is $\delta\omega T_2=3$. In (a) the Rabi frequency corresponds to the first anti-resonance. In (b)-(d) the behavior at the first three subharmonic anti-resonances are shown. The Rabi frequency used in these figures are: (a) $\kappa E_1 T_2=5.75$; (b) $\kappa E_1 T_2=10.55$; (c) $\kappa E_1 T_2=15.3$; (d) $\kappa E_1 T_2=20.03$. The detuning for all figures is zero, $\Delta T_2=0$.

culated but this time with many more points in order to develop an accurate histogram of the atomic behavior. In particular, we will examine the histogram of the atomic inversion. The range of values that the inversion can acquire (ranging from -1 to 1) is broken up into 1000 bins. The phase plot is analyzed over an integral number of periods with many thousand points in order to construct an histogram of the inversion. In Figs 2.4(a-d) I have plotted the histograms for the atomic inversion corresponding to the same parameters as were used to construct the phase plots in Figs 2.2(a-d). The first plot Fig. 2.4(a) represents the histogram for the atomic inversion at the first resonance. The histogram is indicative of harmonic motion which is nearly symmetrical about the point corresponding to zero inversion. The next three histograms depict the atomic behavior at the next three resonances. At each resonance the histogram displays an extra set of peaks. At each successive resonance the motion of the atomic inversion acquires an additional harmonic component.

In order to see the progression between successive resonances I have plotted the histograms for the atomic inversion at the first four anti-resonances. These histograms are shown in Figs 2.5(a-d). The parameters used to construct these histograms are the same as those used to construct the phase-plots in Figs. 2.3(a-d). The first thing to notice is that these histograms have greater extent over the inversion axis (x-axis) than those shown in Figs. 2.4(a-d). It is interesting that while the resonances are defined by the occurrence of local maxima of the dc inversion, the atomic trajectory takes on its minimum extent for the same parameters. In other words, the dc response is maximized while the ac response is minimized. We can learn a bit more from the histogram plots in Figs. 2.5(a-d). The origin of the subsequent peaks in the histogram plots can clearly be seen in this sequence of graphs. While the trajectory takes on its maximum
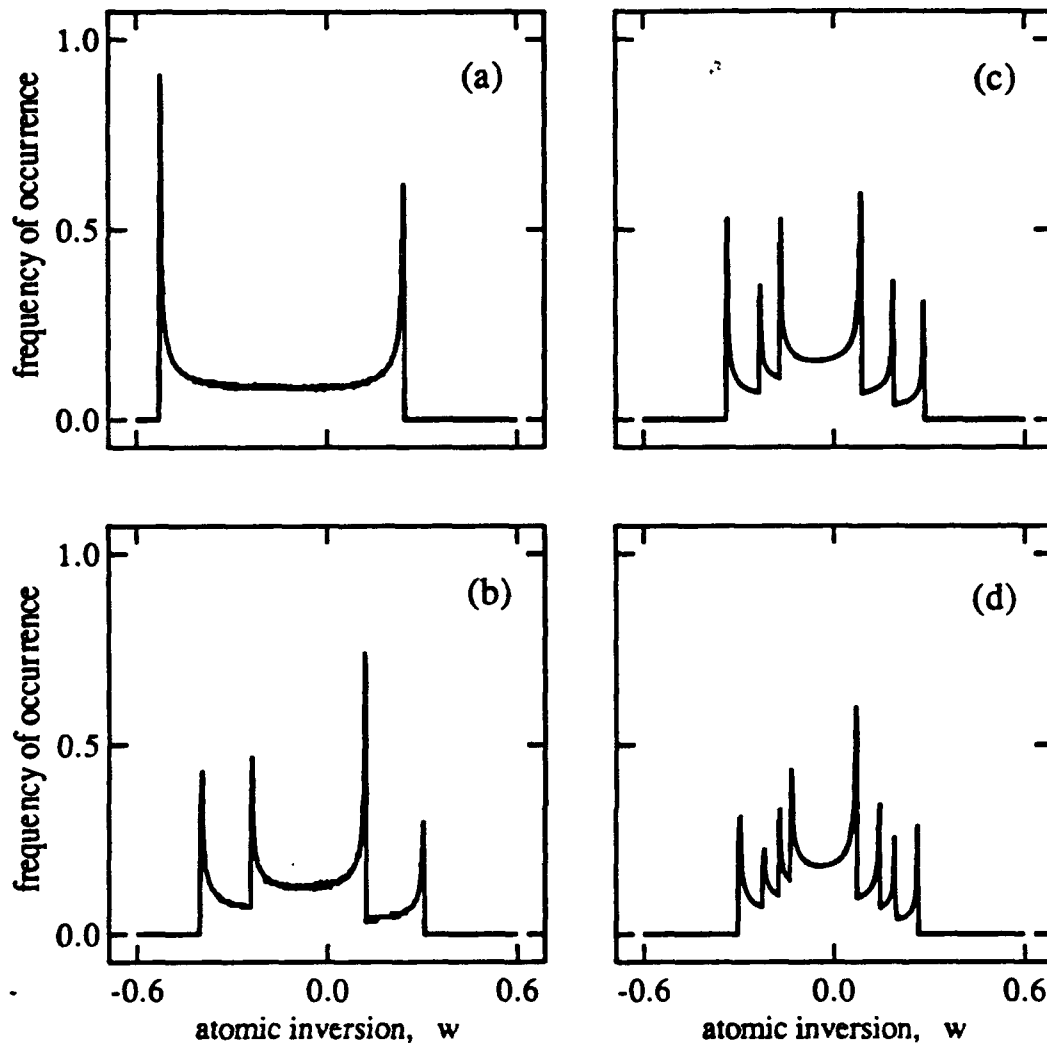
Fig. 2.4 Histograms of the atomic inversion of an atom subjected to 100% AM excitation at the first four resonances. Histograms are constructed of the behavior of the atomic inversion at the first four parameteric resonances for a modulation frequency $\delta\omega T_2=3$. The histograms are constructed using 100000 points and the results are normalized to 4500 occurrences. The parameters used are: (a) $\kappa E_1 T_2=3.9$; (b) $\kappa E_1 T_2=8.43$; (c) $\kappa E_1 T_2=13.1$; (d) $\kappa E_1 T_2=17.8$. These parameters are the same as those used in Fig. 2.4.
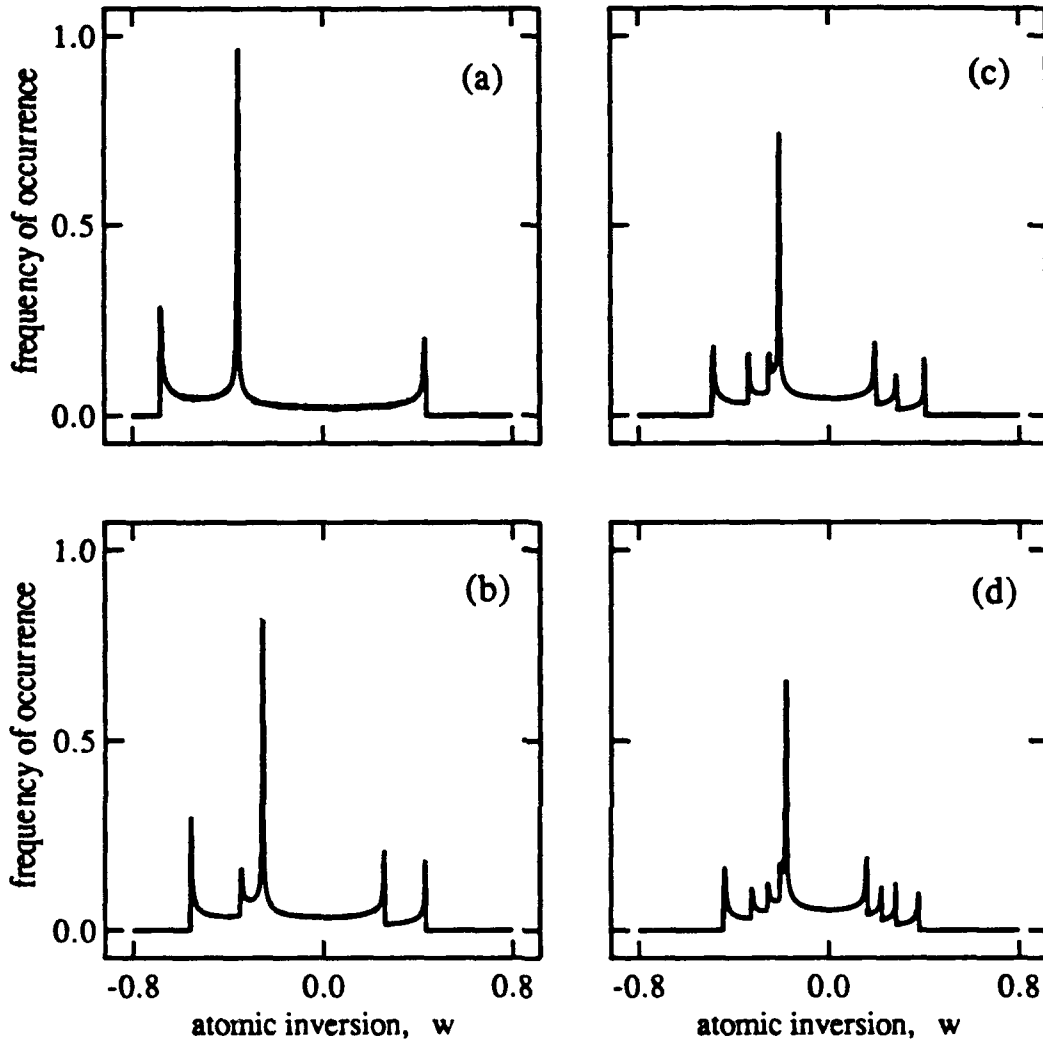
Fig. 2.5 Histograms of the atomic inversion of an atom subjected to 100% AM excitation at the first four anti-resonances. Histogram^ are constructed of the behavior of the atomic inversion at the first four parametric anti-resonances for a modulation frequency $\delta\omega T_2=3$. The histograms are constructed using 100000 points and the results are normalized to 7500 occurrences. The parameters used are: (a) $\kappa E_1 T_2=5.75$; (b) $\kappa E_1 T_2=10.55$; (c) $\kappa E_1 T_2=15.3$; (d) $\kappa E_1 T_2=20.03$. These parameters are the same as those used in Fig. 2.3.

extent near the anti-resonance, a peak in the inversion histogram emanates in the negative inversion region. This peak actually overshadows all other peaks in the histogram. The atomic trajectory stalls at this value of the inversion. Then, this peak bifurcates into two peaks which move apart as the field intensity is further increased. At the same time the entire histogram contracts about the zero inversion value as the intensity is increased to correspond with the next subharmonic resonance. The reader is encouraged to see the movie!

D. The experiment

In order to test the theoretical predictions discussed in the previous sections, we set out to perform an experiment using a radiatively broadened ($T_2 = 2T_1$) two level atomic medium. Atomic sodium was prepared in an atomic beam as the medium. A home-built stabilized dye laser was used to excite the atoms with a 100% amplitude-modulated field. The absorption of the field was determined by monitoring the total fluoresence scattered from the interaction region. In this section I discuss the apparatus and techniques used in this experiment. First, in sub-section 1 I discuss the details of the laser stabilization. This section is devoted primarily to people who might want to employ the stabilized laser in experiments of their own. Then, in the next subsection, I will discuss the atomic-beam system which was also constructed for this experiment. The last subsection is devoted to the details of the overall experimental setup. This includes the production of the 100% AM filed and the collection of the signal. The reader who is not interested in using any of this equipment should skip to subsection 3 for the description of the actual experiment.

1. The stabilized laser

The lasers we use in our experiments are home-built. In this experiment we used a rhodamine 6G dye laser pumped by an argon-ion laser. The dye jet is one which Coherent uses in their commercially available dye lasers. The jet is approximately 300 μ thick by 3 mm wide. The dye is flowed through this jet at 35 psi. Great care is taken to insure that vibrations from the pump are eliminated from the fluid system to prevent these fluctuations from degrading the frequency stability of the dye laser. The vibration isolation is accomplished by using pliable tygon tubing to connect the dye jet to the rest of the system. Further vibrational damping is accomplished by a ballast made of a "Master of the Universe" punching ball which is inflated by the dye's pressure inside of a sealed housing. These precautions insure that the frequency jitter of the laser is roughly 10-20 MHz before active stabilization is employed. Consequently, the stability of our dye laser is superior to the Coherent 699 stabilized dye laser system in the "free-run" mode of operation.

The reader should refer to Fig. 2.6 for the following discussion of the optics employed in the stabilized dye laser. The laser is a standing-wave laser which operates in two longitudinal modes separated by approximately 60 GHz in frequency. For further details into the philosophy of this laser-cavity configuration the reader can see Mary Citron's thesis[28] or the paper we published on the "washing machine instability."[29] Two broadband high-reflector focusing mirrors, each having a 5 cm radius of curvature, are used to focus and recollimate the laser beam through the dye jet. One of the curved high reflectors also serves to focus the argon pump beam into the dye jet. The focusing mirrors are each mounted on Melles Griot translation stages to allow easy adjustment of the focus of each mirror. The pump beam and the dye-laser beam each have
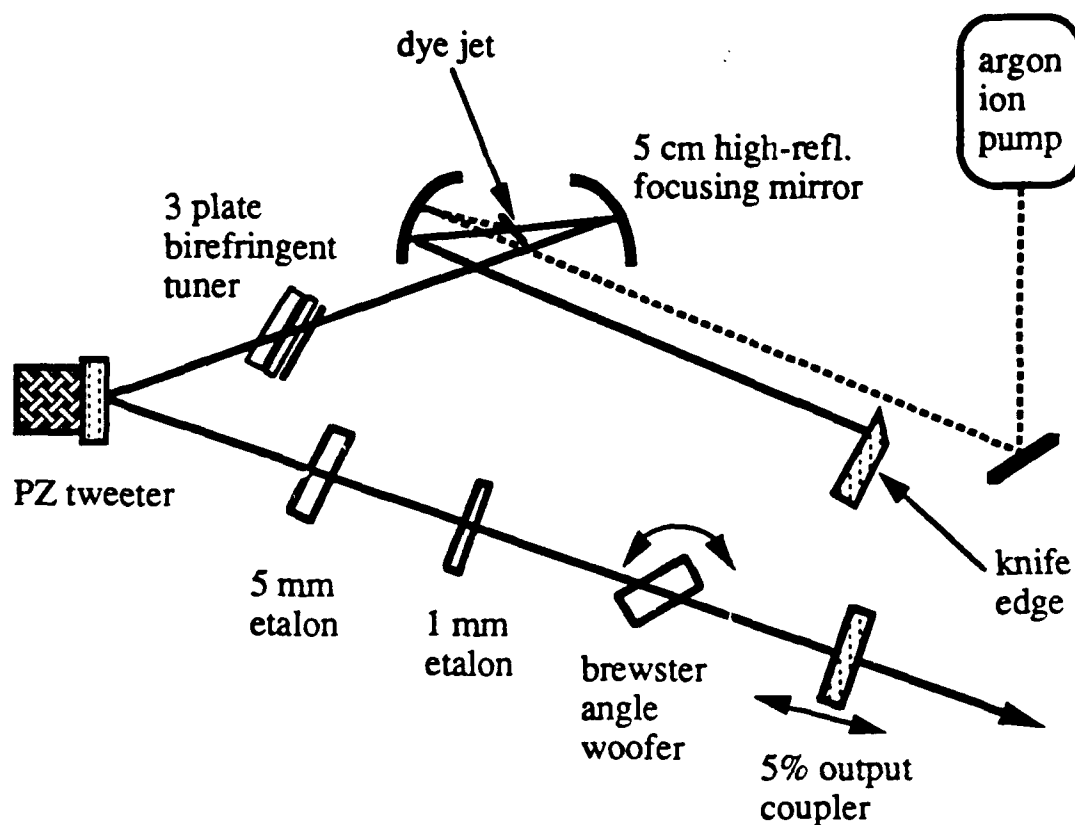
Fig. 2.6 Two-mode standing-wave dye laser layout. The cavity consists of five mirrors: two 5 cm radius high reflectors mounted on translation stages; a knife-edge high reflector; a high reflector flat mounted on a PZ pusher (tweeter); and a 5% output coupler mounted on a translation stage. A three-plate birefringent tuner is used for course tuning. Two etalons are used for mode selection. A third etalon is mounted on a galvo motor and is inserted at brewsters angle to serve as a woofer.

approximately a 15 μ spot size at the dye jet. This pump geometry has been employed in past experiments.[24-27] A knife-edge high-reflector mirror allows the argon pump beam to be brought in parallel to the dye-laser laser cavity axis. The knife-edge also serves as one of the end mirrors of the dye-laser cavity. A fourth high-reflector flat mirror is mounted on a piezoelectric pusher to serve as the tweeter in the stabilization circuit. This mirror folds the cavity axis onto the 5% output coupler which is mounted on another Melles Griot translation stage to facilitate small adjustments of the length of the dye-laser cavity. The coarsest frequency filter used in the dye-laser cavity is a three-plate birefringent filter supplied by Coherent Inc. The birefringent filter provides an initial bandwidth of less than 100 GHz. The next finer tuning element is a 1 mm thick etalon which is coated with a 15% reflective coating on both sides. The finest tuning element is a 5 mm thick etalon with a 15% reflective coating. The free spectral range of the thick etalon is 60 GHz which is the frequency separation of the two lasing longitudinal modes. At this point it is necessary to point out that a homogeneously broadened standing-wave laser with a thin gain medium is unstable in single-mode operation. When a standing-wave laser operates in a single longitudinal mode, spatial hole burning results since the standing-wave pattern of a single mode would utilize only half of the pumped atoms. The sinusoidal interference pattern due to a single-mode standing-wave field produces a condition of spatial hole burning within the gain medium. Two modes separated by as much as 60 GHz can maintain a constant phase difference throughout the 100 μm thick gain medium. Therefore, it is necessary for the laser to operate in at least two modes in order to deplete the gain in a spatially uniform manner. The reason a single-mode unidirectional ring laser is not used is that our unidirectional device (a Faraday rotator and a birefringent crystal) introduces

too much loss to the laser cavity. Furthermore, since the frequency separation between the lasing modes is 60 GHz and the linewidth of the atomic transition in sodium is 10 MHz we can tune one mode to resonance and assume that the other mode does not interact with the atoms.

Stable two-mode operation in the described standing-wave laser configuration occurs only under certain conditions. The position of the end mirrors with respect to the gain medium is an important factor. Therefore, we mount the output coupler on a translation stage. Stable two mode operation occurs for several end-mirror positions. Once one of these positions are found, another position can be found by translating one of the mirrors by the optical path length of the thick etalon. The stability of the laser to two mode operation is related to the position of the nodes and antinodes of the two-mode interference pattern at the end mirrors and in the gain medium. The knife edge is first positioned by hand and then the position of the output coupler is tweeked to produce stable two-mode operation. These steps are repeated until the operator can lean on the table or otherwise deform the dye-laser cavity, causing the laser to mode-hop from one set of two modes to another, without a third mode turning on.

Once the laser is operating in a stable two-mode configuration the active stabilization can be engaged. A thick glass plate is used to produce two pick-off beams for the stabilization circuit (see Fig. 2.7). One beam is directed onto a fast detector (bandwidth of over 1 MHz) and the other is directed into a thermally stabilized pressure-scanned confocal Fabry Perot interferometer (FPI). The details of the construction of this FPI are outlined in a paper by M. Hercher[30] and I will only briefly discuss them here. A combination of Super Invar and Cervit (a ceramic) are used in the mechanical cavity. These materials have small coefficients of thermal expansion but of opposite sign. The lengths of each material
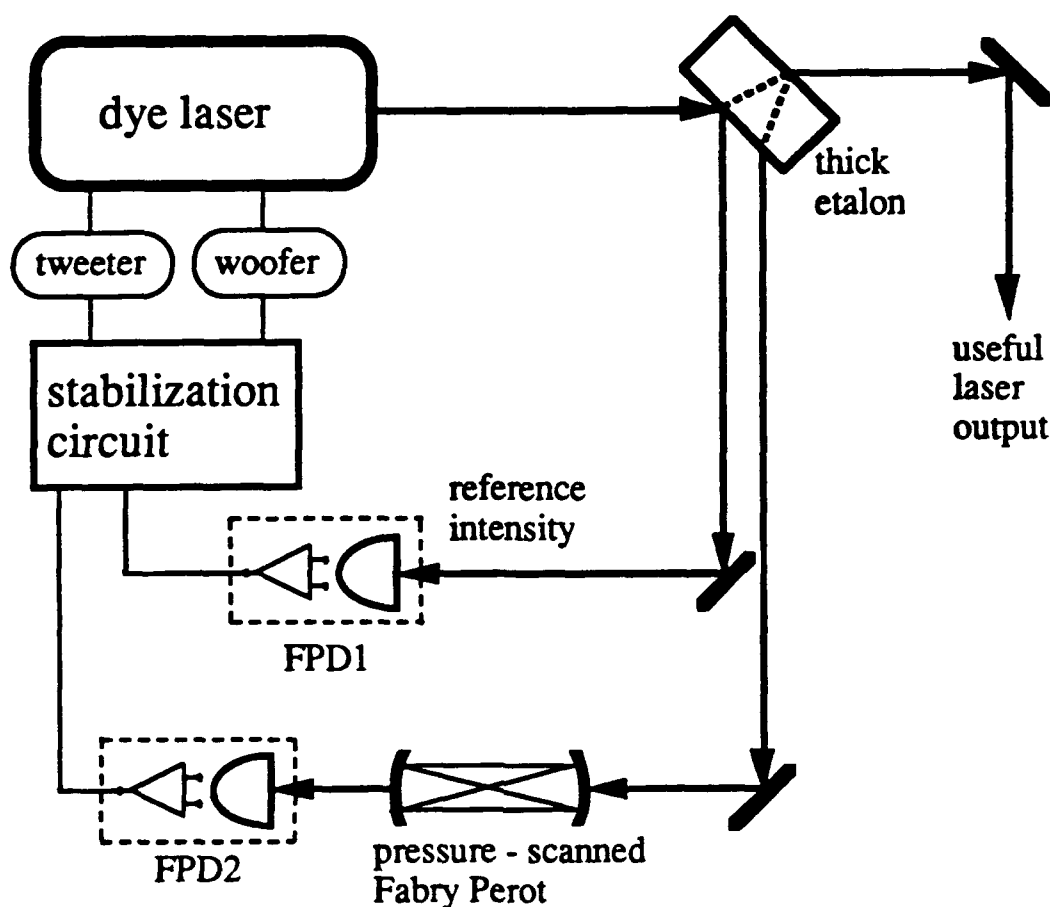
Fig. 2.7 Optical layout for the frequency stabilization of the dye laser. Shown is the layout of the optical components involved in the stabilization process together with the routes of the electrical signals involved. Two pick-off beams are used: one for a reference-intensity measurement; the second is used for the frequency measurement. The frequency is monitored via a detector positioned in back of a temperature-stabilized pressure-scanned Fabry Perot interferometer. The stabilization circuit performs a fast divide operation on the two signals. The resulting error signal is fed through a crossover circuit to drive the woofer and tweeter correcting elements in the laser cavity.

are chosen to produce a structure which is invariant to small uniform changes in temperature. The optical path length of the FPI is changed by a micrometer screw which pushes on a diaphragm which is exposed to the cavity via an air passage. Once the desired cavity resonant frequency is obtained the cavity can be valved off from the diaphragm to isolate the cavity from pressure fluctuations in the room. A second fast photodiode is positioned in back of the FPI to monitor the transmitted intensity from the cavity. The stabilization circuit divides the transmitted signal from the Fabry Perot by the intensity reference signal to obtain a voltage whose value represents the difference of the laser's frequency from the resonant frequency of the FPI. The intensity of the laser is divided out to prevent intensity fluctuations from obscuring the frequency measurement. The normalized FPI signal represents a nearly linear conversion of small frequency fluctuations into voltage fluctuations. This is the error signal for the stabilization circuit. If the laser is locked onto the side of a transmission peak of the FPI and the fluctuations are small compared to the linewidth of the FPI then the conversion of frequency fluctuations to voltage fluctuations is a linear process.

The stabilization circuit is based on a fast divide chip (3091D) from RCA. The circuit diagram for the stabilization circuit is shown in Figs. 2.8 - 2.10. The signals from the detectors are first amplified by a factor of ten using the two op-amps shown in Fig. 2.8. The amplified signals are fed into the fast divide chip as shown in Fig. 2.9. The divide circuit puts out one signal which is proportional to the frequency error. This signal is split between the tweeter driver and the woofer driver. These cross-over circuits are shown in Fig. 2.10.

The tweeter circuit is diagrammed in Fig. 2.10. The tweeter circuit has been designed to provide large low-frequency gain. The idea is to provide two
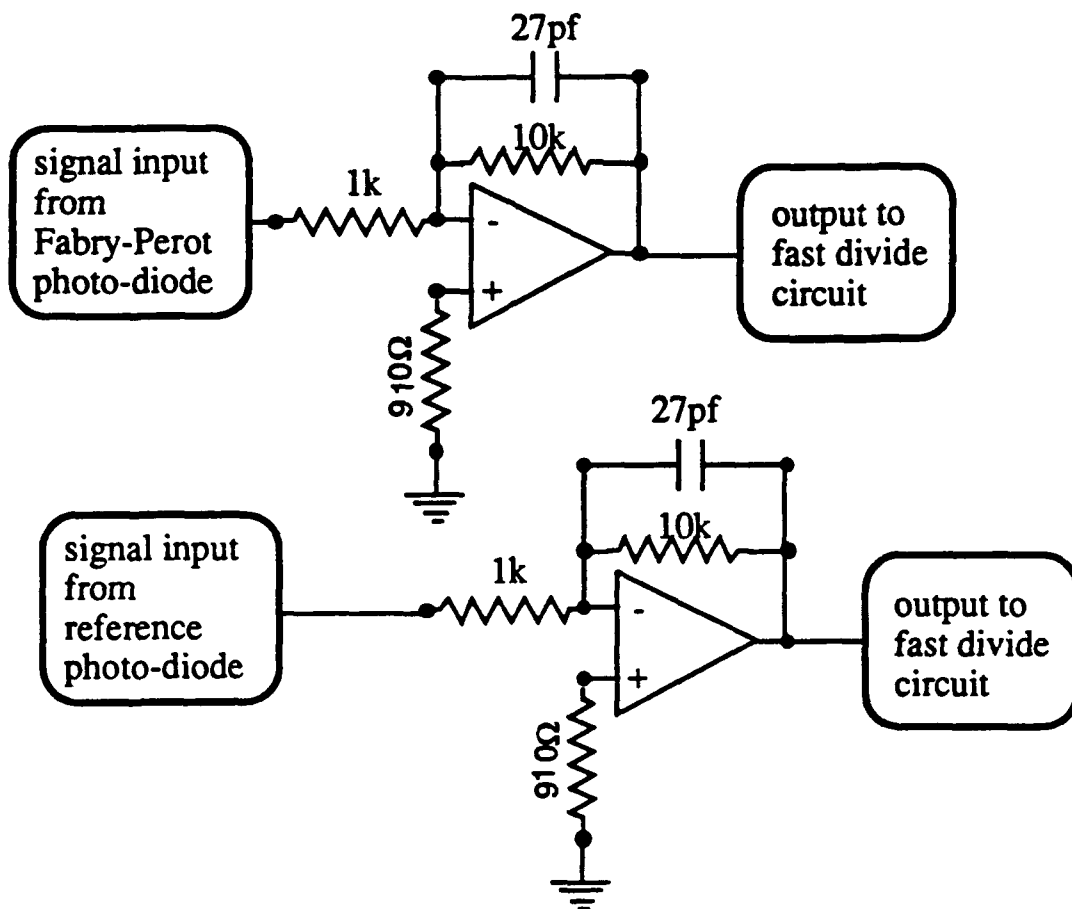
Fig. 2.8 Circuit diagram of the input amplifiers in the frequency-stabilization circuit. Two Motorola 356 op-amps are employed. Each amplifier provides a 10X amplification with a bandwidth of over 1MHz. The input signals come directly from the detectors used in the intensity and frequency measurements of the laser beam. The amplified signals from these amplifiers are fed into the fast-divide circuit.
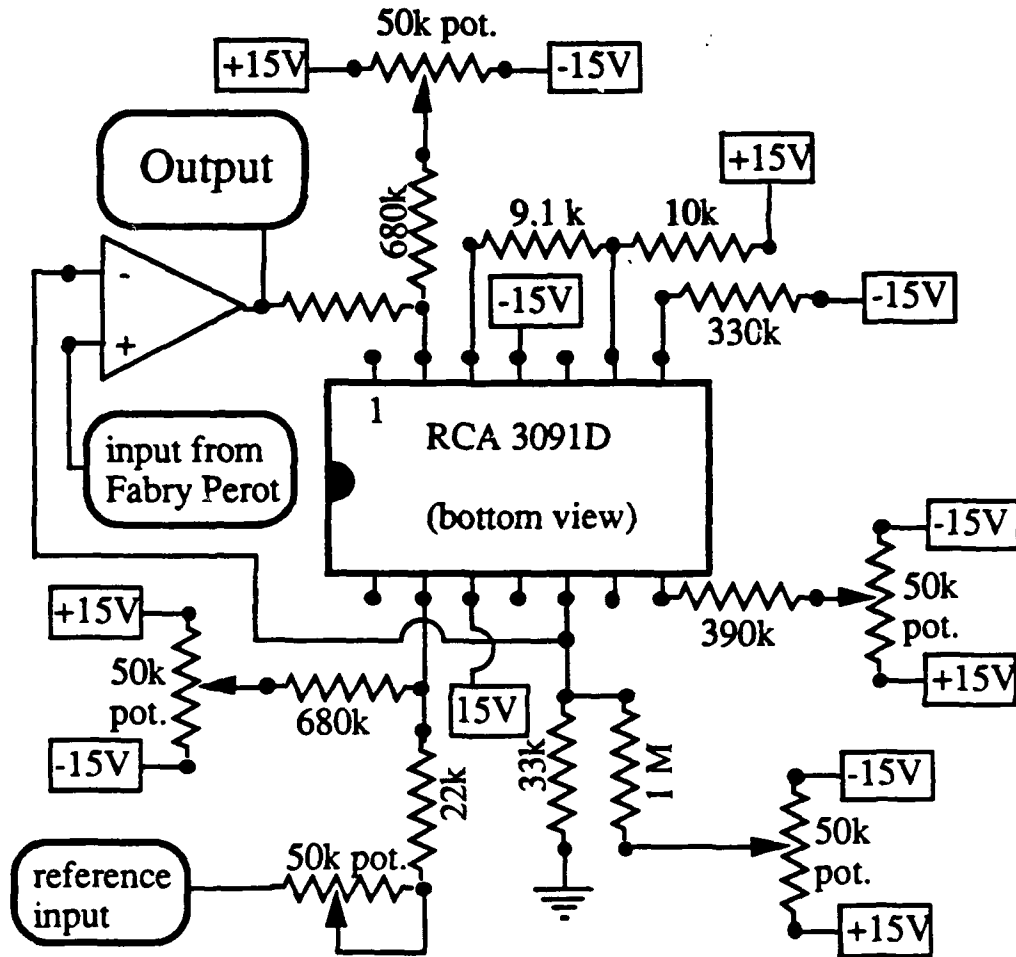
Fig. 2.9 Schematic of the fast-divide chip circuit. Shown is the circuit diagram for the RCA 3091D fast-divide chip and associated circuitry. The circuit takes inputs from the input amplifiers for the reference intensity and the Fabry Perot transmitted intensity. The output signal is proportional to the Fabry Perot signal divided by the reference intensity. This output signal goes to the crossover circuit. The op-amp shown is a Motorola 356 op-amp.
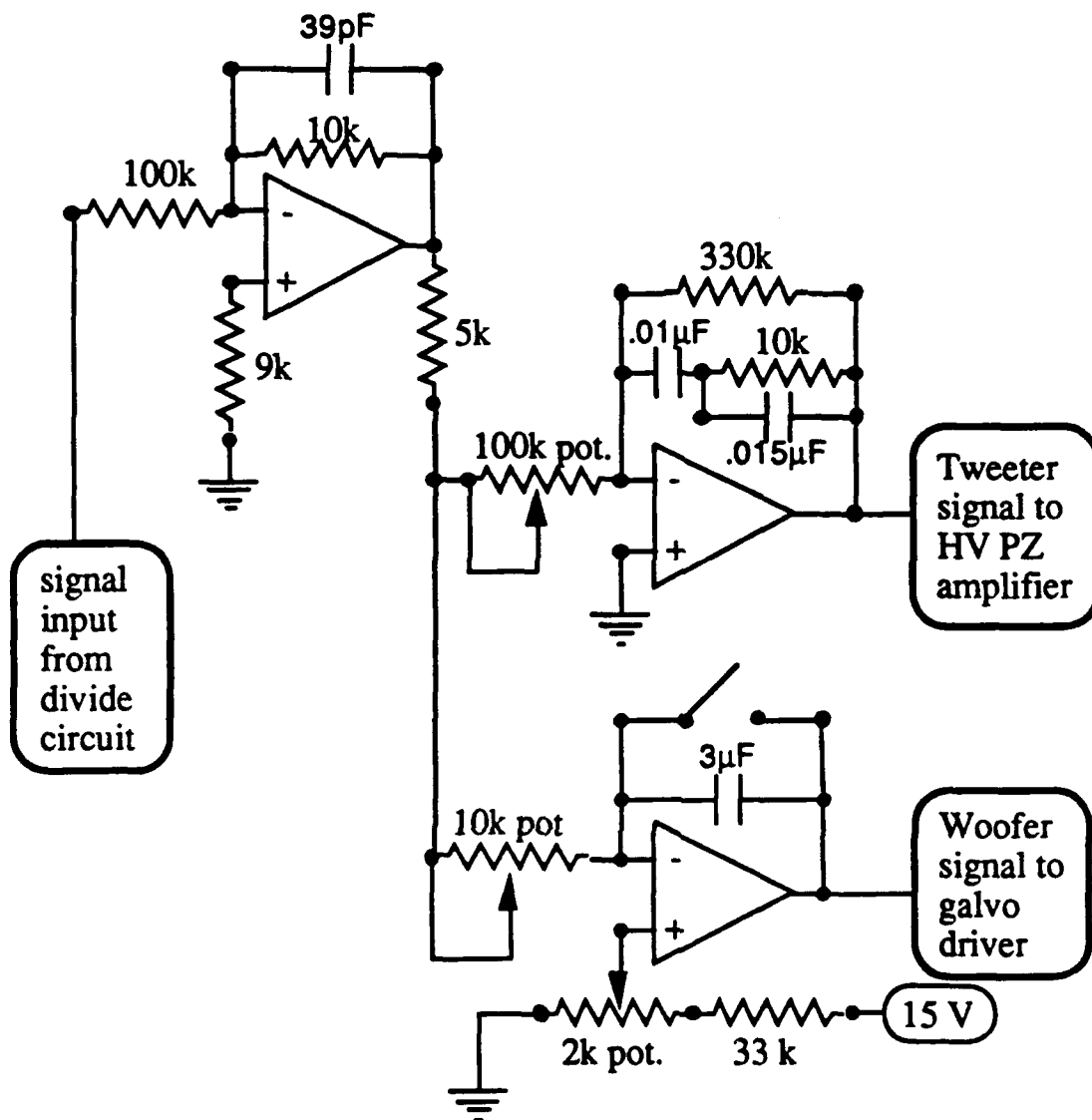
Fig. 2.10 The cross-over network for the laser frequency stabilization circuit. This circuit takes the error signal from the output of the fast-divide circuit and amplifies it for proper signal strength and bandwidth for the woofer and the tweeter drivers. The tweeter circuit is designed for high gain-bandwidth product at low frequencies as well as maximum bandwidth. Then woofer amplifier performs and integration of the error signal. All op-amps are Motorola 356 op-amps.

gain roll-off points ocurring at two different frequencies. The high frequency gain roll-off is designed to provide unity gain at the 90-degree phase error point. The lower frequency RC constant is designed to allow greater gain at the lower frequencies to provide greater stability at these lower frequencies than a mere factor of two above unity gain (characteristic of a simple RC roll-off). The 330k resistor is used to top off the low frequency gain to prevent runaway integration of voltage at extremely low frequencies. The tweeter signal is fed into a Trek 601-2 high-voltage op-amp which provides a voltage gain of 100 to drive the tweeter piezoelectric crystal on which is mounted one of the cavity mirrors. An additional RC compensation circuit is placed in parallel with the piezoelectric crystal in order to pull the apparent impedance seen by the Trek amplifier into the first quadrant of the phase plane and maintain a phase error of less than 90 degrees out to 5 kHz.

A diagram of the woofer driving circuit is shown in Fig. 2.10. The signal for the woofer is integrated about a voltage value set by the user. The woofer acts not only as a low-frequency correction device but it also integrates any DC charge off of the tweeter circuit so the piezoelectric crystal always operates in the center of its dynamic range. The woofer signal is sent to a galvo circuit which rotates a glass flat in the cavity oriented at brewsters angle to minimize loss and etaloning effects. The procedure for locking the laser is to first stabilize the laser with the feedback in the woofer circuit shorted. This is accomplished by tuning the Fabry-Perot reference cavity around until locking occurs. Then the woofer circuit is activated by opening the short.

2. The atomic beam system

In this section I describe the atomic beam apparatus which we constructed

for this experiment and other experiments involving the gathering of scattered light from an atomic beam. The system features a large F-number for efficient collection of scattered radiation from the interaction region. Windows of 1.5 inch clear aperture are situated at 2.5 inches from the beam on three sides. A diagram of the system is shown in Fig. 2.11. The atomic beam axis points vertically through a portable table with a steel top. The steel top on this table allows convenient clamping for optical mounts on magnetic bases.

The system was designed to isolate the optical interaction region from the alkali cloud usually associated with the oven chamber of an atomic beam system. The relatively dirty oven chamber is pumped by a diffusion pump. A liquid nitrogen cold trap is used to condense the alkali gas before it reaches the diffusion pump. During operation of the atomic beam the only connection between the the oven chamber and the interaction region is through the uppermost pinhole. During periods when the oven is filled with alkali but it is not being used, the diffusion pump can be valved off from the oven and turned off. The turbo-molecular pump (Balzers TPU 170) which pumps the optical interaction region can now be used to pump the cool oven chamber as well as the interaction region. This is accomplished by opening a ball valve which separates the two high vacuum regions during operation of the atomic beam. During operation of the beam, the turbo pump is used to pump the interaction region since turbo pumps are intrinsically cleaner than diffusion pumps. A cold finger at the top of the interaction region is filled with liquid nitrogen during beam operation to collect the atoms after they pass through the interaction region. This helps to keep the optical interaction region clear of an atomic cloud. Both the diffusion pump and the turbo pump are rough-pumped by the same mechanical floor pump.
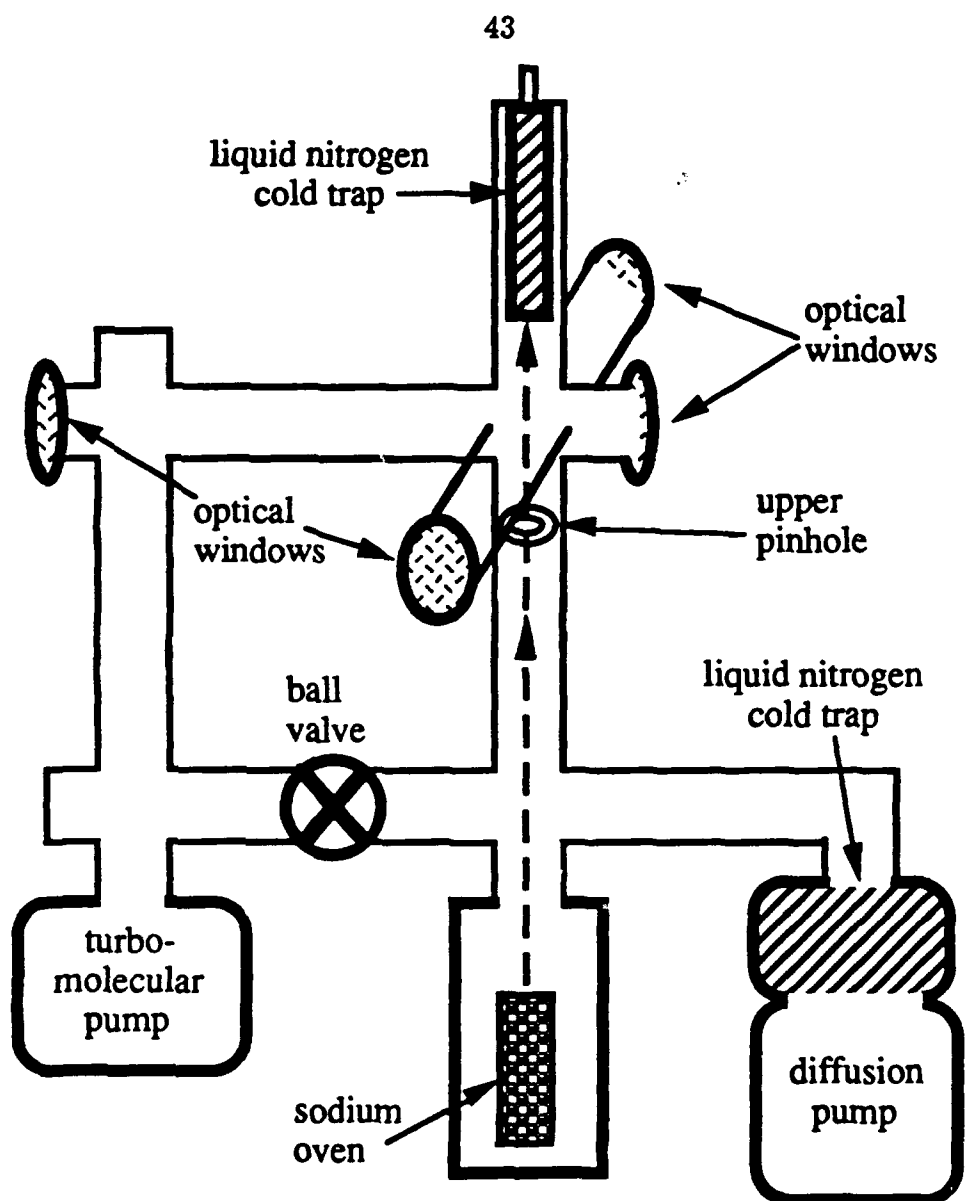
Fig. 2.11 The atomic beam system. The beam of sodium atoms runs vertically originating from a pinhole in the top of the sodium oven and defined by a second pinhole beneath the interaction region. The interaction region is isolated from the oven portion of the vacuum system by a ball valve and the upper pinhole. A diffusion pump is used to pump the oven portion of the va⋯ ⋮n system. A Balzers turbo-molecular pump is used to pump the interaction region portion of the vacuum system. Four windows allow optical access to the interaction region.

A $400\mu m$ pinhole is sealed to the top of the oven and a second $400\mu m$ pinhole is spaced approximately 25 cm above the oven to define an atomic beam with an angular divergence of about 1.5 milliradians. This angular divergence allows roughly 2 MHz of Doppler broadening of the atomic transition frequency. The oven is heated by two separate electrical cartridge heaters which are fastened to the side of the oven. When the beam is started the upper heater is turned on first in order to evaporate any alkali metal which may have deposited onto the pinhole of the oven during the last cool-down. Once the upper part of the oven reaches the proper temperature the lower heater is powered in parallel with the upper heater. The oven is fastened at its base through a ceramic spacer to the base of the oven chamber. Therefore, the lower part of the oven maintains a lower temperature than the pinhole since heat is removed through the bottom of the oven by slow conduction. The pinhole on the oven chamber must always be the hottest part of the oven to prevent its clogging. When the system is to be cooled the lower heater is unplugged first to allow the alkali to condense away from the pinhole on the bottom half of the oven away from the pinhole.

3. The experimental setup

The experimental apparatus that we used to study the rate of absorption of the 100% AM field is shown in Fig. 2.12. The absorption is determined by measuring the total fluorescent intensity from a small portion of the interaction region. A lens is used to image the fluorescence from the interaction region onto a pinhole placed in front of a photomultiplier tube. The pinhole is used to filter the fluorescence signal to that originating from a small volume in the center of the interation region where the intensity of the excitation is constant to within 20%. By spatially filtering the image of the interaction region we can

study atoms with nearly equal Rabi frequencies. The detectors are dc-coupled to measure the time-averaged fluorescence.

Atomic sodium was chosen as the atomic medium because it has a large oscillator strength and is readily made into a two-level atomic system. To obtain a two-level atomic system we resonantly excited the $3s - 3p$ transition with circularly polarized light. A two-level system results from the pumping of the population into the aligned magnetic sublevels.[31] The atomic beam is collimated to provide a divergence angle of 1.5 mrad with an associated Doppler width of less than 2 MHz [this is 20% of the natural linewidth (FWHM) of the sodium transition]. The atoms were excited by a circularly polarized laser beam whose angular divergence was less than 1 mrad (this angular divergence provides for no more than 1-MHz Doppler broadening). The laser beam is the output of a frequency stabilized Rhodamine 6G dye laser whose full-width jitter is less than 1 MHz (see section D1 for details). The combined broadening mechanisms listed above account for a total systematic frequency broadening of less than 4 MHz, or 40% of the natural linewidth (FWHM). This systematic linewidth is verified by measuring the full spectral width of the atomic transition to be 14 MHz [the natural linewidth is 10 MHz (FWHM)].

We produced a 100% AM laser field with a modulation frequency, $\delta\omega/2\pi$, of no less than 15 MHz, which is three times the polarization relaxation rate of the sodium D_2 line. The modulated field was produced using a method recommended to us by S. Ezekiel.[31] The laser beam is passed through a high efficiency acousto-optic modulator operating in the cw diffraction mode. A portion of the beam was upshifted by the drive frequency of the acousto-optic modulator (AOM). The diffraction efficiency is adjusted so the intensity diffracted into the first-order beam is equal to that remaining in the zeroth-order undiffracted

Fig. 2.12 Experimental apparatus. The following labeling convention is used in this figure: SDL- stabilized dye laser; AOM- acousto-optic modulator; M- mirrors; BS- beam splitter; LP- linear polarizers; EOM-electro-optic modulator; λ/4- quarter wave plate; Na- sodium oven; PH- pinhole; PMT- photmultiplier tube; PD-photdiode. The 100% AM field is created by recombining the zeroth and the first-order diffracted beams from the AOM. The EOM is used to control the intensity of the field. Circularly polarized light is used to maintain the atoms in a two-level system.

beam. The diffraction efficiency of the AOM is adjusted by varying the amount of rf power supplied to the AOM crystal. The bichromatic field is created by recombining the first-order diffracted beam with the zeroth-order (undiffracted) beam. The two beams are aligned with interferometric precision so that a strong beat note at the AOM drive frequency can be clearly detected by a fast photodiode measuring the far-field intensity. After recombination, the field state can be described in terms of a carrier, at the mean frequency of the two frequency components, that is 100% AM modulated at one half the drive frequency of the AOM. Because the recombination geometry is different for each modulation frequency, it was inconvenient to vary the modulation frequency in search of the resonances. Instead, we held the modulation frequency fixed and varied the Rabi frequency by sweeping the intensity of the laser. This was done with a set of linear polarizers and an electro-optic cell driven by our computer.

At each power setting we recorded the incident laser intensity along with the intensity of the fluorescence emitted by the atoms. Each data point was averaged 100 times over several milliseconds to integrate out any fast intensity fluctuations of the laser field. All data were recorded with a 12-bit analog-to-digital converter on a PDP-11/23 micromputer. The 36-dB dynamic range provided by the digitization is necessary to match the dynamic range of the data.

E. Experimental results

1. DC fluorescence signal

We collected data for the AM excitation for several different modulation frequencies and several different detunings for each modulation frequency. In this section I will present this data in raw form and with theoretical fits. I show

the effects of detuning on the resonances. Also I will show a figure which reveals the behavior of the extrema in the response of the fluorescence for different detunings and excitation strengths.

In Fig. 2.13 I have plotted the data in raw form (fluorescence signal versus intensity) together with the best theoretical fit to this data. The theory has been modified to account for slight experimental complications such as intensity averaging over the Gaussian laser beam profile and a mismatch in the intensity of the two frequency components. The data is plotted versus the time-averaged dimensionless intensity $2I_1$. The squares in Fig. 2.13 represent the data taken with a dimensionless modulation frequency $\delta\omega T_2 = 5$. for resonant excitation $\Delta T_2 = 0$. The solid line represents the best theoretical fit with 20% intensity averaging and a 25% mismatch in the intensity of the bichromatic field components. The mismatch in the intensity of the field components can be due to imperfections in the AOM or in the alignment of the two frequencies at the atomic beam. The effects of Doppler broadening are probably present as well but I have not included them in the fit.

We also collected data at a 40 MHz AOM drive frequency which corresponds to $\delta\omega T_2 = 4$. At this modulation frequency we took data for 4 values of detuning: $\Delta T_2 = 0.0$; $\Delta T_2 = 2.0$; $\Delta T_2 = 4.0$; $\Delta T_2 = 6.0$. Data is shown at each of these detunings in Figs. 2.14(a-d). In each figure I plot the raw data together with the unmassaged theory for the same parameters. The x-axis of each graph is the square-root of the time-average of the squared Rabi frequency [ie. the root-mean-square (RMS) Rabi frequency]. I attribute the mismatch in the position of the first extrema of the data and theory to the Doppler and intensity averaging which were present in the experiment but not in the theoretical plots shown here. These experimental complications also explain the mismatch in the depth
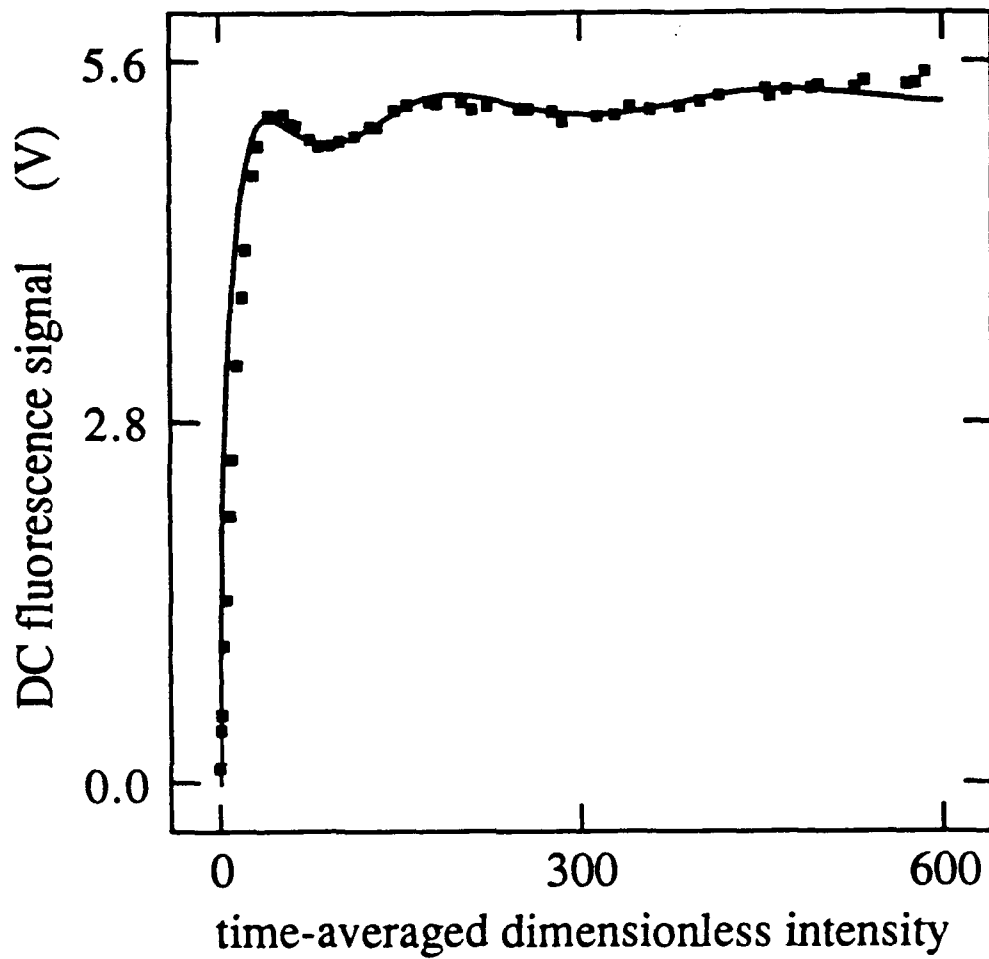
Fig. 2.13   The time-averaged fluorescence signal versus the time-averaged dimensionless intensity. The time-averaged fluorescence signal collected from atoms in the atomic beam excited by a 100% AM modulated field is plotted versus the time-averaged dimensionless intensity of the excitation. Data (squares) is shown for a modulation frequency of $\delta\omega T_2 = 5.0$. The solid line is the best theoretical fit to the data after intensity averaging and inhomogeneities in the excitation are taken into account.

of the resonances. From Figs. 2.14(a-d) it is apparent that the effect of detuning is to cause the resonances to occur at a smaller value of the Rabi frequency than for resonant excitation. This indicates that the generalized Rabi frequency is involved in the occurrence of the parametric resonances.

In Fig. 2.15 I have plotted the parameters corresponding to the first three local extrema of data similar to those shown in Fig. 2.14. Plotted is the RMS Rabi frequency versus the detuning for the first three local maxima (squares) and for the first three local minima (circles) for the fluorescence versus Rabi frequency curves for $\delta\omega T_2 = 4.0$ and three different values of detuning: $\Delta T_2 = 0.0, 2.0, 4.0$. As the detuning increases the theory predicts that the corresponding extrema (ie. 1st maximum and 1st minimum) will coalesce. This effect is shown in Fig. 2.15 for the first extrema. The data corresponding to the first extrema seems to lie on a narrower contour than the theory predicts. I attribute this effect to Doppler averaging and intensity smearing present in the experiment. Except for this effect, the data and theory shown in Fig. 2.15 agree.

2. Derivative of the fluorescent response

Until this point we have concentrated on the total time-averaged intensity emitted via fluorescence from the interaction region. However, measuring the total fluorescence as a function of excitation strength is a background-limited detection process. The reason for this is that the resonances lie on a saturation curve which is at least an order of magnitude larger than the depth of the resonance structure. Our interest in signal-limited detection schemes has led us to devise a method to observe the resonances of modulation without the saturation curve as a background.

If we take a derivative of the saturated response curve, the modulation-
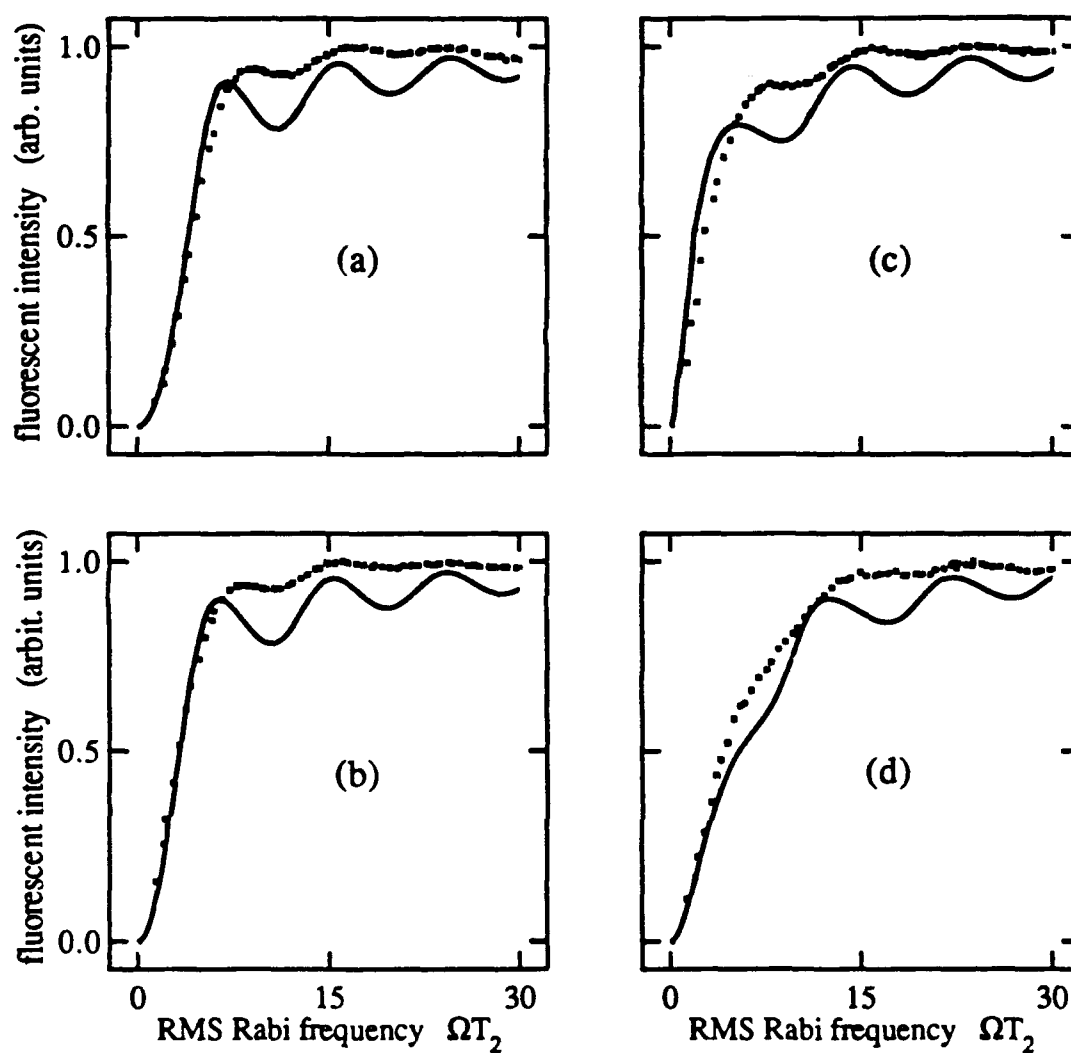
Fig. 2.14 Fluorescent intensity versus the dimensionless RMS Rabi frequency. Data and theory are shown for a dimensionless modulation frequency $\delta\omega T_2 = 4.0$ and four dimensionless detunings: (a) $\Delta T_2 = 0.0$; (b) $\Delta T_2 = 2.0$; (c) $\Delta T_2 = 4.0$; and (d) $\Delta T_2 = 6.0$. The squares represents the data and the solid lines represents the theory. Y-axes for the data and theory have been normalized to unity.
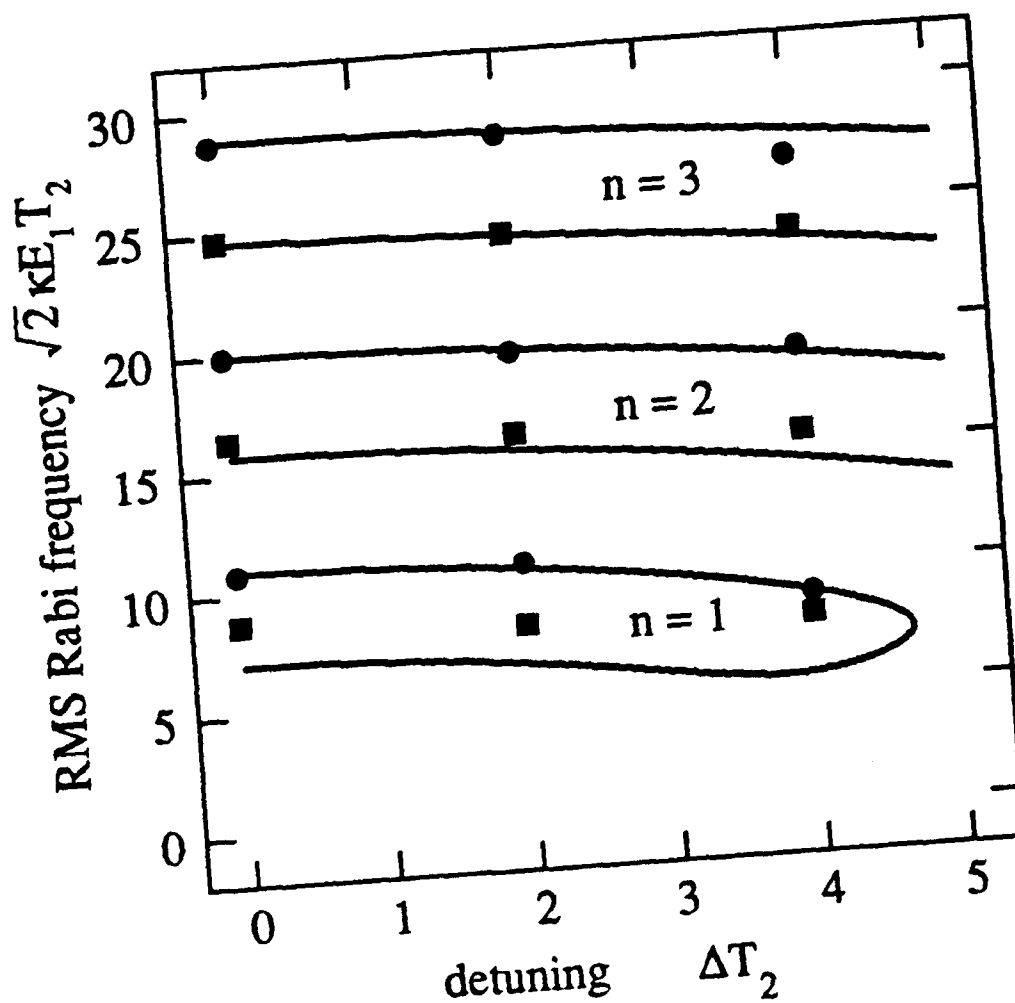
Fig. 2.15 The dimensionless root-mean-square (RMS) Rabi frequency versus the dimensionless detuning for the first three resonances. Plotted are the parameters corresponding to the first three extrema (n=1,2,3) in the fluorescence-versus-Rabi-frequency data (see Fig. 2.14) for three different detunings: $\Delta T_2 = 0.0$; $\Delta T_2 = 2.0$; and $\Delta T_2 = 4.0$. The squares correspond to the local maxima in the fluorescence data while the circles correspond to local minima in the data. The solid lines represent the theoretical positions for the extrema.

resonance extrema lie symmetric about zero signal. The derivative measurement is a signal-limited detection. However, numerically extracting a derivative from our previous data would be too noisy. Instead, we devised a method to directly record the derivative of the fluorescent response with respect to intensity. In Fig. 2.16 is a diagram of the experimental apparatus. This setup is similar to that shown in Fig. 2.12. We have added the AOM2 driven by a signal generator (Wavetek model 188 sweep/function generator), and a lock-in amplifier (EG&G PARC model 5210 dual-phase Lock-in Amplifier). The AOM2 provides a weak audio-frequency amplitude modulation to the excitation intensity. The signal generator provides the modulation signal at the audio modulation frequency to the AOM2 and the reference signal to the lock-in amplifier. In this experiment the signal from the PMT is fed into the lock-in amplifier. The lock-in amplifier reports the in-phase signal to the computer. The response curve of the fluorescent intensity to the 100% AM excitation acts as a transfer function to the weak modulation in the excitation intensity [see Fig. 2.1(b)]. The effect of all this is that the lock-in measurement is analogous to a derivative measurement. The signal from the lock-in amplifier is actually the derivative of the fluorescent response with respect to intensity.

The results of this experiment are plotted together with the theoretical predictions in Fig. 2.17(a-d). The derivatives were recorded for a modulation frequency of 22.5 MHz (ie. $\delta\omega T_2 = 4.5$). We recorded data for four values of the detuning. In Fig. 2.17(a) is shown data and theory for resonant excitation $\Delta T_2 = 0$. The first peak of the curve represents the rising edge of the response curve where the derivative is the largest. The falling edge of the derivative passes through zero at the first-harmonic resonance. The curve goes through its first minimum at the inflection point of the response curve. After this,
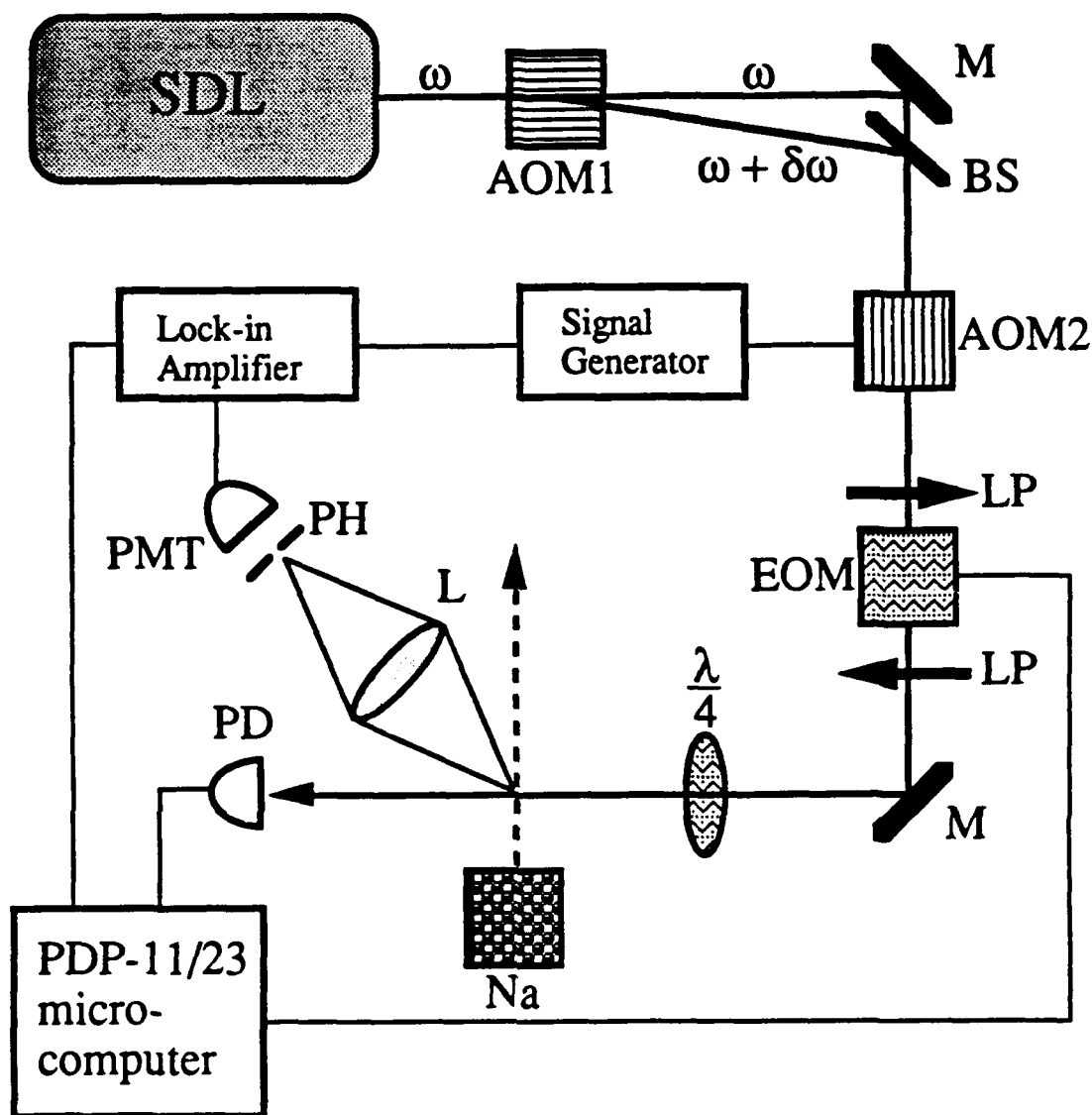
Fig. 2.16 Experimental apparatus for the derivative measurement. The AOM2 and the lock-in amplifier and signal generator are added to the apparatus shown in Fig. 2.12 in order to weakly modulate the excitation intens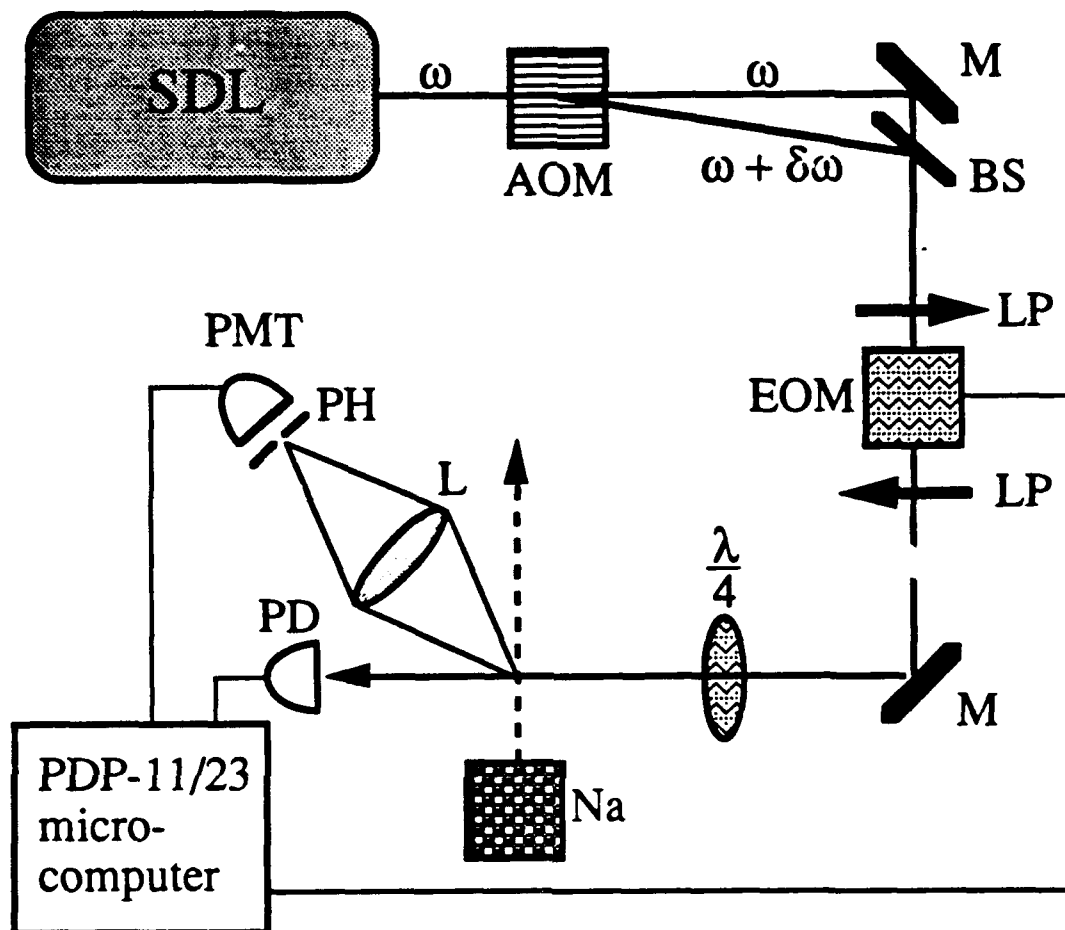ity. The following labeling convention is used in this figure: SDL- stabilized dye laser; AOM- acousto-optic modulator; M- mirrors; BS- beam splitter; LP- linear polarizers; EOM-electro-optic modulator; $\lambda/4$- quarter wave plate; Na- sodium oven; PH- pinhole; PMT- photmultiplier tube; PD- photodiode.

the derivative passes through zero again at the first minimum of the response function. Whenever the derivative signal crosses zero from the positive side a subharmonic resonance is encountered. Whenever the derivative crosses zero from the negative side an anti-resonance is encountered.

In Figs. 2.17(b-d) I plot the derivative signals for detuned excitation. I plot signals for $\Delta T_2 = 2$. in Fig. 2.17(b). In this figure it is barely apparent that the position of the resonances are moving toward lower intensity. In Fig. 2.17(c) I plot the derivative for $\Delta T_2 = 4$. At this detuning it is obvious that the positions of the resonances occur for smaller values of intensity than they did for resonant excitation as shown in Fig. 2.17(a). Also, the first minimum in the derivative has moved toward the zero value on the y-axis. This means that the zero crossings of the derivative for the first resonance and anti-resonance are beginning to coalesce. Finally in Fig. 2.17(d) the first resonance is gone since the derivative does not cross zero. The first minima and maxima of the fluorescent response are now no more than an inflection point. I will emphasize that the theoretical curves plotted here are unmassaged. Experimental complications such as Doppler averaging and intensity averaging lead to any discrepancies between theory and data.

F. Harmonic and pulsed excitation of a two-level atom

In this section I hope to provide further physical insight into the modulation problem by making an analogy between modulated excitation and pulsed excitation. In this section I will discuss the physics of the modulated interaction with pulsed excitation in mind. I will treat the 100% AM interaction as a sinusoidal pulse interaction. I present this discussion as both an explanation of the physics of these interactions and a motivation for future work in this area.
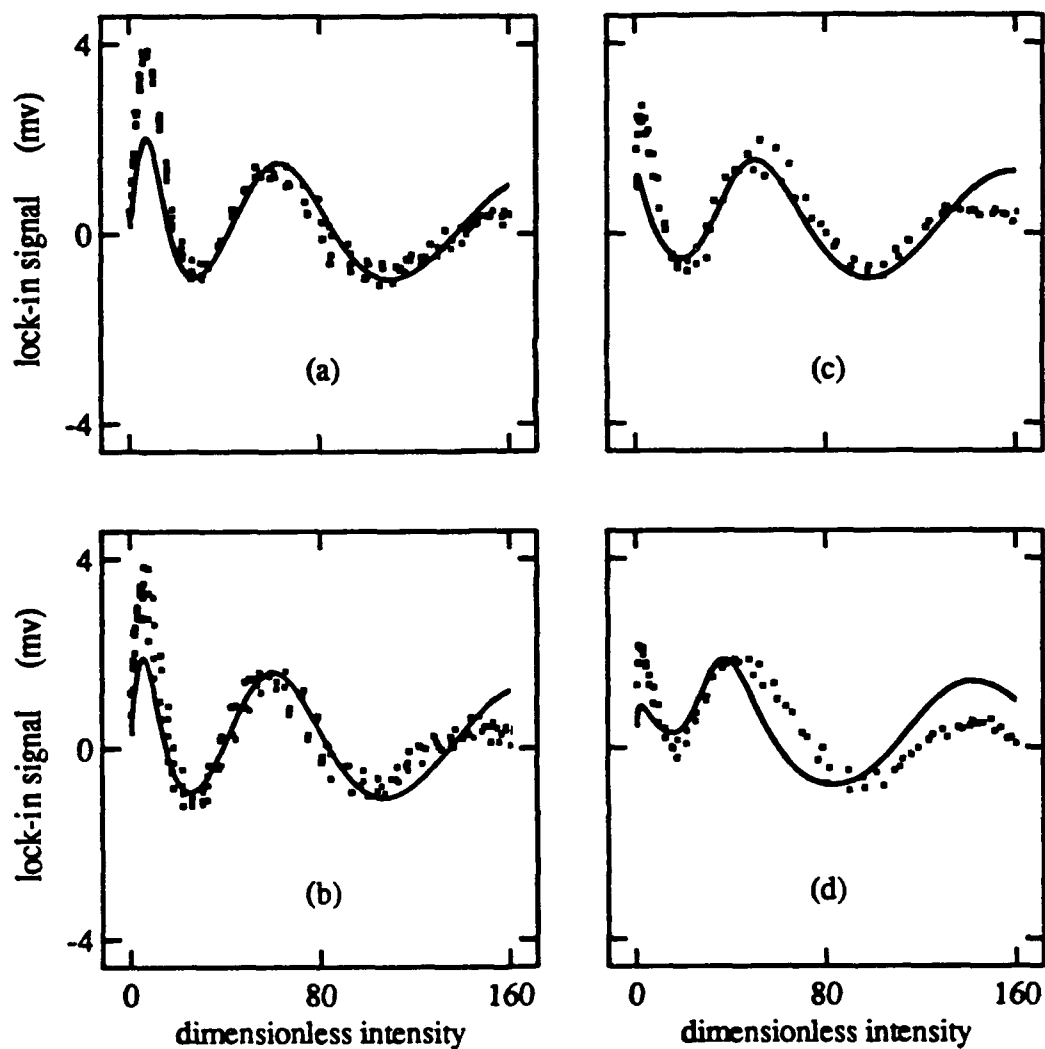
Fig. 2.17 Derivative of the fluorescent response of a two-level atom to 100% AM excitation versus the dimensionless intensity. The signal from the lockin is plotted versus the excitation intensity for a dimensionless modulation frequency $\delta\omega T_2 = 4.5$ and four values of the dimensionless detuning: (a) $\Delta T_2 = 0.0$; (b) $\Delta T_2 = 2.0$; (c) $\Delta T_2 = 4.0$; (d) $\Delta T_2 = 6.0$. For weak modulation, the first-harmonic signal reported by the lock-in amplifier is the derivative of the response curve.

To motivate the analogy between the 100% AM interaction and pulsed interactions I have plotted the time-averaged excited-state population versus excitation strength for a series of harmonic excitations of the form

$$E(t) = E_0 \left(1 + \sum_{n=1}^{N} 2cos(n\delta\omega t) \right), \tag{2.11}$$

for several values of the number of harmonics N. In Fig. 2.18 the excited-state population versus the excitation strength κE_0 for excitation consisting of 0, 2, 5, 7, 10, and 20 harmonics of the modulation fundamental $\delta\omega$. As the number of harmonics increase the depth of the modulation in the response of the excited-state population versus excitation strength increases. As the number of harmonics gets larger the response curve begins to look sinusoidal. This type of response is characteristic of pulsed interactions. To demonstrate this effect I have plotted the excited-state population versus pulse area for an ideal (infinitesimally short pulses) pulse train incident on an ensemble of two-level atoms. In Fig. 2.19 I have plotted the excited-state population versus pulse area for several different pulse repetition rates. In the limit of large repetition rate the response of the population is a sinusoidally varying function of the pulse area. Also, whenever the pulse area is a multiple of 2π the time-averaged population in the excited-state is zero. With this in mind I will now consider the interaction of a 100% AM field with two-level atoms.

To further the analogy between the bichromatic interaction and pulsed interactions I will calculate the area of a sinusoidal pulse. In Fig. 2.20 is a plot of the sinusoidally varying Rabi frequency in the rotating frame for a resonant 100% AM field. The indicated area A is the "pulse" area I will calculate. The area is

$$A = \int_0^{\frac{\pi}{\delta\omega}} 2\kappa E sin(\delta\omega t) \, dt = \frac{4\kappa E}{\delta\omega}. \tag{2.12}$$
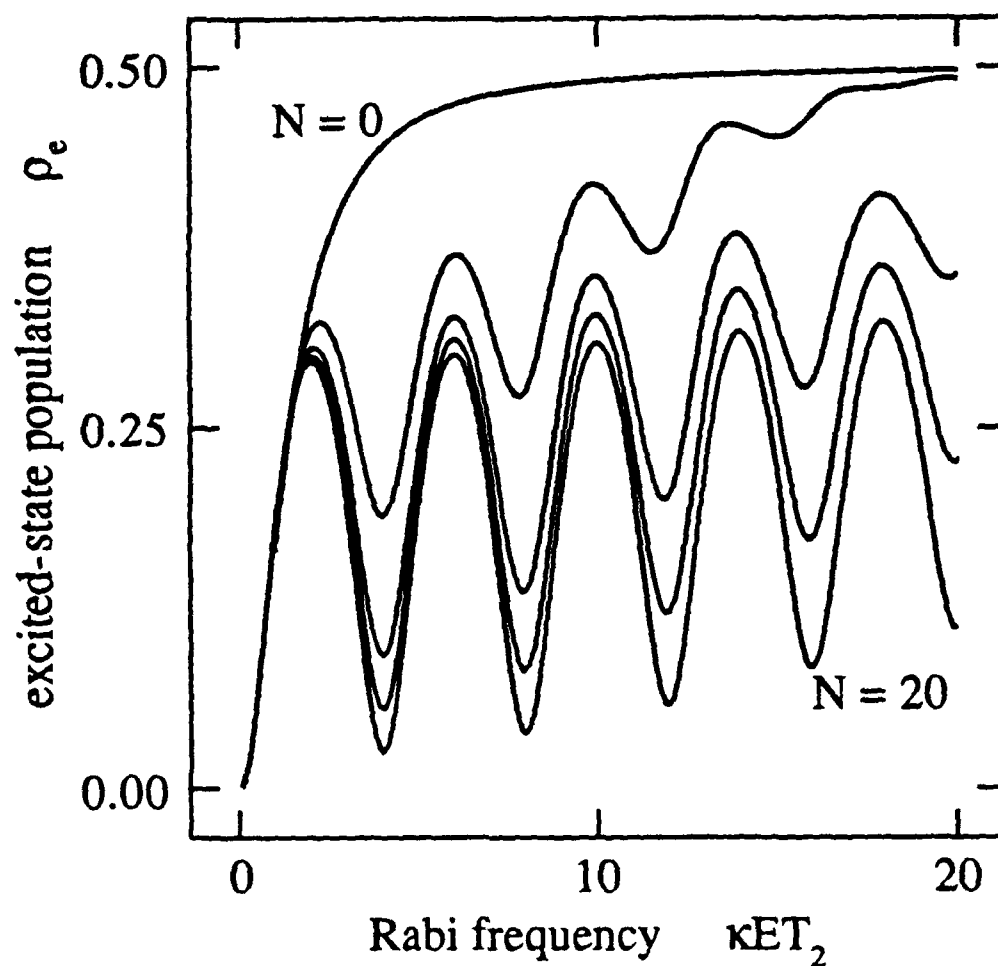
Fig. 2.18 DC or time-averaged excited-state population versus Rabi frequency kET_2. The response of the excited-state population to harmonic excitation containing different numbers of harmonics is plotted. The excited-state population is plotted for $\delta\omega T_2 = 4.0$. The calculations shown are for the number of harmonics $N = 0, 2, 5, 9,$ and 20.
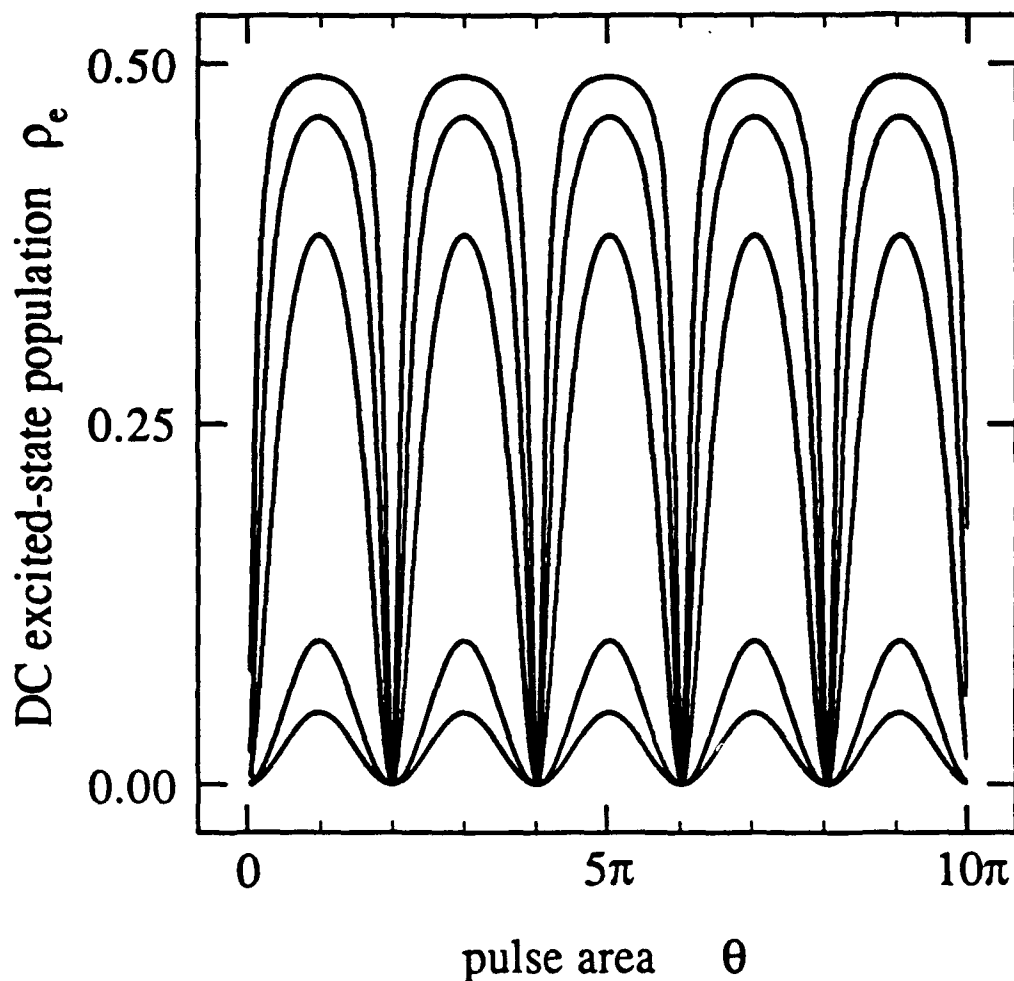
Fig. 2.19 The DC or time-averaged excited-state population versus the pulse area θ. The response of a two-level atom to a train of infinitessimally short pulses is shown. The curves shown are (from bottom to top) for a pulse repetition rate of RT_2 = 0.1, 0.2, 1.0, 2.0, 4.0. As the repetition rate is increases the depth of the modulation in the response becomes deeper. Each curve goes to zero for pulse area of 2π multiples.
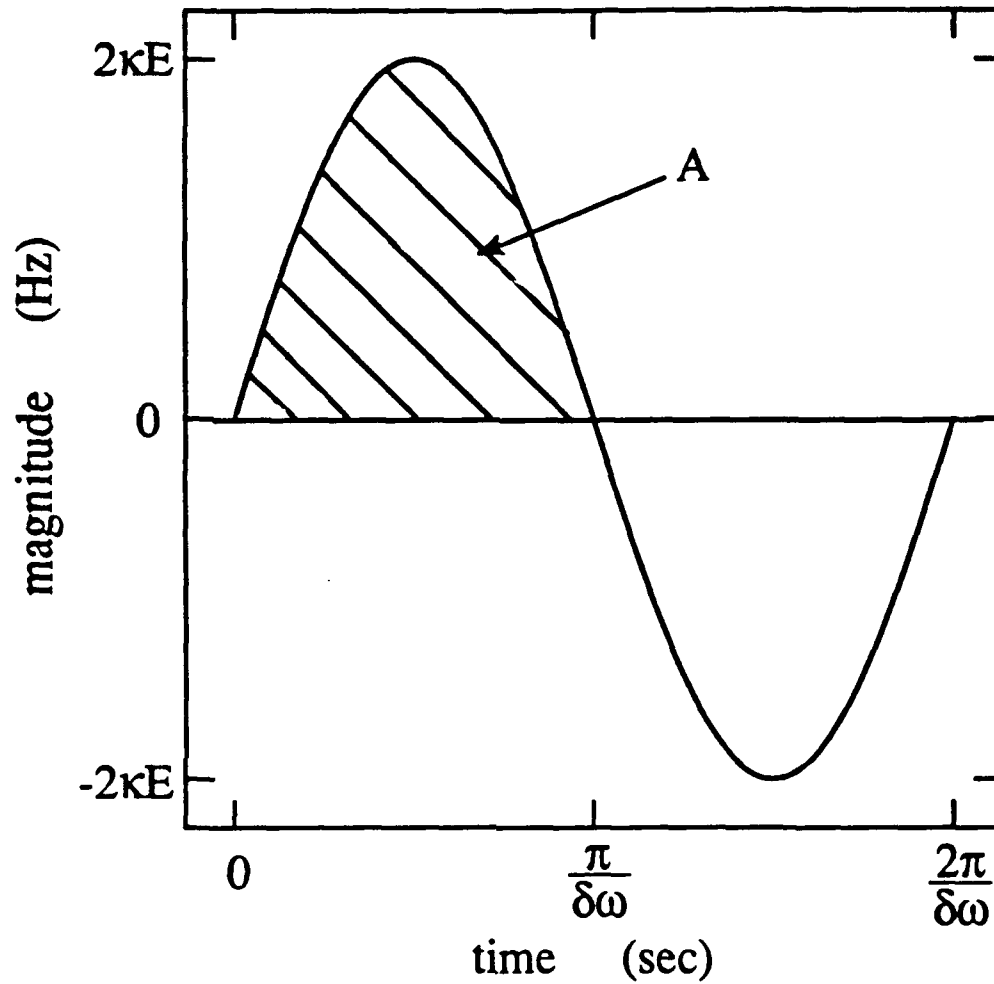
Fig. 2.20 Magnitude of a sine-wave versus time. The function $2\kappa E \sin(\delta \omega t)$ is plotted versus time. The area under the first maximum is highlighted. This area is $A = 4\kappa E/\delta \omega$.

I have already indicated in section B of this chapter that the resonances occur whenever the Bessel function $J_0\left(\frac{2\kappa E}{\delta\omega}\right)$ is equal to zero. For large arguments the zeros of $J_0(x)$ are equally spaced such that

$$x = \frac{\pi}{4} + n\pi. \tag{2.13}$$

We can use the expression for the area of the sinusoidal pulse [Eq. (2.12)] and Eq. (2.13) to arrive at an expression for the sinusoidal pulse area corresponding to the resonances of the 100% interaction

$$A = \frac{\pi}{2} + n2\pi. \tag{2.14}$$

The resonances occur whenever the area indicated in Fig. 2.20 is increased by a multiple of 2π. This behavior is reminiscent of the response of the atoms to the ideal pulsed excitation in Fig. 2.19.

G. Conclusion

I have presented both theory and experiment for the absorption of a 100% AM field by a closed two-level atomic system. The interaction reveals resonances at subharmonic multiples of the Rabi frequency. We observed the first three subharmonic resonances with resonant and detuned excitation. In this chapter I have presented an experimental, theoretical, and numerical study of these subharmonic resonances. I have discussed both the time-averaged and the harmonic responses of the atoms to the modulated excitations.

The data presented in section E of this chapter shows the saturated absorption of the 100% AM optical excitation. The subharmonic resonances appear as enhancements and reductions of the fluorescent intensity over the usual single-field fluorescent response as a function of excitation intensity. In calculating the

theoretical fits I have accounted for experimental complications such as intensity averaging and imperfect modulation conditions. The data is well fit by this type of theory. I have also analyzed the extrema in the response of the fluorescence. A plot is constructed showing the parameters corresponding to each extrema for different detunings and excitation strength. The parameters corresponding to the extrema from the data are compared with the theoretical predictions. Again, the agreement between experiment and theory is good.

In section C I have considered the dynamic behavior of the atomic variables. The phase plots of the polarization versus the inversion show that the trajectory takes on an additional pair of cycles at each resonance. This conclusion has been substantiated by histogram plots. The histograms contain characteristic harmonic peaks. An additional pair of harmonic peaks occurs at each resonance in the absorption. The atomic trajectory oscillates in period n fashion where n is the number of the subharmonic resonance.

The data presented in this chapter shows that the amplitude of the absorption of the bichromatic field is enhanced at the first-order resonance and at each of the subharmonic resonances. This result differs from that obtained by Thomann.[12] The results of that experiment showed a decrease in the absorption at each resonance. In that experiment the field-modulation index was no larger than 0.65, so there was always a significant field component at the carrier frequency. When the carrier frequency is present, it can beat with each of the modulation sidebands to produce overtones, at harmonics of the modulation frequency, in the atomic response. This beat frequency is one half of the beat frequency arising from the interference between the two modulation sidebands. The harmonic overtones of these two sets of beat notes can destructively interfere in a three-field experiment. This interference causes the absorption to

diminish at each resonance.

I have presented a signal limited detection scheme for observing the subharmonic resonances. In the second part of the section containing experimental results I demonstrated that by using lock-in detection and a weakly modulated excitation intensity the derivative of the response of the fluorescent intensity to the bichromatic fields can be measured. The theory and experiment agree quite well using this superior detection scheme. Thomann[12] used lock-in detection in his experiment to measure the difference between modulated (three-field) and single-field excitation. Employing the technique used by Thomann in the three field experiment would not have been possible in our two field experiment. However, both techniques get around the errors encountered in measuring the resonances on top of the saturation curve.

I have also shown that the interaction of a 100% AM field is comparable to an interaction involving a pulse train. The subharmonic resonances occur whenever the area under the sinusoidal pulse in the 100% interaction is increased by 2π. This type of behavior is similar to pulsed interactions in which the dynamics repeat themselves for pulses whose areas are multiples of 2π.

I have demonstrated the complicated behavior of a purely bichromatic field interacting with a closed two-level atomic system. Subharmonic resonances occur because of the coherent nonlinear interaction of a multifrequency field with an isolated atomic resonance. It is exactly this type of nonlinear interaction that determines the competition or cooperation between cavity modes in a laser gain medium. The same set of subharmonic resonances occurs in a saturated two-level amplifier interacting with a modulated laser field. This provides a possible mechanism for multimode instabilities in homogeneously broadened lasers.

References

1. B.R. Mollow, "Stimulated emission and absorption near resonance for driven systems," Phys. Rev. A **5**, 2217-2222 (1972).

2. S. Haroche and F. Hartmann, "Theory of saturated absorption line shapes," Phys. Rev. A **6**, 1280-1300 (1972).

3. F.Y. Wu, S. Ezekiel, M. Dulcoy, and B.R. Mollow, "Observation of amplification in a strongly driven two-level atomic system at optical frequencies," Phys. Rev. Lett. **38**, 1077-1080 (1977).

4. M.T. Gruneisen, K.R. MacDonald, and R.W. Boyd, "Induced gain and modified absorption of a weak probe beam," J. Opt. Soc. Am. B **5**, 123-129 (1988).

5. R.W. Boyd, M.G. Raymer, P. Narum, and D.J. Harter, "Four-wave parametric interactions in a strongly diven two-level system," Phys. Rev. A **24**, 411-423 (1981).

6. D.J. Harter, P. Narum, M.G. Raymer, and R.W. Boyd, "Four-wave parameteric amplification of Rabi sidebands in sodium," Phys. Rev. Lett. **46**, 1192-1195 (1981).

7. D.J. Harter and R.W. Boyd, "Four-wave mixing enhanced by ac-Stark-split levels in self-trapped filaments of light," Phys. Rev. A **29**, 739-748 (1984).

8. L.W. Hillman, R.W. Boyd, and C.R. Stroud, Jr., "Natural modes for the analysis of optical bistability and laser instability," Opt. Lett. **7**, 426-428 (1982).

9. M.A. Kramer, R.W. Boyd, L.W. Hillman, and C.R. Stroud, Jr., J. Opt. Soc. Am. B **2**, "The propagation of modulated optical fields through saturable absorbing media: a general theory of modulation spectroscopy," 1444-1455 (1985).

10. A.M. Bonch-Breuvich, T.A. Vartanyan, and N.A. Chigir, "Subradiative structure in the absorption spectrum of a two-level system in a biharmonic radiation field," Sov. Phys. JETP **50**, 901-906 (1979).

11. P. Thomann, "Optical parametric resonances," J. Phys. B **9**, 2411-2419 (1976).

12. P. Thomann, "Optical resonances in strong modulated laser beam," J. Phys. B **13**, 1111-1124 (1980).

13. G.I. Toptygina and E.E. Fradkin, "Theory of subradiative absorption in the interaction between two intense waves in a nonlinear medium," Sov. Phys. JETP **55**, 246-251 (1982).

14. An. A. Mak, S.G. Przhibel'skii, and N.A. Chigir, "Nonlinear resonance phenomena in bichromatic fields," Ser. Fiz. **47**, 1976-1983 (1983).

15. G.S. Agarwal, and N. Nayak, "Multiphoton processes in two-level atoms in two intense pump beams," J. Opt. Soc. Am. B **1**, 164-169 (1984).

16. R.E. Silverans, G. Borghs, P. De Bisschp, and M. Van Hove, "Phase effects in bichromatic field interactions with two-level atom," Phys. Rev. Lett. **55**, 1070-1073 (1985).

17. J.H. Eberly and V.D. Popov, "Phase-dependent pump-probe line-shape formulas," Phys. Rev. A **37**, 2012-2016 (1988).

18. G.S. Agarwal, "Subharmonic Raman effect in nonlinear mixing," J. Opt. Soc. Am. **13**, 482-484 (1988).

19. G.S. Agarwal, "Generation of squeezed states of radiation at submultiple Rabi resonances," J. Opt. Soc. Am. B **5**, 180-183 (1988).

20. W.M. Ruyten, "Harmonic behavior of the multiple quantum resonances of a two-level atom driven by a fully-amplitude-modulated field," Phys. Rev. A, **40**, 1447-1455, (1989).
W.H. Ruyten, "Subharmonic resonances in terms of multiphoton processes and generalized Bloch-Siegert shifts," J. Opt. Soc. Am. B, **6**, 1796-1802 (1989).

21. B.J. Feldman and M.S. Feld, "Theory of high-intensity gas laser," Phys. Rev. A **1**, 1375-1396 (1970).

22. H. Risken and K. Nummedal, "Instability of off resonance modes in lasers," Phys. Lett. **26A**, 275-276 (1968).
H. Risken and K. Nummedal, "Self pulsing in laser," J.Appl Phys. **39**, 4662-4672 (1969).

23. R.G. Harrison, J.V. Moloney, J.S. Uppal, and W. Forysiak, "Analysis of instability and chaos in optically pumped three level lasers," **Instabilities and Chaos in Quantum Optics II**, (Plenum Press, New York, 1988).

24. L.W. Hillman, J. Krasinski, R.W. Boyd, and C.R. Stroud, Jr., "Observation of higher order dynamical states of a homogeneously broadened laser," Phys. Rev. Lett. **52**, 1605-1608 (1984).

25. L.W. Hillman, J. Krasinski, K. Koch, and C.R. Stroud, Jr., "Dynamics of homogeneously broadened lasers: higher-order bichromatic states," J. Opt. Soc. Am. B **2**, 211-217 (1985).

26. L.W. Hillman, "Interaction of modulated optical fields with saturable media and its application to laser instability," University of Rochester, Ph.D. Thesis (1984).

27. K.W. Koch III, "Dynamics and instabiliies in homogeneously broadened lasers," University of Rochester, Ph.D. Thesis (1989).

28. M. Citron "Study of a two-level system in sodium using laser optical pumping," University of Rochester, Ph.D. Thesis (1977).

29. S. Chakmakjian, K. Koch, L.W. Hillman, and C.R. Stroud, Jr. "Multi-mode instabilities of homogeneously broadened lasers," Optical Bistability III, (Springer-Verlag, N.Y. 1986).

30. M.Hercher "The spherical mirror Fabry-Perot interferometer," Appl. Opt. **7**, 951-966 (1968).

31. J.A. Abate, "Preparation of atomic sodium as a two-level atom," Opt. Commun. **10**, 269-272 (1974).

32. private communication with S. Ezekiel.

Chapter 3

A FOUR-LEVEL LASER AMPLIFIER
WITH AN AMPLITUDE MODULATED PUMP

A. Introduction

It has long been realized that population oscillations or pulsations play an important role in laser dynamics.[1-4] By population oscillations I mean the modulation that occurs in the atomic inversion of a laser gain medium. Population oscillations can occur at the laser's intermodal beat frequency and couple together different longitudinal cavity modes. This coupling is important in the onset of mode locking as well as in the occurrence of laser instabilities.[2,3]

Population oscillations have been studied in homogeneously broadened absorbers.[5-14] When a two-level absorber is driven by a strong saturating field as well as one or more weak probe fields, the rate of absorption of the probe fields depends on the probe-field detuning from the saturating field. At small probe-field detunings the absorption of the probe field is decreased producing an induced spectral hole in the homogeneous absorption spectrum.[5-14] This effect was first predicted by Schwartz and Tan.[5] They predicted that if a collisionally-

broadened (eg. $T_2 \ll T_1$) saturable absorbing media were driven by a strong resonant field and an additional weak probe field were applied, the weak probe field would experience diminished absorption if it were detuned from the strong field by an amount less than the population decay rate T_1^{-1}. Throughout this chapter this induced-gain feature will be referred to as the "$1/T_1$ hole." In a later work, Sargent et al.[6] extended this research to show that weak amplitude modulation (AM) could be applied to the saturating field and the absorption spectrum of the AM sidebands would exhibit the same spectral hole at zero modulation frequency. Furthermore, Sargent et al.[6] showed that the spectral width of the hole in the absorption spectrum of the modulation sidebands broadens proportionally to the dimensionless intensity of the saturating field. The work I report on in this chapter is a direct extension of these early works[5,6] and of more recent research performed at The Institute of Optics at the University of Rochester.[7-14]

Hillman et al.[7] and Kramer et al.[8] have showed that a "natural modes" formalism can be used to describe the physics behind the population-oscillation induced spectral holes in a homogeneously broadened absorber. Furthermore, Boyd and Mukamel[10] presented an explanation of the physical cause of the spectral holes by describing the multiphoton interactions between the strong field, the probe field, and the absorber. Another way to examine the physics is to consider that when the atomic population is capable of following the beat frequency between two optical fields, the absorption of both these fields by the atoms is reduced. This argument is further justified by the fact that the response of a harmonic oscillator is 90° out of phase with the driving field at resonance (resonance is defined by the frequency at which the driving field experiences maximum absorption).

The experimental realization of the T_1^{-1} spectral hole has been obtained in a series of three experiments at The Institute of Optics. The first experiment was performed by Hillman et al.[11,14] in ruby. In this experiment an argon-ion laser beam was used to pump the ruby crystal. The intensity of the pump beam was weakly amplitude modulated at a variable modulation frequency and the amplitude of the modulation in the transmitted pump-beam intensity was recorded by a lock-in amplifier. This transmission data was used to obtain the saturated absorption spectrum of the modulation sidebands. Although the observation of the population-oscillation-induced spectral dip was confirmed, the value of T_1 obtained using the modulation measurement did not agree with previously reported values of T_1 for ruby.

In a later experiment, Malcuit et al.[12] performed a similar experiment in alexandrite. The value of T_1 derived from the modulation data in this experiment agreed with previously reported values of T_1 for alexandrite. A further interesting feature was observed in this experiment when the pump laser was tuned to a wavelength at which the excited-state absorption cross section was larger than the ground-state absorption cross section. In this case the population pulsations lead to an increase in the absorption of the modulation sidebands for small modulation frequencies. That is to say that the T_1^{-1} dip became a T_1^{-1} tip!

The third such experiment was carried out by Kramer et al.[8,13] In this experiment an argon-ion laser was used to pump a fluorescein-doped boric acid glass (FBAG). This purpose of this experiment was to understand the mechanisms involved with the triplet-state quenching of the fluorescence in the FBAG. When the sample was cooled to liquid nitrogen temperatures the width of the T_1^{-1} hole was reduced to less than 1 Hz. This spectral feature was, at the time,

the narrowest spectral feature ever observed. This experiment demonstrates the usefulness and the versatility of these modulation techniques. It is possible to obtain sub-laser-linewidth resolution with AM spectroscopy.

The work in this chapter is a direct extension of these three experimental works. These previous experiments involved a weakly modulated laser tuned to the pump-transition of various laser materials, and the absorption spectrum of the pump was studied. We have tuned a weakly modulated laser to the pump-transition of the alexandrite crystal and studied the AM spectrum of the amplification experienced by a second laser tuned to the inverted transition of alexandrite. In this manner we were able to measure the modulation throughput of the laser amplifier, or rather, the transmission and amplification of modulations from the pump laser to the amplified laser.

In this chapter I will explore the response of a four-level atomic system to modulations in one or two fields each of which is applied to a different optical transition. The only interaction of these fields is via the atomic medium. The atoms act to transfer modulation from the pump-beam intensity to the intensity of the field being amplified and visa versa. The rate at which modulations can be transferred from one optical field to the other is related to the bandwidth of the atomic system. I will show that this bandwidth depends not only on the properties of the atoms but also on the strength of the field components which pump atomic population around the various energy levels. In the theoretical section of this chapter a rate equation formalism is developed to describe the modulations of the atomic population and the modulations induced in the intensity of the pump and amplified laser intensities. This theory is developed for collisionally broadened media with the assumption that the polarization dephasing rate T_2^{-1} is more rapid than any other spontaneous or induced rate.

For very strong excitation the population rate equations are not valid and the polarization equations for the atomic system should be included as I did in the previous chapter for a two-level system driven by strong optical fields.

I describe an experiment we performed to demonstrate the validity of this theory. The experiment is carried out with two dye lasers; a rhodamine 6G laser is used as a pump; an LDS 698 laser is tuned to the inverted transition to probe the gain of the system. Alexandrite is used as a four-level atomic medium which is strongly collisionally broadened. In this experiment the pump intensity is modulated and the modulated gain is measured. We measure the modulated gain by detecting the modulation signal, at the pump-modulation frequency, in the intensity of the LDS probe-laser beam after it has passed through the gain medium.

This chapter is devoted to the material dynamics of a driven laser medium. The medium is in free space to simplify this study. If the cavity dynamics are included, the temporal response of the laser system to pump fluctuations can be slower than either the atomic dynamics or cavity dynamics would dictate separately.[15] In this chapter I concentrate on the dynamics of the interaction of the laser medium with various optical fields. The treatment of the dynamics of a complete laser system is carried out in the next chapter of this thesis.

B. Theory of modulation in a four-level atomic system

I present a theoretical analysis based on a canonical four-level system. The four-level model is commonly used to model the energy levels of the alexandrite crystal. Of course, no real laser is quite so simple as this model, but we can get a basic qualitative understanding of many physical effects by studying this simple four-level model. For systems such as alexandrite in which a band of

levels exists, Fu and Haken[16] have developed a band model which has been proven to be successful in describing some instabilities which occur in dye-laser dynamics.[17]

I restrict the theoretical treatment to the case of strong collisional broadening. In this limit we are able to adiabatically eliminate the polarization equations of motion and start with the equations of motion for the population density matrix elements of the four-level system shown in Fig. 3.1:

$$\frac{d}{dt}\rho_g = -\lambda\rho_g + \gamma_1\rho_1, \tag{3.1a}$$

$$\frac{d}{dt}\rho_e = \lambda\rho_g - \gamma_e\rho_e, \tag{3.1b}$$

$$\frac{d}{dt}\rho_2 = \gamma_e\rho_e - R(\rho_2 - \rho_1) - \rho_2/T_1, \tag{3.1c}$$

and

$$\frac{d}{dt}\rho_1 = -\gamma_1\rho_1 + R(\rho_2 - \rho_1) + \rho_2/T_1. \tag{3.1d}$$

The ground-level population equation, Eq. (3.1a), contains the pump rate, λ, and the rapid non-radiative decay rate, γ_1. The equation of motion, Eq. (3.1b), for the population of the initial excited state contains the rapid non-radiative decay rate, γ_e. Finally, the spontaneous decay rate from level 2 is denoted by $1/T_1$.

Since the non-radiative decays in the ρ_e and ρ_1 equations are more rapid than all other decay rates and modulation rates, I adiabatically eliminate these variables from the system dynamics. When I do this and invoke conservation of population we are left with two independent equations:

$$\frac{d}{dt}\rho_2 = -(R + \lambda + 1/T_1)\rho_2 + \lambda \tag{3.2a}$$

and

$$\frac{d}{dt}\rho_g = -(R + \lambda + 1/T_1)\rho_g + R + 1/T_1. \tag{3.2b}$$
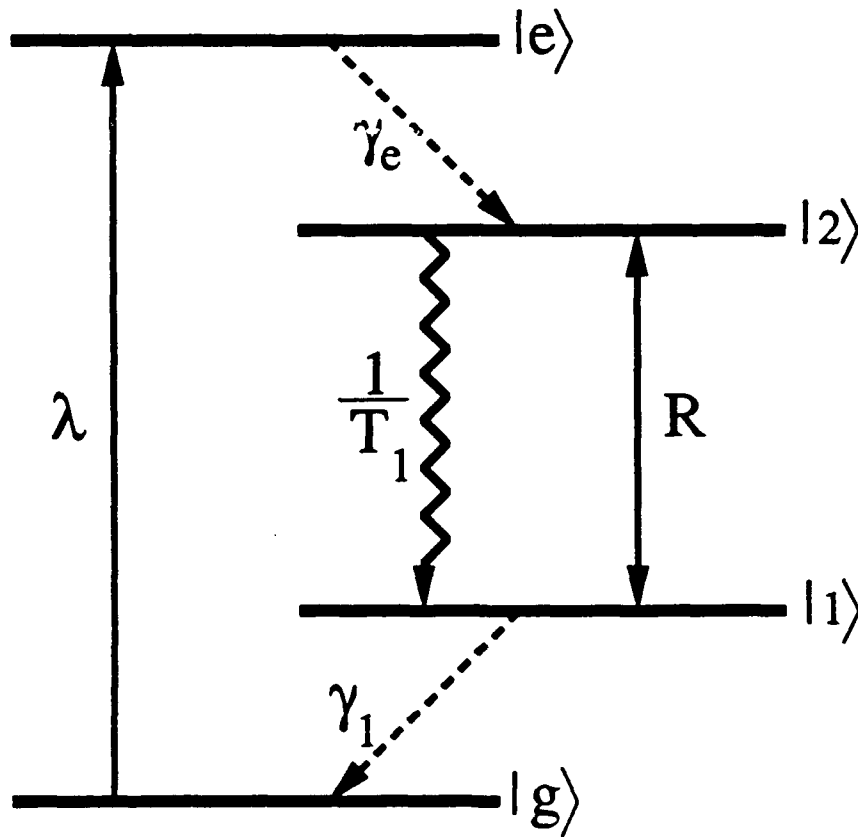
Fig. 3.1 Energy-level diagram for a canonical four-level laser system. Population is pumped from the ground state g to the initial excited state e by the pump rate λ. The population rapidly decays from level e to the upper lasing level, level 2, at a rate γ_e. The transition from level 2 to level 1 is naturally inverted since $\gamma_1 >> 1/T_1$. Population is stimulated from level 2 to level 1 by the laser-field stimulated rate R.

The factor $R + \lambda + 1/T_1$ appears as a homogeneous coefficient in both Eqs. (3.2a) and (3.2b). This term is the sum of the spontaneous-emission rate, $1/T_1$, and the two stimulated rates, R and λ; it is the population cycling rate, or rather the rate at which a population perturbation can circulate through the system's energy levels. This result demonstrates the value of modulation spectroscopy. The modulation bandwidth of a closed atomic system is a measure of the complete cycling rate of population through the system. In the limit of weak excitation rates $(R, \lambda \ll 1)$, the cycling rate is the slowest decay rate, in this case $1/T_1$. A modulation measurement can therefore be used to find any hidden slow decay rates which would act as a bottleneck for population through the atomic levels.

In the experiment we sinusoidally modulate the intensity of the pump laser. This modulation can be mathematically expressed as

$$\lambda(t) = \lambda_0 + 2\delta\lambda \cos(\delta\omega t), \qquad (3.3)$$

where λ_0 is the dc or time-averaged pump rate, $\delta\lambda$ is the strength of the modulation ($\delta\lambda \ll \lambda_0$ in this work), and $\delta\omega$ is the modulation frequency in radians per second.

Although we modulate only the pump laser, a modulation signal develops on the probe-laser stimulated rate, which we represent as

$$R(t) = R_0 + 2\delta R \cos(\delta\omega t + \Phi), \qquad (3.4)$$

where Φ is a phase lag that results from the finite response time of the atomic system. The modulation of the probe laser results from the modulated gain produced by the modulated pump rate, $\lambda(t)$. In general, because of nonlinearities, the resulting modulation on R is anharmonic and contains higher harmonics of the modulation frequency, $\delta\omega$. However, since the magnitude of the modula-

tion sidebands, $\delta\lambda$, is small in our experiment we neglect these higher-harmonic terms.

Floquet's theorem tells us that since the system is driven harmonically, the stationary-state response of the population expectation values will consist of harmonic overtones of the fundamental modulation frequency. The population for each of the levels in the system can be written as

$$\rho_j(t) = \sum_{n=-\infty}^{\infty} \rho_{j,n} \exp(in\delta\omega t), \tag{3.5}$$

where $\rho_{j,n}$ represents the nth-harmonic component of the populatio. expectation value of energy level j. We substitute the expressions for the time-dependent driving terms, Eqs. (3.3) and (3.4), and the expression for the time-dependent populations, Eq. (3.5), into the rate equations, Eqs. (3.2a) and (3.2b). When we equate terms of equal time dependence we get the following recurrence relations:

$$(1 + I_R + I_\lambda + in\delta\omega T_1)\rho_{2,n} + (\delta I_R^* + \delta I_\lambda)\rho_{2,n+1} + (\delta I_R + \delta I_\lambda)\rho_{2,n-1}$$
$$= I_\lambda \delta_{n,0} + \delta I_\lambda(\delta_{n,1} + \delta_{n,-1}) \tag{3.6a}$$

and

$$(1 + I_R + I_\lambda + in\delta\omega T_1)\rho_{g,n} + (\delta I_R^* + \delta I_\lambda)\rho_{g,n+1} + (\delta I_R + \delta I_\lambda)\rho_{g,n-1}$$
$$= (1 + I_R)\delta_{n,0} + \delta I_R \delta_{n,1} + \delta I_R^* \delta_{n,-1}, \tag{3.6b}$$

where I_λ and I_R are the dimensionless intensities of the pump laser and the probe laser given by

$$I_\lambda = \lambda_0 T_1 \tag{3.7a}$$

and

$$I_R = R_0 T_1. \tag{3.7b}$$

The normalization of the stimulated rates by the population lifetime of level 2 was done since this lifetime is believed to be the bottleneck of the system (the slowest decay rate). It is this lifetime which determines the saturation intensity of the individual lasers. In more complicated systems the normalization may be less obvious. In a similar manner, the dimensionless intensity of the modulation sidebands are given by

$$\delta I_\lambda = \delta\lambda T_1 \tag{3.8a}$$

for the pump laser, and

$$\delta I_R = \delta R T_1 \exp(i\Phi) \tag{3.8b}$$

for the probe laser. The asterisks in Eqs. (3.6a) and (3.6b) denote the complex conjugate.

These recurrence relations can be solved iteratively to give an analytic solution for the population in terms of continued fractions. In this chapter I consider the case when the modulation index is small ($\delta I_\lambda, \delta I_R \ll 1$). This assumption allows us to truncate the continued fraction and obtain a solution to first-order with respect to the modulation variables, δI_λ and δI_R. The first-harmonic responses of the upper laser level (level 2) and the ground level (level g) in phase with the modulation are given by

$$\text{Re}(\rho_{2,1}) = \frac{\delta I_\lambda(1 + I_R) - \delta I_R I_\lambda}{(1 + I_R + I_\lambda)^2 + (\delta\omega T_1)^2} \tag{3.9a}$$

and

$$\text{Re}(\rho_{g,1}) = \frac{\delta I_R I_\lambda - \delta I_\lambda(1 + I_R)}{(1 + I_R + I_\lambda)^2 + (\delta\omega T_1)^2} \tag{3.9b}$$

respectively. Similarly, the atomic response 90° out of phase with the modulation is given by the imaginary part of $\rho_{2,1}$

$$\text{Im}(\rho_{2,1}) = \left(\frac{-\delta\omega T_1}{1 + I_R + I_\lambda}\right) \frac{\delta I_\lambda(1 + I_R) - \delta I_R I_\lambda}{(1 + I_R + I_\lambda)^2 + (\delta\omega T_1)^2} \tag{3.10a}$$

and the imaginary part of $\rho_{g,1}$

$$\text{Im}(\rho_{g,1}) = \left(\frac{-\delta\omega T_1}{1 + I_R + I_\lambda}\right) \frac{\delta I_R I_\lambda - \delta I_\lambda(1 + I_R)}{(1 + I_R + I_\lambda)^2 + (\delta\omega T_1)^2} \tag{3.10b}$$

The in-phase first-harmonic response of the atomic population to a modulation of either stimulated rate, R or λ, is a Lorentzian of half-width at half-maximum (HWHM) $(1+I_\lambda+I_R)/T_1$. In the limit of weak excitation ($I_\lambda, I_R \ll 1$) the cycling rate is $1/T_1$. These Lorentzian terms give rise to homogeneous hole burning or the $1/T_1$ hole.[7-14] The hole in the absorption spectrum of the modulation sidebands of the pump, δI_λ, arises from the negative term in Eq. (3.9b). The pump experiences decreased absorption when the population can follow the modulation frequency; another consequence of this is that a probe laser that is being amplified will experience a modulated amplification. Modulated amplification is the subject of this chapter.

In the rate-equation limit we can write the propagation equation for the probe-laser intensity as

$$\frac{d}{dz} I_R(t,z) = \alpha I_R(t,z)\rho_2(t,z), \tag{3.11}$$

where α is the inverse Beer absorption length. Equating terms of equal time dependence, we get an expression for the spatial dependence of the probe field, δI_R:

$$\frac{d}{dz} \delta I_R(z) = \alpha \left\{ \delta I_R(z)\rho_{2,0}(z) + I_R(z)Re\left[\rho_{2,1}(z)\right] \right\}. \tag{3.12}$$

The first term on the right-hand side of Eq. (3.12) is an exponential gain term, which is responsible for the growth of fields modulated at frequency $\delta\omega$. The exponential gain term is independent of modulation frequency for weak modulation. The second term on the right-hand side of Eq. (3.12) is a linear gain term. This linear gain term provides an avenue for pump fluctuations to be

transmitted to the amplified probe-laser intensity, $I_R(t)$. In our experiment, the exponential gain term is insignificant since the amplitude of the modulation sidebands, δI_R, remains small. It is the linear gain term that is responsible for the initial growth of the modulation signal in the intensity of the amplified probe laser. Furthermore it is the linear gain term that gives the amplifier a low-pass response to pump fluctuations. The physics of this behavior lies in the first-harmonic response of the excited-state population $\rho_{2,1}$. In our experiment we measure the response of an optical amplifier to amplitude fluctuations of the pump intensity, $I_\lambda(t)$. We have devised a signal-limited detection scheme to measure the spectrum of the amplifier's response to the fluctuations as a function of the pump modulation frequency, $\delta\omega$.

In Fig 3.2 I have plotted the real part of the first-harmonic component of the excited-state population, $\rho_{2,1}$ [as given by Eq. (3.9a)], for various values of I_λ and small probe-laser intensity ($I_R \ll 1$). It is evident from the figure that the population behaves as a low-pass filter. The low frequency gain maximizes for $I_\lambda = 1$. The bandwidth of the gain increases with increasing pump intensity but the maximum gain occurs for $I_\lambda = 1 + I_R$.

C. Experimental apparatus

A schematic of the experimental apparatus is shown is Fig. 3.3. The experiment involves two dye lasers. The pump laser is a rhodamine 6G dye laser which is tuned to a wavelength of 6000 angstroms using an intracavity Pellin-Brocha prism. This wavelength is the center of the pump band of the alexandrite crystal. The maximum output power of our laser at this wavelength is approximately 500 mw. The second dye laser is a LDS 698 dye laser which is tuned to the four-level vibronic transition of the alexandrite crystal. The center of
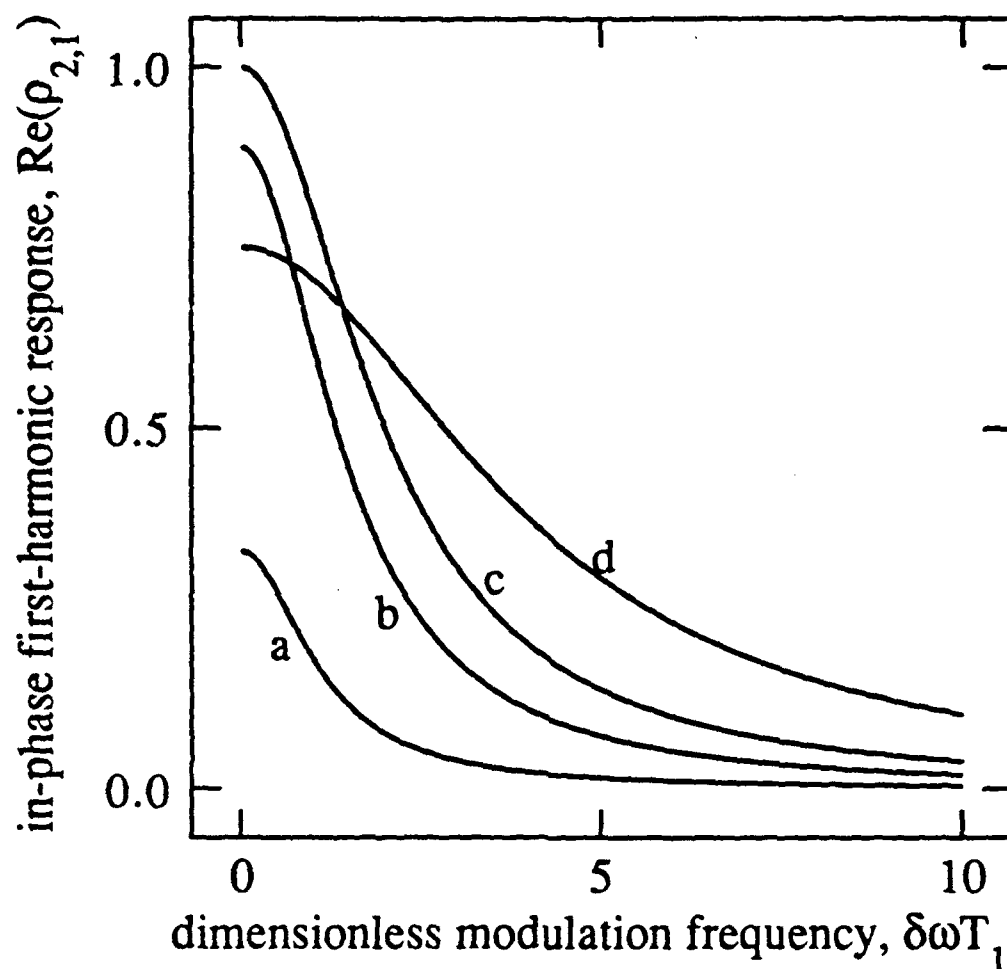
Fig. 3.2 The in-phase first-harmonic linear gain, at the modulation frequency of the pump laser, experienced by the probe-laser tuned to the inverted transititon in a four-level laser system. Plotted is $\text{Re}(\rho_{2,1})$ as it appears in Eq. (3.9a). The signal has been normalized to the maximum signal which occurs for dimensionless-pump intensity $I_\lambda = 1$. The linear gain is plotted for negligible probe-laser intensity ($I_R \ll 1$) for four different dimensionless pump-laser intensities: (a) $I_\lambda = 0.1$; (b) $I_\lambda = 0.5$; (c) $I_\lambda = 1.0$; (d) $I_\lambda = 3.0$.

the vibronic transition is actually at a wavelength of 7500 angstroms but we tuned the LDS laser to 7200 angstroms instead since a laser operating at 7200 angstroms is still visible to the eye facilitating alignment.

The lasers operate in multiple longitudinal modes. The multimode operation of the lasers does not degrade the experimental results since the modulation frequencies we used were much less than the frequency separation of the cavity modes, and the bandwidth of the pump and vibronic transitions in alexandrite is hundreds of angstroms while the bandwidths of the dye lasers are less than an angstrom. The bandwidth of the laser is narrow compared with the transitions and the modulation frequency is small compared with the free spectral range of the laser cavities.

The alexandrite crystal can behave as a three level laser like ruby or a four-level system like a dye. The three level operation occurs at a wavelength of 6900 angstroms while the four level vibronic operation occurs between 7000 and 8000 angstroms. In this experiment we tune the probe laser to resonance with the vibronic transition.

The rhodamine 6G laser beam is passed through a fast acousto-optic modulator (AOM) (see Fig. 3.3). An Isomet 1205C AOM driven by a 232A-1 driver is driven by a weak sine wave of variable frequency generated by a Wavetek model 188 Sweep/Function Generator. The sinusoidally varying voltage causes the AOM to diffract a sinusoidally varying amount of intensity out of the path of the rhodamine laser beam. A weak sinusoidal amplitude modulation of the pump-laser intensity results. The Wavetek also supplies a reference signal to a lock-in amplifier which measures the amount of modulation in the intensity of the amplified LDS laser.

The modulated rhodamine laser beam is now combined colinearly with the
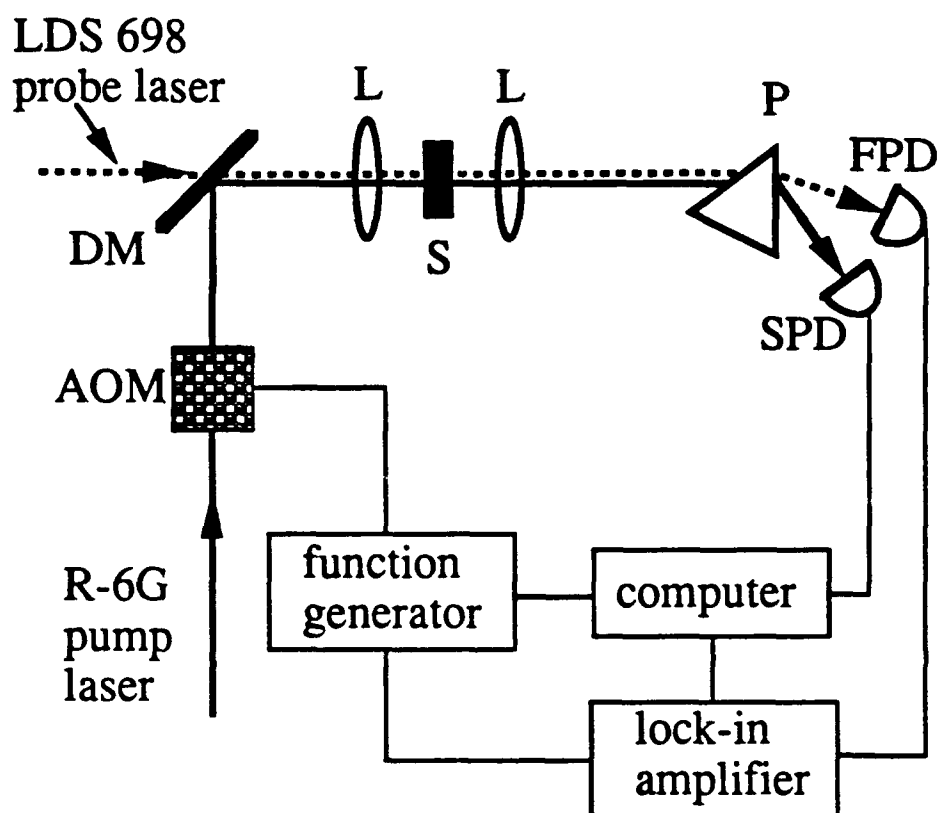
Fig. 3.3 Experimental apparatus in block-diagram form. I use the following abbreviations: AOM- acousto-optic modulator; DM- dichroic mirror; L- lens; S- alexandrite sample; P- prism; SPD- slow photo-diode; FPD- fast photo-diode.

LDS laser beam using a dichroic mirror which reflects the rhodamine beam but allows light from the red LDS laser to pass through. The alignment of the two lasers are tweaked to maximize the amplification of the LDS laser beam which is transmitted through the pumped alexandrite crystal. The colinear lasers are focused into the alexandrite crystal sample using a 25 mm focal length lens, and the transmitted beams are recollimated with another 25 mm focal length lens. After being recolimated the colinear lasers are separated using a prism. The isolated LDS laser beam is focused onto a fast photodiode whose bandwidth is adequate to detect the AM signal in the intensity of the laser. The isolated rhodamine laser beam is focused onto a slow photodiode which is used to measure the average intensity of the rhodamine laser in order to determine the intensity of the pump beam.

A modulation run consists of several modulation frequency settings. The computer supplies a voltage to a voltage-controlled oscillator (VCO) in the Wavetek in order to set the modulation frequency. The computer records the in-phase and in-quadrature components of the first-harmonic response of the intensity of the probe laser at each modulation frequency. The lock-in readings are collected to acquire the modulation spectrum of the probe-laser amplification. Prior to each modulation run the intensity of the pump laser is recorded by the computer. In order to convert the voltage from the slow photodiode into a dimensionless intensity value of the pump laser beam we record a saturation measurement prior to taking the modulation spectra. The saturation measurement is accomplished by measuring the incident and transmitted values of the pump laser intensity through the alexandrite crystal. These values are then fit to a simple saturated absorption theory to arrive at a scale factor for converting the voltage measured by the slow photodiode to the actual dimensionless

intensity of the pump laser.

D. Experimental results

In Fig. 3.4 I have plotted the in-phase modulation signal measured in the intensity of the amplified probe laser. This form of the data is useful if one is interested in transferring information through the system with no phase lag. Agreement between theory and experiment is good. I have plotted the amplification spectra for four different pump laser intensities. All four spectra are fit simultaneously with the same theory. The free parameter used in the fitting process is the overall signal strength. The dimensionless intensity of the pump laser was derived from the saturation data. In fitting the saturation data I derive a scalar which relates the digitized value of the pump intensity to the dimensionless intensity used in the theory. This scalar is then applied to the digitized intensity measurement performed before each modulation run in order to determine the dimensionless intensity of the laser. The in-phase signal behaves approximately as a Lorentzian. The bandwidth of the in-phase signal increases as the intensity of the pump laser is increased, even though the amplification occurs at a different transition than the pumping process. As the theory predicts the population cycling rate is increased by the pump intensity.

I have plotted the in-quadrature modulation signal from the amplified probe in Fig. 3.5. Again I report good agreement between experiment and theory. These curves increase in size and width with increasing pump intensity. The in-quadrature signal behaves similarly to a dispersion curve. Since this response lags the in-phase response by 90°, the data and the theory are actually negative, but I have inverted them before plotting.

For applications to data communication the in-phase and in-quadrature
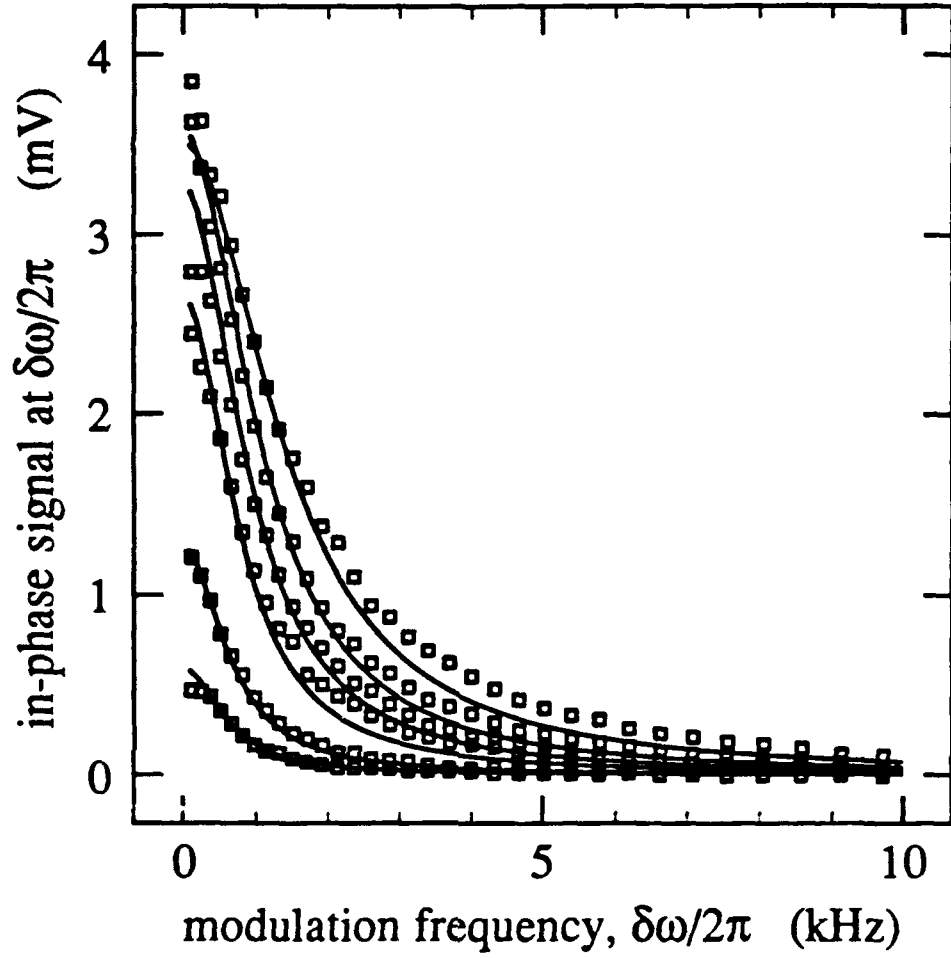
Fig. 3.4 Theory and experiment for the in-phase amplification signal at the modulation frequency $\delta\omega/2\pi$. The squares represent data points and the solid curves represent the best-theoretical fit using Eq. (3.9a). All the data shown are fit simultaneously to the same parameters. The in-phase signals are shown for negligible probe-laser intensity ($I_R \ll 1$) for six different pump intensities. The pump intensities shown are (from bottom to top): $I_\lambda = 0.05, 0.12, 0.37, 0.59, 0.89, 1.49$.
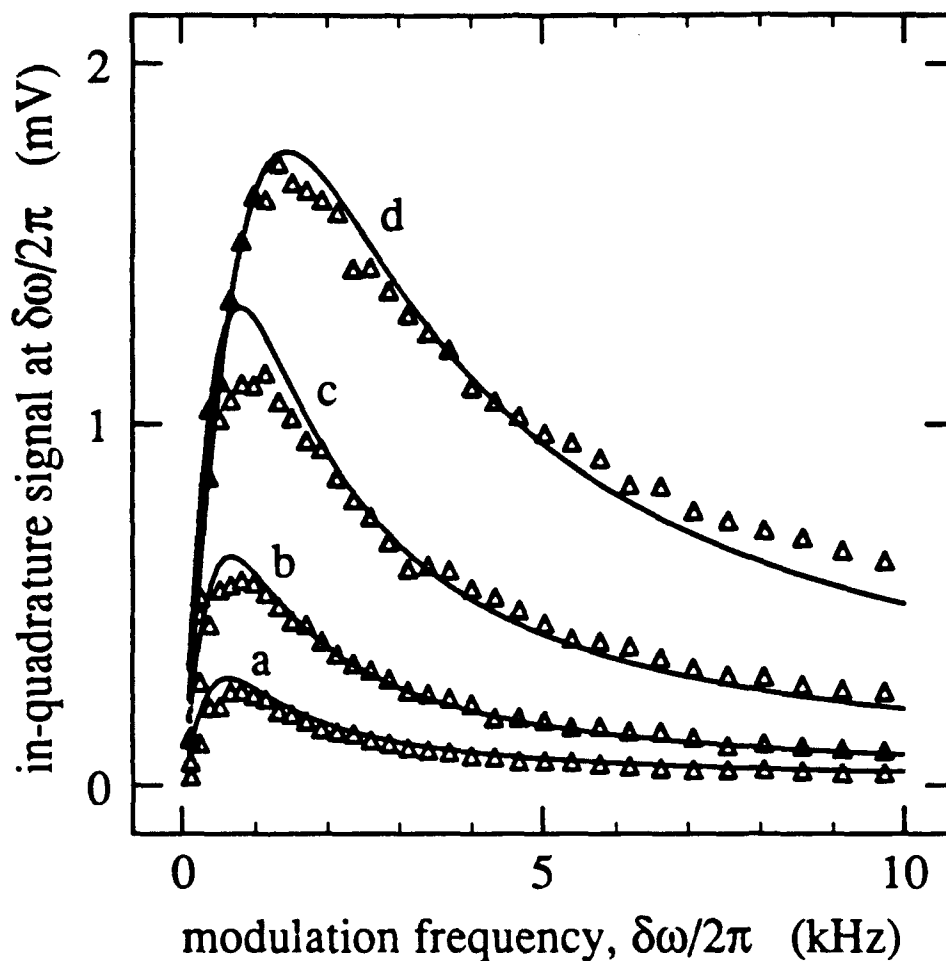
Fig. 3.5 Theory and experiment for the in-quadrature amplification signal at the modulation frequency $\delta\omega/2\pi$. The squares represent data points and the solid curves the best theoretical fit using Eq. (3.10a). The signal is actually negative since we measure the modulation signal, which lags the modulation of the pump laser by 90 degrees. With this in mind I have inverted the data and theory before plotting. Shown are the in-quadrature signals for weak probe-laser intensity for four different pump intensities: (a) $I_\lambda = 0.05$; (b) $I_\lambda = 0.12$; (c) $I_\lambda = 0.37$; (d) $I_\lambda = 1.49$.

data are of interest. If, however, the effect of multiplicative noise is the issue, then the phase of the modulation transfer is immaterial. The modulus of the modulation signal is analogous to the noise-transmission ability of the system.[15] In Fig. 3.6 I have plotted the modulus of the data (squares) and the theoretical value for the modulus (solid curves). The modulus signal increases with pump intensity and broadens, as did the in-phase signal. However, the modulus falls off with increasing modulation frequency more slowly than the in-phase signal does. The modulus behaves as the square root of the in-phase signal. The in-phase signal falls off as a Lorentzian; therefore the noise transmission spectrum of the amplifier is the square-root of a Lorentzian.

A final interesting way to characterize the data is through the modulation bandwidth of the amplifier as a function of pump intensity. In Fig. 3.7 I have plotted the half width at half maximum (HWHM) of the in-phase signal and the signal modulus versus the dimensionless intensity of the pump laser. The bandwidth of the in-phase signal is always smaller than that of the signal modulus. Figure 3.7 shows that the bandwidth of the amplified signal increases with the dimensionless intensity of the pump laser. For the in-phase signal this increase is linear, and the slope is just the stimulated emission rate of the pump laser, $I_\lambda/2\pi T_1$ (for alexandrite T_1 is the room-temperature fluorescent lifetime, $262\mu s$). The y-intercept is the spontaneous emission rate, $1/2\pi T_1$.

E. Alexandrite model with thermal pumping included

To demonstrate a rather esoteric application of AM spectroscopy I will present a theoretical model for the energy levels of the alexandrite crystal which includes the multi-level nature of the alexandrite energy level diagram and modulated thermal pumping. In fitting the data I will arrive at a parameter which
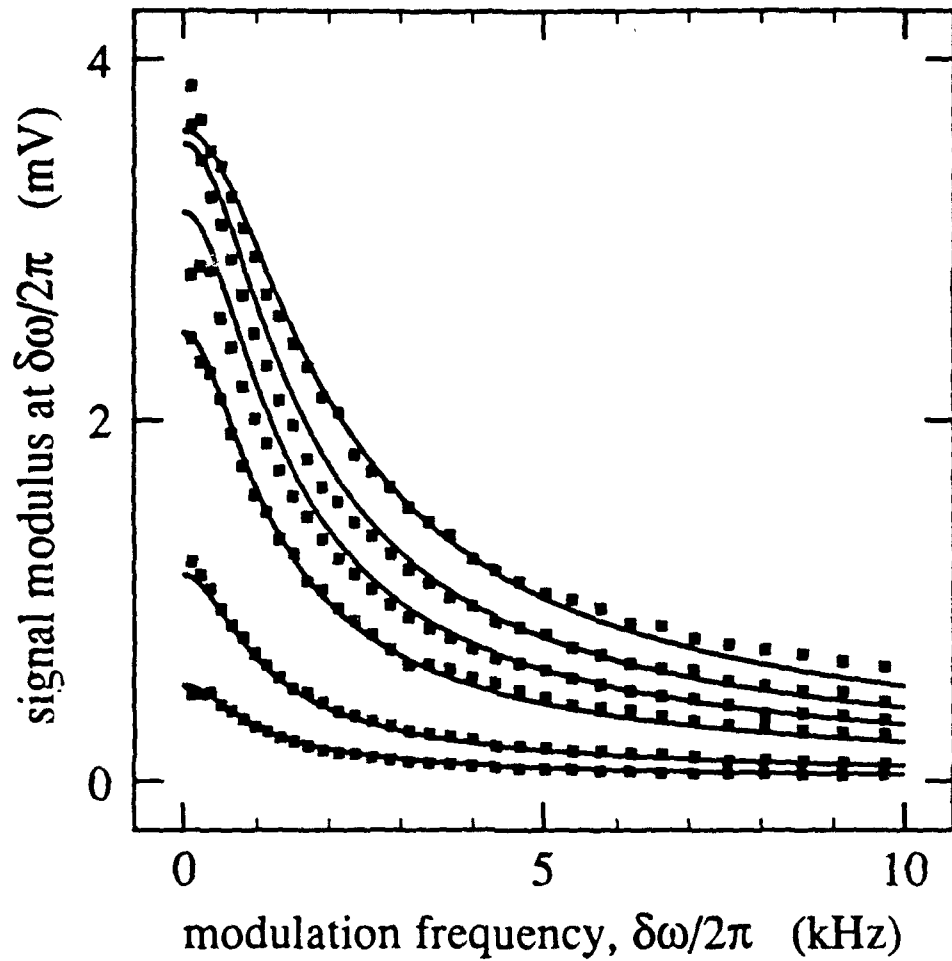
Fig. 3.6 Theory and experiment for the modulus of the amplification signal at the modulation frequency $\delta\omega/2\pi$. The squares represent data points and the solid curves represent the best-theoretical fit using Eqs. (3.9a) and (3.10a) to obtain an expression for the modulus of ρ_{21}. The moduli of the amplification signals at $\delta\omega$ are plotted for negligible probe-laser intensity ($I_R \ll 1$) for six different pump intensities, $I_\lambda = 0.05, 0.12, 0.37, 0.59, 0.89, 1.49$, as shown from bottom to top.
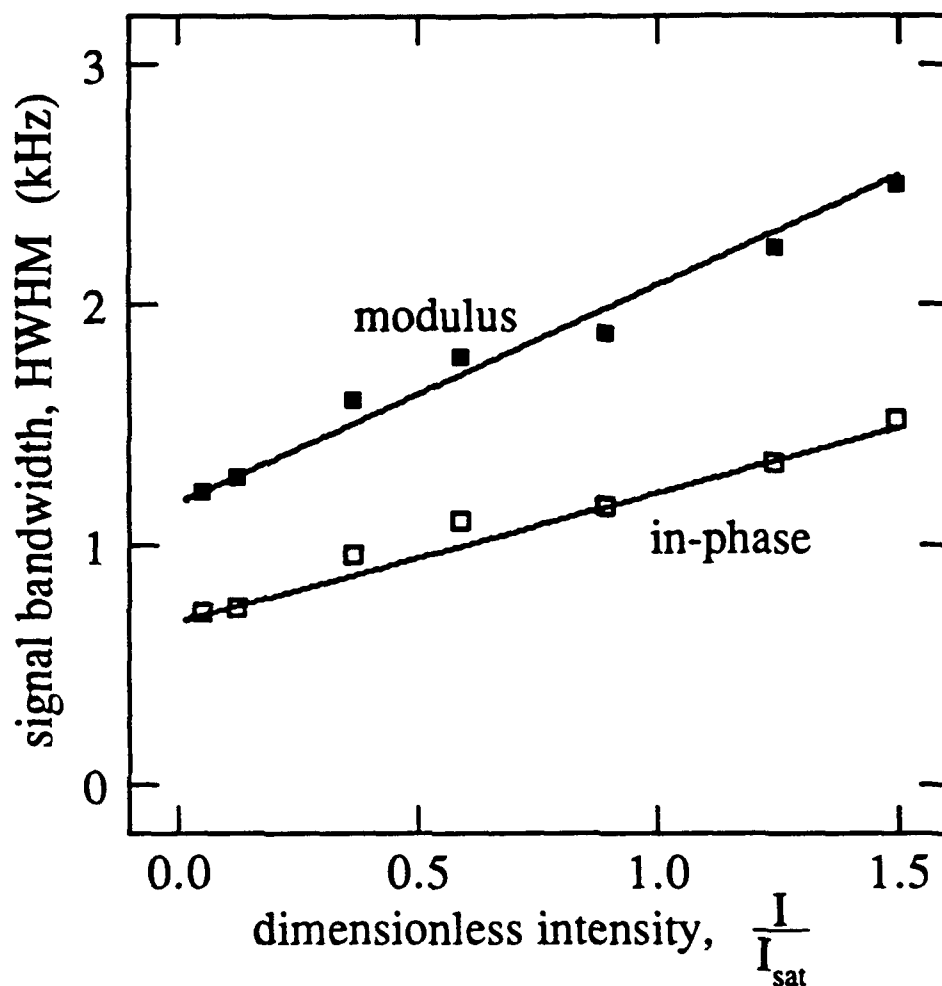
Fig. 3.7 Modulation bandwidth (HWHM) of the probe-laser amplification signal versus the dimensionless intensity of the pump laser. Plotted are the HWHM of the in-phase signals and the HWHM of the signal moduli of the modulation-amplification spectrum of the probe laser. The HWHM of the in-phase data signal is represented as empty squares, and the HWHM of the signal modulus is represented by the solid squares. The solid lines represent the theoretical predictions.

relates the temperature of the crystal to the intensity of the pump beam. While this elaborate model offers no better a fit to the data than the simple four level theory does, this treatment is more realistic in keeping with what is known about alexandrite,[18-23] and it provides information about the thermal state of the crystal which is an integral part of the performance of an alexandrite laser.

In this section I will describe the equations I use to describe the alexandrite crystal. The system of equations are based on what is known about the alexandrite crystals from research done at Allied Signal Corp. In this model I include the storage level for the atomic population and the upper and lower levels of the four-level vibronic transitions. Once again the band model developed by Fu and Haken[16] could be used to provide a more accurate description of these levels. However, the aim of this section is to develop an understanding of the thermal dynamics of the alexandrite crystal. I use this five-level model to describe the response of the alexandrite crystal to pump intensity modulations just as I did in section B of this chapter. In describing the response of the population expectation values in this model to pump modulations I develop an expression for the temperature in the interaction region of the crystal due to heating by the incomplete conversion of pump photons into light. When the data is fit an accurate figure can be arrived at for this temperature increase coefficient. In this way I employ AM spectroscopy to develop an understanding of the thermal state of the alexandrite crystal. In the past, photo-acoustic spectroscopy has been used to determine the temperature change within the alexandrite crystal due to heating by the pump.[23] In this experiment a microphone is used to detect sound waves generated due to the modulated convective heating of the atmosphere in the vicinity of the pumping region. The microphone and the alexandrite crystal are placed in an acoustic cell for this purpose. As the pump beam is modulated, the

acoustic response of the system reveals the rate at which heat can be removed from the interaction region by optical and thermal methods. Such parameters as the *quantum efficiency* and the *temperature rise* can be measured in such a manner. I will show in this section that an AM measurement involving only optical detection can be used to measure the temperature of the interaction region in the alexandrite crystal.

I start with the equations of motion of the five significant levels of alexandrite (see Fig. 3.8). The significant levels are the ground state g, the excited state e to which population is pumped, the upper level of the three-level laser system 3, the upper level of the four-level vibronic system 2, and the lower vibronic level 1. I want to point out that a more accurate treatment of this problem would include the vibronic multilevel nature of the state 1 (see for instance Haken and Hong[16]). The equations of motion for these levels with this notation are:

$$\frac{d}{dt}\rho_g = \gamma_1\rho_1 + \gamma_3\rho_3 - \lambda\rho_g, \qquad (3.13a)$$

$$\frac{d}{dt}\rho_e = \lambda\rho_g - \gamma_e\rho_e, \qquad (3.13b)$$

$$\frac{d}{dt}\rho_2 = -(\rho_2 - \rho_1)R - (\rho_2 - \rho_3)R_T - \gamma_2\rho_2, \qquad (3.13c)$$

$$\frac{d}{dt}\rho_3 = (\rho_2 - \rho_3)R_T + \gamma_e\rho_e - \gamma_T\rho_3, \qquad (3.13d)$$

and

$$\frac{d}{dt}\rho_1 = \gamma_2\rho_2 + (\rho_2 - \rho_1)R - \gamma_1\rho_1, \qquad (3.13e)$$

Since the decay rates γ_e and γ_1 are rapid, the equations of motion for ρ_e and ρ_1 can be adiabatically eliminated from the dynamics. Also, I invoke conservation of population in order to eliminate the ρ_g equation of motion.
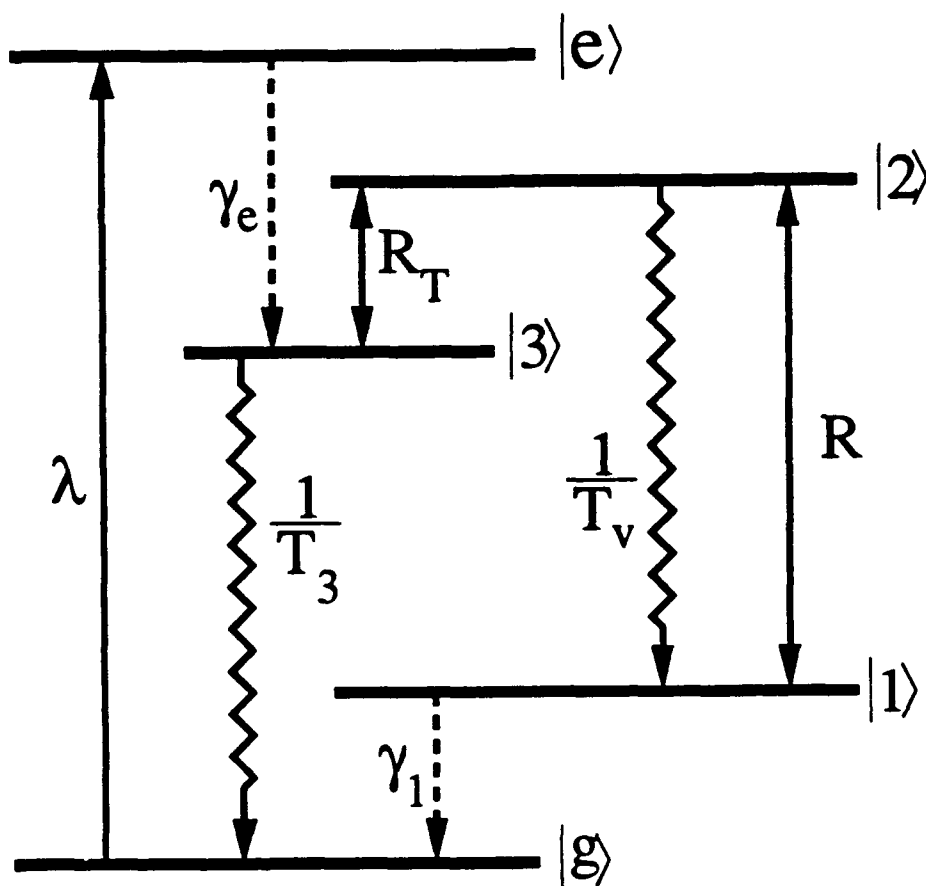
Fig. 3.8   Energy-level diagram for the alexandrite crystal with thermal pump-rate R_T included. The pump rate λ takes population from the ground state, g, to the excited state, e, from where it rapidly decays at the rate γ_e to the storage level, level 3. The thermal pump rate R_T connects the storage level with the excited vibronic level, level 2. The spontaneous optical-decay rates are denoted by $1/T_3$ and $1/T_v$. The probe-laser pump rate is denoted by R.

Making these eliminations leaves us with the equations for ρ_3 and ρ_2

$$\frac{d}{dt}\rho_2 = -\left(R + R_T + \gamma_2\right)\rho_2 + R_T\rho_3, \qquad (3.14a)$$

$$\frac{d}{dt}\rho_3 = -\left(\gamma_3 + R_T + \lambda\right)\rho_3 + (R_T - \lambda)\rho_2 + \lambda. \qquad (3.14b)$$

Again I apply a modulation of the pump rate λ to these equations. In this case the modulation of the pump rate not only results in a modulation of the stimulated rate $R(t)$ but the thermal pump rate R_T also becomes modulated. The modulated parameters in this case are

$$\lambda(t) = \lambda_0 + 2\delta\lambda\cos(\delta\omega t), \qquad (3.15)$$

$$R(t) = R_0 + \delta R\exp(i\delta\omega t) + \delta R^*\exp(-i\delta\omega t), \qquad (3.16)$$

and

$$R_T(t) = R_{T,0} + \delta R_T\exp(i\delta\omega t) + \delta R_T^*\exp(-i\delta\omega t). \qquad (3.17)$$

The modulated parameters can be substituted into the equations of motion Eqs. (3.14a-b). I truncate the coefficients in these equations to first-order with respect to the modulated parameters to derive the recurrence relations for the first- and zeroth-harmonic responses of the population of levels 2 and 3

$$\begin{pmatrix} R_0 + R_{T,0} + \gamma_2 + i\delta\omega & -R_{T,0} \\ \lambda_0 - R_{T,0} & R_{T,0} + \lambda_0 + \gamma_3 + i\delta\omega \end{pmatrix} \begin{pmatrix} \rho_{2,1} \\ \rho_{3,1} \end{pmatrix}$$

$$= \begin{bmatrix} \delta R_T\rho_{3,0} - (\delta R + \delta R_T)\rho_{2,0} \\ \delta\lambda + (\delta R_T - \delta\lambda)\rho_{2,0} - (\delta\lambda + \delta R_T)\rho_{3,0} \end{bmatrix} \qquad (3.18)$$

The two equations given in the matrix Eq. (3.18) can be solved simultaneously to find both $\rho_{2,1}$ and $\rho_{3,1}$. However, in order to get an analytic solution it is first necessary to have an expression for the modulated thermal pump rate

$R_T(t)$. To do this I assume that the thermally-induced transition rate takes the form

$$R_T(t) = \sigma L_{\nu_0}(t), \qquad (3.19)$$

where L_{ν_0} is the integrated phonon irradiance and σ is the cross-section for absorption of the phonon radiation. The irradiance is integrated over all frequencies capable of inducing a transition from the storage level, level 3, to a level at or above level 2 in energy (eg. the phonon irradiance is integrated from the 800 cm^{-1} separation of levels 3 and 2 to infinite frequency). I assume that there are an infinite number of degrees of freedom within the crystal lattice and therefore the phonon irradiance is given by Planck's blackbody distribution. In appendix A I have calculated the phonon irradiance L_{ν_0} capable of inducing a transition from level 3 to an energy level at or above level 2

$$L_{\nu_0}(t) \approx \left(\frac{8\pi h}{c^3}\right) \exp[\phi(t)\nu_0] \sum_{n=0}^{3} (-1)^n \frac{3!\nu_0^{3-n}}{(3-n)!\phi(t)^{n+1}}, \qquad (3.20)$$

where $\phi(t) = -h/kT(t)$. The temperature is a function of time since the time varying absorption of the pump laser intensity induces a time-dependent heating of the interaction region.

Once the integrated phonon irradiance is found as a function of temperature the modulation of the temperature is derived. In appendix B I calculate the modulated temperature T(t) due to heating by the modulated pump intensity, $I_\lambda(t)$. I substituted the expression for the modulated temperature into the expression for the integrated phonon irradiance given by Eq. (3.20). Then, I linearized the resulting expression for $L_{\nu_0}(t)$ with respect to δT, the weak modulation amplitude of the temperature. The linearized expression for the time-dependent phonon irradiance is

$$L_{\nu_0}(t) = \left(\frac{8\pi h}{c^3}\right) \exp\left(\frac{-h\nu_0}{kT_0}\right) \left\{ (AT_0 + BT_0^2 + CT_0^3 + DT_0^4) \right. \tag{3.21}$$

$$\left. + \left[\delta T \left(A\frac{h\nu_0}{kT_0} + 4A + 12BT_0 + 24CT_0^2 + 24DT_0^3\right) \exp(i\delta\omega t) + C.C.\right] \right\}$$

where the coefficients A,B,C, and D are given in appendix B. In Eq. (3.21) the temperature of the interaction region of the crystal is assumed to be of the form

$$T(t) = T_0 + [\delta T \exp(i\delta t) + C.C.], \tag{3.22}$$

where T_0 is the DC or time-averaged temperature given by

$$T_0 = T_{room} + \psi I_\lambda(\alpha\epsilon\rho_{g,0} + \beta\rho_{3,0}), \tag{3.23}$$

and the modulated component of the temperature δT is given by

$$\delta T = \psi[\alpha\epsilon(\rho_{g,0}\delta I_\lambda + \rho_{g,1}I_\lambda) + \beta(\rho_{3,0}\delta I_\lambda + \rho_{3,1}I_\lambda)]. \tag{3.24}$$

The ground-state absorption coefficient α and the excited-state absorption co-efficient β are both known quantities along with the thermal quantum efficiency ϵ [18-23] (the thermal quantum efficiency ϵ is one minus the fluorescent quantum efficiency). Since the saturation intensity of the alexandrite crystal is defined in terms of the ground-state absorption coefficient, α, I normalize this quantity to unity, and the excited-sate absorption coefficient β is normalized with repect to α. The scalar ψ relates the dimensionless intensity of the pump laser to the temperature of the crystal. This constant is found by fitting the data. The phonon absorption cross section σ in Eq. (3.19) is found by setting the pump intensity to zero: the thermal pump rate is now equal to the room temperature value. This quantity corresponds to a population lifetime of 262 μs.

The expression for the time-dependent phonon irradiance in Eq. (3.21) together with the expression for the time-dependent thermal pump rate $R_T(t)$ given in Eq. (3.19) can be used to evaluate the DC thermal pump rate

$$R_{T,0} = \sigma \left(\frac{8\pi h}{c^3}\right) \exp\left(\frac{-h\nu_0}{kT_0}\right) (AT_0 + BT_0^2 + CT_0^3 + DT_0^4), \qquad (3.25)$$

and the expression for the modulated component of the thermal pump rate

$$\delta R_T = \sigma \delta T \left(\frac{8\pi h}{c^3}\right) \exp\left(\frac{-h\nu_0}{kT_0}\right)$$
$$\left(A\frac{h\nu_0}{kT_0} + 4A + 12BT_0 + 24CT_0^2 + 24DT_0^3\right). \qquad (3.26)$$

These expressions in Eqs. (3.25) and (3.26) can be used to solve the matrix equation Eq. (3.18). The solutions for $\rho_{2,1}$ and $\rho_{3,1}$ are solved for simultaneously in an iterative manner since the expression for δR_T contains the variable δT which itself depends on $\rho_{2,1}$ and $\rho_{3,1}$.

The resulting expression for $\rho_{2,1}$ and that for $\rho_{2,0}$ are used together with Eq. 3.12 in order to fit the data with this model. The results of this fit are shown in the Fig. 3.9. In fitting the data I have evaluated the constant ψ that related the temperature in the crystal to the intensity of the pump laser. The best fit for the data shown in Fig. 3.9 was arrived at using $\psi = 3.6° K/$(unit dimensionless intensity). This is equivalent to saying that a dimensionless intensity of 1 causes a temperature change in the crystal of $3.6° K$. This constant has been studied in the past via photo-acoustic spectroscopy.[23] Photo-acoustic techniques involve modulated heating of the sample and detection of the sound waves generated by the periodic convective cooling of the sample by the surrounding atmosphere. In these studies the quantum efficiency and the rate of heat absorption by the sample can be derived. Using modulated pumping and purely optical detection methods we have derived the relation between the temperature and the
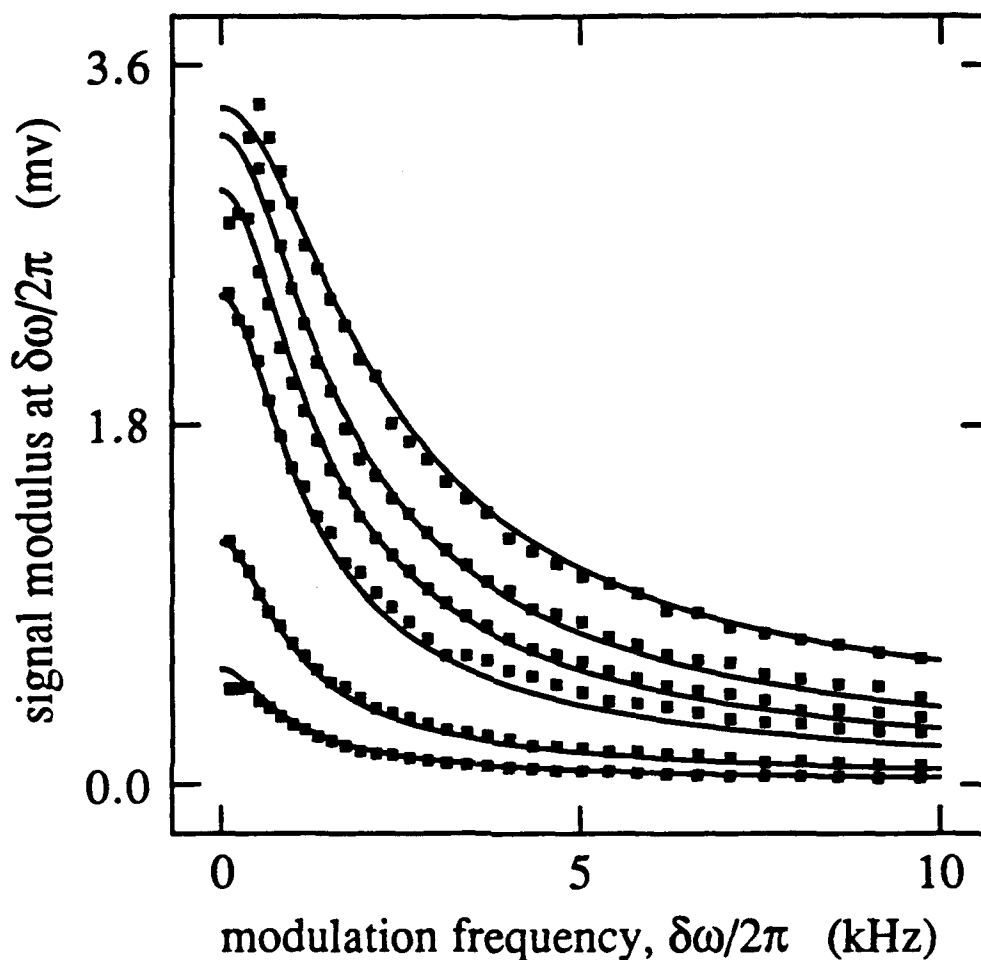
Fig. 3.9 Theory and experiment for the modulus of the amplification signal at the modulation frequency $\delta\omega/2\pi$. The experimental data is plotted along with the alexandrite-thermal-pump-theory. The squares represent data points and the solid lines represent the best-theoretical fit to the data using the thermal-pumping theory outlined in section E of this chapter. The moduli of the amplification signal are ploted for six different pump intensities (from bottom to top): I_λ = 0.06, 0.15, 0.43, 0.70, 1.06, 1.77. The thermal pump coefficient giving this fit is $3.6^\circ K$ per unit dimensionless pump-intensity.

dimensionless intensity of the pump laser. The intensity dependence of the temperature of the sample we report ($\psi = 3.6°K/($unit dimensionless intensity)) is in good agreement with the value of this quantity reported by Shand and Jensson.[23]

F. Conclusion

In this chapter I have reviewed an experiment studying the temporal response of a four-level laser amplifier to a modulated pump intensity. Using a rate-equation formalism, valid for collisionally-broadened homogeneous media, I have derived an expression for the response of the atomic population to a weak harmonic modulation of the pump rate of the amplifier. When the modulation sidebands are weak the response is a Lorentzian whose HWHM is the sum of the spontaneous-emission rate and the dimensionless intensities of the pump laser, I_λ, and the probe laser, I_R (the probe laser was tuned to the inverted transition). The HWHM is the rate at which population can cycle freely through the atomic system and is equal to $(1 + I_R + I_\lambda)/T_1$. In the limit of weak driving ($I_R, I_\lambda \ll 1$) the population responds at the spontaneous emission rate $1/T_1$. Therefore, I propose this type of AM spectroscopy as a means of determining slow decay rates in optically active media.

I report an experimental test of these predictions. By modulating the pump of an alexandrite crystal at a frequency $\delta\omega$ and measuring the amplification of the probe laser at the modulation frequency $\delta\omega$, we measure the spectrum of the atomic response to the modulation. The probe laser undergoes modulated amplification only when the modulation frequency is less than the population cycling rate (eg. $\delta\omega \ll (1 + I_R + I_\lambda)/T_1$). Furthermore, I showed that by measuring the modulus of the amplification signal one can measure the response

of the amplifier to multiplicative pump noise.

The remarkable aspect of these results is that the intensity of the pump I_λ can affect the modulation bandwidth of amplification occuring at a different optical transition in a multilevel system. The pump is not coherent with the amplified probe, yet, through population oscillations it has a marked effect on the modulation bandwidth of the amplifier.

In the last section of this chapter I have demonstrated a technique to measure the temperature rise of the crystal due to the incomplete conversion of pump photons into fluorescent or stimulated-emission photons. The temperature of the crystal due to this heating can be derived using modulation spectroscopy and a data fitting algorithm. This AM technique is similar to thermo-acoustic techniques which also involve a modulated pumping of the sample. However in the photo-acoustic measurements a pressure transducer is needed whereas in this experiment only intensity measurements are necessary.

The behavior and the stability of a laser depends on both the atomic dynamics and the cavity configuration. I have shown that a proper treatment of the atomic dynamics must include the multilevel nature of the gain medium and the multifrequency nature of the field.

References

1. H. Risken and K. Nummedal, "Self pulsing in laser," J.Appl Phys. **39**, 4662-4672 (1969).

2. T. Ogawa and E. Hanamura, "Dynamical properties of the multi-mode laser with modulated inversion," Opt. Commun. **61**, 49-54 (1987). item T.Ogawa and E. Hanamura, "Numerical analysis of multimode laser with modulated inversion," Appl. Phys. B **43**, 139-153 (1987).

3. T. Ogawa, "Quasiperiodic instability and chaos in the bad-cavity laser with modulated inversion: numerical analysis of a Toda oscillator system," Phys. Rev. A **37**, 4286-4302 (1988).

4. M. Sargent III, M.O. Scully, and W.E. Lamb, Jr., *Laser Physics*, (Addison-Wesley, Reading, Mass., 1974).

5. S.E. Schwartz and T.Y. Tan, "Wave interactions in saturable absorbers," Appl. Phys. Lett. **10**, 4-6 (1967).

6. M. Sargent III, P.E. Toschek, and H.G. Danielmeyer, "Unidirectional saturation spectroscopy. I, Theory and short dipole lifetime limit," Appl. Phys. **11**, 55-62 (1976).
M. Sargent III and P.E. Toschek, "Unidirectional saturation spectroscopy II, General lifetimes, interpretations, and analogies," Appl. Phys. **11**, 107-120 (1976).

7. L.W. Hillman, R.W. Boyd, and C.R. Stroud, Jr., "Natural modes for the analysis of optical bistability and laser instability," Opt. Lett. **7**, 149-151 (1982).

8. M.A. Kramer, R.W. Boyd, L.W. Hillman, and C.R. Stroud, Jr., "Propagation of modulated optical fields through saturable-absorbing media: a general theory of modulation spectroscopy," J. Opt. Soc. Am. B **2**, 1444-1455 (1985).

9. R.W. Boyd, "Spectral holes due to population oscillations in a homogeneously broadened media," in *Coherence and Quantum Optics V*, L. Mandel and E. Wolf, eds. (Plenum, New York, 1984).

10. R.W. Boyd and S. Mukamel, "Origin of spectral holes in pump-probe studies of homogeneously broadened lines," Phys. Rev. A **29**, 1973-1983 (1984).

11. L.W. Hillman, R.W. Boyd, J. Krasinski, and C.R. Stroud, Jr., "Observation of a spectral hole due to population oscillations in a homogeneously broadened optical absorption line," Opt. Commun. **45**, 416-419 (1983).

12. M.S. Malcuit, R.W. Boyd, L.W. Hillman, J. Krasinski, and C.R. Stroud, Jr., "Saturation and inverse-saturation absorption line shapes in alexandrite," J. Opt. Soc. Am. B **1**, 73-75 (1984).

13. M.A. Kramer, "Nonlinear Optical Properties of Impurity-Doped Solids," University of Rochester, Ph.D. Thesis (1985).

14. L.W. Hillman, "Interaction of modulated optical fields with saturable media and its application to laser instability," University of Rochester, Ph.D. Thesis (1984).

15. A.W. Yu, G.P Agrawal, and R. Roy, "Noise propagation from pump to secondary lasers," Opt. Lett. **12**, 806-808 (1987).

16. H. Fu and H. Haken, "Semiclassical theory of dye lasers: the single frequency and multifrequency steady states of operation," J. Opt. Soc. Am. B **5**, 899-906 (1988).
    H. Fu and H. Haken, "Multichromatic operations in cw dye lasers," Phys. Rev. Lett. **60**, 2614- (1988).

17. K.W. Koch III, "Dynamics and instabilities in homogeneously broadened lasers," University of Rochester, Ph.D. Thesis (1989).

18. J.C. Walling, O.G. Peterson, H.P. Jenssen, R.C. Morris, and E.W. O'Dell, "Tunable alexandrite lasers," IEEE J. Quantum Electron. **QE-16**, 1302-1314 (1980).

19. J.C. Walling, D.J. Heller, H. Samuelson, D.J. Harter, J.A. Pete, and R.C. Morris," Tunable alexandrite lasers: development and performance," IEEE J. Quantum Electron. **QE-21**, 1568-1581 (1985).

20. J.C. Walling, "Alexandrite lasers: Physics and performance," Laser Focus, 45-50 (Feb., 1982).

21. M.L. Shand, J.C. Walling, and R.C. Morris, "Excited-state absorption in the pump region of alexandrite," J. Appl. Phys. **52**, 953-955 (1981).

22. S. Guch, Jr., and C.E. Jones, "Alexandrite laser performance at high-temperature," Opt. Lett. **7**, 608-610 (1982).

23. M.L. Shand and H.P. Jenssen, "Energy kinetics in alexandrite," **Proceedings of International Conference on Lasers '82**, 559-562 (1982).

Chapter 4

A LASER OPERATING NEAR THRESHOLD WITH AN AMPLITUDE MODULATED PUMP INTENSITY

A. Introduction

The work described in this chapter has been motivated by a desire to understand the behavior of laser systems subjected to noise sources. The two types of noise sources which affect lasers are additive noise and multiplicative noise. The dominant source of additive noise is spontaneous emission fluctuations, while multiplicative noise arises from loss or gain fluctuations. In this chapter I will study the effects of multiplicative fluctuations on the amplitude stability of lasers.

The dynamics of a single-mode laser with multiplicative fluctuations can be very different from those of a laser with purely additive noise.[1-13] Early evidence of this fact came from studies of the statistical properties of lasers with multiplicative noise. Kaminishi *et al.*[1] measured an anomalously large normalized variance of the intensity in a single-mode laser when the laser is operated near the lasing threshold. They attributed this effect to the presence of multiplicative

noise in their laser system. A later theoretical work by Graham et al.[2] provided a theory to explain this effect which included white multiplicative noise in the third-order equations. However, in a later experiment Short et al.[3] measured the two time correlation function of a single-mode dye laser for several pump parameters. They find that while the third-order theory with white multiplicative noise explained the data for the laser operating near threshold, the data taken at higher pump parameters was not well fit by this theory. This discrepancy was later rectified by Dixit and Sahni[4], Schenzle and Graham[5], and by Fox et al.[6] Their theories included colored multiplicative fluctuations in the third-order equations. The pump fluctuations affecting dye lasers are actually much slower than the spontaneous emission fluctuations which are usually modeled by white noise. The reason that the white multiplicative noise was successful in describing the behavior of the laser near threshold is that the fast components of the white noise were incapable of affecting the laser due to critical slowing down in the laser dynamics. Higher above threshold the high frequency components of the white multiplicative noise affected the theoretical predictions in a physically incorrect manner leading to a disagreement between experimental and theoretical results.

Multiplicative noise causes other interesting effects in lasers operating near threshold. Roy and Mandel[7] observed a double-peaked probability distribution in a two-mode dye laser operating near threshold. This phenomenon was attributed to the competition between the counterpropagating modes in the laser, however their data was best fit when the affects of multiplicative fluctuations were included in their theory. Jung and Risken[8] predicted that a double-peaked intensity-distribution function results when colored multiplicative fluctuations are included in the laser theory. The significance of this result is that the double-

peaked distribution is accompanied by a discontinuous mode of the intensity of the laser as the pump parameter is increased. This discontinuity is an indication of a first-order phase transition. The existence of the double-peaked distribution function and a first-order phase transition was experimentally observed in a single-mode dye laser by Lett et al.[9] More recent experiments in a Helium Neon laser system with white multiplicative noise exhibited only second order phase transition behavior and no double-peaked distribution was observed.[10] More experiments need to be done to understand this phenomenon.

Researchers in the field of laser physics have also found it useful to study the first-passage-time (FPT) statistics of lasers. The statistics of the characteristic time in which a laser passes from the off state to the on state is affected by the presence of multiplicative fluctuations. In single mode lasers[11-13] researchers find that the second-order statistics of the FPT data are best modeled by the inclusion of multiplicative fluctuations in the theory. The two mode laser FPT problem is also best fit by a theory which includes multiplicative fluctuations[14].

These studies have concentrated on the dynamics of single-mode and two-mode lasers. To date, little attention has been given to extremely multimode laser systems. Also, most treatments have concentrated on the laser intensity, while the atomic behavior has been eliminated from the dynamics. In this chapter I address both problems by examining the response of the total intensity of the laser and the response of atomic inversion of the atoms in the gain medium of multimode lasers subjected to multiplicative fluctuations. I apply weak amplitude-modulation spectroscopy to a homogeneously broadened laser operating near the lasing threshold. The pump intensity of the laser is modulated and the behavior of the system, in response to the modulation, is studied. In particular, I treat the special case of a collisionally broadened four-level laser

system. This model was selected because it is a fairly accurate and popular description for a dye laser which is the subject of the experiment. Recently, a more thorough description of dye-laser systems has been proposed by Fu and Haken[15]. Their model describes the lower laser level as a band of vibronic levels. This model is accurate and has been successful in the description of instabilities in dye lasers; however, we find that the four-level theory is quite adequate in the description of the dynamics in our experiment.

I will formulate a theoretical analysis based on the four-level population rate equations for the material and the intensity rate equation for the field inside the cavity. The theoretical analysis is a single-mode traveling-wave theory which I compare with an experiment performed using multimode dye lasers. I show that the response of the total intensity of multimode lasers to multiplicative pump fluctuations is identical to the response of the intensity of a single mode laser. This agreement depends on the condition that the fluctuations occur over a bandwidth which is small compared to the frequency separation of longitudinal cavity modes in the multimode laser. Ogawa and Hanamura[16] show that when the modulation depth is large and the modulation frequency is comparable to the intermodal frequency spacing the operation of the laser becomes unstable.

In this chapter I measure the response of the laser intensity and the fluorescent intensity emitted by the atoms in the interaction region of the laser. The laser intensity and the fluorescent intensity represent the two output ports by which modulation energy may leave the laser system. I also consider the input port for the modulation energy. I measure the absorption of the modulation energy from the pump intensity. This is the third and final port for the modulation energy in or out of this system. With this information I perform a complete energy-balance analysis of the problem.

B. Behavior of a laser operating near threshold

A laser is an example of a fairly simple optical system which displays threshold behavior and critical slowing down. These are universal properties of nonlinear systems operating near a critical point. This behavior has attracted numerous theoretical and experimental researchers to the field of laser instabilities.[1-24] In this section I will review some of this work to prepare the reader for the experimental topic of this chapter. Perhaps the most logical place to start this problem is with the basic equations of motion for a laser. For an idealized four-level laser these are the equation for the excited-state population of the inverted transition, the equation for the atomic polarization, and the equation for the electric field inside the cavity. Since the experiment I am reporting involves a dye laser which is strongly collisionally broadened, I start with the rate equations for a four-level laser which include the rate equation for the atomic population in the excited state

$$\frac{d}{dt}\rho = -\frac{1}{T_1}(1 + I_p + I)\rho + \frac{I_p}{T_1}, \qquad (4.1)$$

and the rate equation for the intensity of the laser field inside the cavity

$$\frac{d}{dt}I = \left[g\rho - \frac{1}{\tau_c}\right]I. \qquad (4.2)$$

The dimensionless intensity of the laser, I, is defined as the rate of stimulated emission times the excited-state population lifetime T_1. The dimensionless intensity of the pump is I_p (the dimensionless intensity of the pump is the pump laser's stimulated rate times T_1), the passive cavity decay rate is τ_c, and the gain is given by

$$g = \frac{\alpha c}{L}, \qquad (4.3)$$

where α is the integrated absorption coefficient (i.e., the gain per pass) of the interaction region of the gain medium, L is the optical path length of the cavity,

and c is the speed of light. Recently, a more accurate model for the material dynamics of dye lasers has been developed. Fu and Haken[15] have developed a band model which takes into account the multilevel structure of the dye molecule. However, we find that simple four-level rate equations are adequate to describe the dynamics observed in our experiments.

Setting the time derivatives in Eqs. (4.1) and (4.2) equal to zero, we solve for the steady-state response of the excited-state population and the laser intensity. Setting the time derivatives to zero in Eq. (4.1) yields the steady-state value for the excited-state population

$$\rho_{ss} = \frac{I_p}{1 + I_p + I}. \tag{4.4}$$

This relation is always true in the steady-state. However the steady-state solution to Eq. (4.2) yields two possible steady-state conditions for the intensity of the laser I. The first possibility we will consider is the steady-state solution of the laser intensity for below threshold operation which

$$I_{ss} = 0, \tag{4.5a}$$

and then the expression for the steady-state population becomes

$$\rho_{ss} = \frac{I_p}{1 + I_p}. \tag{4.5b}$$

The interpretation of Eqs. (4.5a) and (4.5b) is that when the laser is off the atomic population behaves as it does in the absence of the laser cavity. When you perform a linear stability analysis about this laser-off solution (see Appendix C), two eigenvalues result. One eigenvalue is always negative (indicating stability) for all values of the pump, I_p. The other eigenvalue is negative for values of the pump intensity such that

$$I_p \le I_{p,thr}. \tag{4.6}$$

This is another way of saying that the laser stays off when the pump intensity is below the threshold value.

Next we consider the on solution for which the laser intensity is nonzero. The steady-state solution for the intensity is

$$I_{ss} = \frac{I_p}{I_{p,thr}} - 1, \tag{4.7a}$$

and substituting this expression for I_{ss} into Eq. (4.4) yields the result that the population, and therefore the gain, clamps to a constant value and is independent of the pump intensity above threshold,

$$\rho_{ss} = \frac{1}{g\tau_c}. \tag{4.7b}$$

This phenomenon is referred to in the literature as gain or inversion clamping[25] and it represents discontinuous behavior for both the laser intensity and the inversion as the pump intensity is varied near its threshold value, $I_{p,thr}$. Once again a stability analysis (Appendix C) yields that one eigenvalue is negative for all values of pump intensity while the other eigenvalue displays an instability at $I_p = I_{p,thr}$. This second eigenvalue is

$$\lambda = -\left(\frac{1}{\tau_c}\right)\frac{I_{ss}}{1 + I_{ss} + I_p}. \tag{4.8}$$

The significance of this eigenvalue will be made apparent later in this chapter. The discontinuous behavior in the atomic variables can be seen if we plot the intensity of the laser versus pump power and the atomic inversion versus pump power in Fig. 4.1. The unstable branches of the solutions are represented with dotted lines while the stable branches are represented with solid lines. The laser intensity is zero until the pump intensity reaches the threshold value. Similarly, the excited-state population increases smoothly with increasing pump power

until the threshold pump intensity is reached at which point there is no further increase.

Up until now we have studied the static behavior of a laser. The dynamic behavior of a laser can be quite different from the steady-state behavior and furthermore there is much more information to be gained by considering the dynamic response of a nonlinear system to transients in the behavior of a control parameter, such as the pump intensity in this case. To illustrate the dynamic behavior of a laser near the lasing threshold I have plotted data from a simple experiment in which the pump intensity is swept back and forth through its threshold value in a linear fashion. The results of this experiment are shown in Figs. 4.2(a-d). In Fig. 4.2(a) I have plotted the intensity of the laser as a function of the pump intensity for a slow sweep rate of 100Hz. This behavior is quite similar to the steady-state behavior plotted in Fig 4.1. The similarities disappear as the sweep rate is increased to 40 kHz for the data shown in Fig 4.2(c). In this case the laser seems to remain off as the pump intensity is increased beyond the threshold value and then the laser jumps rapidly to the on state. As the pump intensity is rapidly decreased the laser remains on past the threshold intensity instead of returning abruptly to zero as in the steady-state case. A similar behavior is seen in the response of the intensity of the fluorescence emitted from atoms in the interaction region of the gain medium. In Fig. 4.2(b) the fluorescent intensity versus pump-laser intensity is plotted for a sweep rate of 100Hz. The behavior of the fluorescent intensity as a function of pump intensity displays a discontinuity as did the response of the excited-state populaton in Fig. 4.1. The response of the fluorescent intensity does not flatten out completely as in Fig. 4.1 however. The reason for this is that the multi-level nature of the dye molecule allows for a build-up of population in
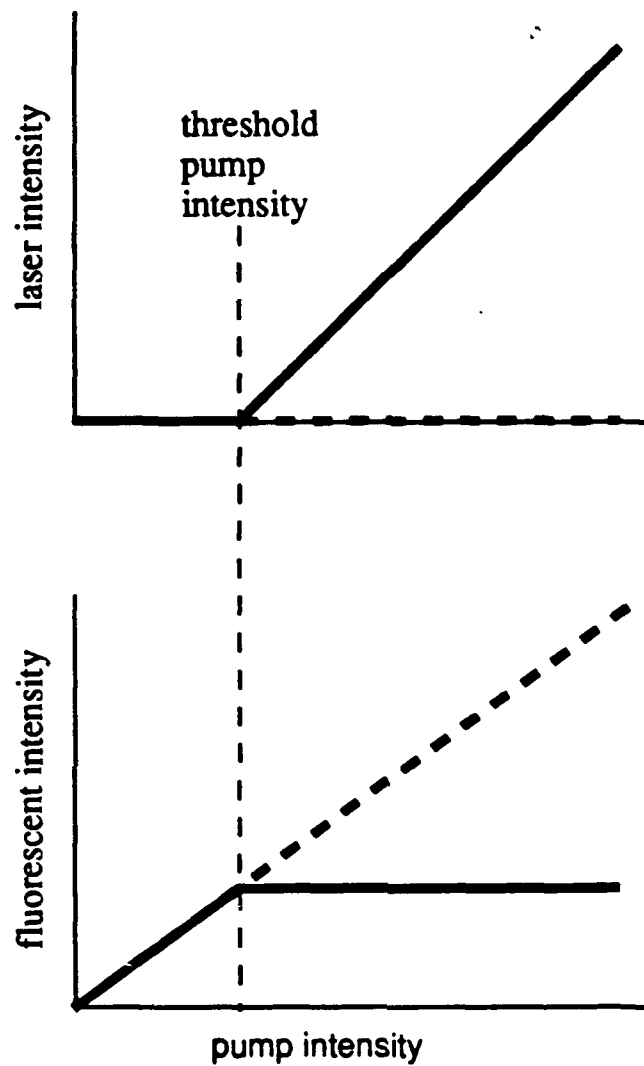
Fig. 4.1 Steady-state response of the laser intensity and the fluorescent intensity. The steady-state response of the intensity of a canonical four-level laser is plotted versus the pump intensity in the upper graph in this figure. The steady-state behavior of the fluorescent intensity for a four-level laser is plotted in the lower graph of this figure. The solid lines represent the behavior of the stable solutions for these variables above and below threshold while the dotted lines represent the behavior of the unstable "off-solutions" above threshold.

the lasing levels and therefore the excited-state population merely increases at a different rate above threshold rather than clamping to a constant value. This discontinuous response changes when the sweep rate is increased to 40 kHz as in Fig. 4.2(d). The fluorescent intensity overshoots the on solution and a hysteresis loop develops here as in the response of the laser intensity. This behavior has been studied theoretically and experimentally and is referred to as a delayed bifurcation.[17-22] The laser's behavior does not make the transition to the stable solution when a control parameter is swept faster than some characteristic time constant.

The delayed bifurcation in the behavior of the laser's intensity near the first threshold has been theoretically treated by Mandel and co-workers[17] and others[18-20]. They predict the delayed bifurcation as a control parameter is swept through a critical point. Sharpf et al.[21] explored the response of an argon ion laser as the loss of the cavity is swept through the threshold value. They found that the laser undergoes a delayed bifurcation as the loss is swept through the threshold value. Furthermore, the width of the delay in units of loss increases as the rate of the sweeping is increased. In a similar experiment Papoff et al.[22] studied a delayed bifurcation with a square-wave modulation. The mean switching time increases as a control parameter is brought near a period-doubling bifurcation point. Also, Gage and Mandel[23] carried out an experiment in a bidirectional ring dye laser. They observed hysteresis in the first passage time of the opposite running modes of the ring laser as the asymmetry of the cavity loss was swept at a rate of 10 Hz. These experiments demonstrate the usefulness of modulating the gain or the loss of a laser to study non-steady-state laser dynamics. The presence of the delayed bifurcation in the dynamics of the laser is an example of critical slowing down. The time constant which
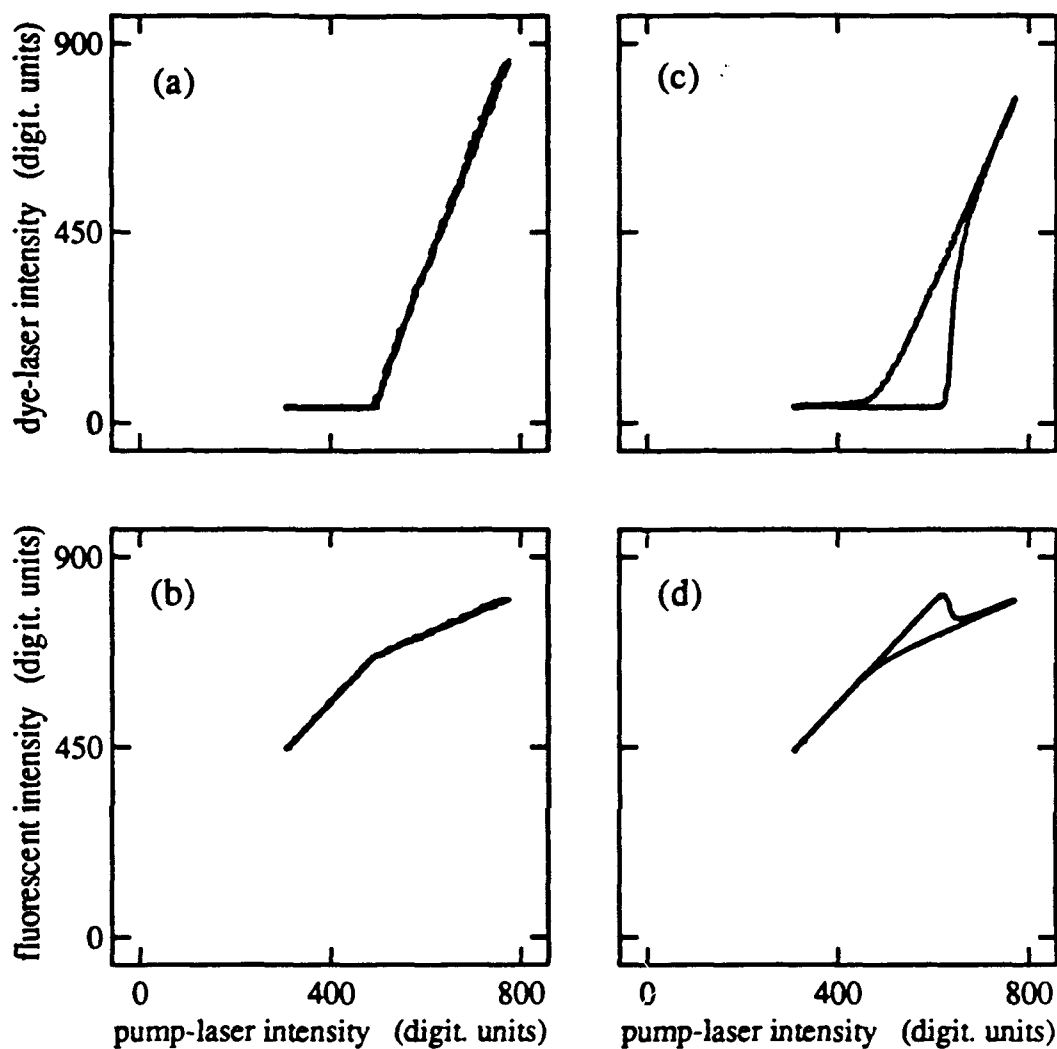
Fig. 4.2(a-d) Dynamic response of the dye-laser intensity and the fluorescent intensity. The intensity of the dye laser is plotted versus a pump-laser intensity which is swept with a triangle wave at: (a) 100 Hz and (c) 40 kHz. The intensity of the fluorescence emitted from the interaction region of the gain medium is plotted versus a pump-laser intensity which is swept with a triangle wave at: (b) 100 Hz and (d) 40 kHz.

characterizes the response of the laser is large because the driving forces (i.e. the stimulated emission rate) diminish to zero at the lasing threshold.

The critically-slowed behavior of a laser is manifested in the laser's inability to follow the rapid temporal fluctuations of the pump intensity. These effects can in part be characterized by examining the power spectrum of the laser's intensity when it is driven by a fluctuating pump intensity. Yu *et al.*[24] measured the power spectrum of the intensity of an argon-pumped single-mode cw dye laser. The intensity of the laser behaves as a low-pass amplifier to the amplitude fluctuations of the pump. Furthermore, the bandwidth of the fluctuations of the intensity of the laser decreases as the intensity of the pump is reduced to the threshold value. This intensity-dependent bandwidth is a good example of critical slowing down in a nonlinear system operating near a critical point. Similar behavior has been predicted in an electrically pumped solid-state laser with current noise. Agrawal and Roy[25] show that at high intensities, the power spectrum of the intensity of a semiconductor laser is affected by current noise in the pumping mechanism. The bandwidth of the intensity noise spectrum of a laser is determined by a systematic time constant that depends on the intracavity laser-field intensity.

These studies have concentrated on the dynamics of single-mode lasers. To date very little attention has been given to multimode systems. How does the behavior of the intensity of a multi-mode laser compare to the behavior of a single mode laser's intensity? Also, most treatments have concentrated on the laser intensity, while the atomic dynamics have received little attention. In this chapter, I address both problems by examining the response of the total intensity and the atomic inversion in multimode lasers subjected to multiplicative fluctuations. I calculate the response of a single-mode laser to a sinusoidally

modulated pump. Expressions for the first-harmonic response of the laser intensity and the excited-state population of the laser transition are derived. I compare these theoretical predictions with experiments in multimode cw dye-laser systems. Amplitude modulation (AM) spectroscopy is used to probe the near-threshold dynamics of these lasers. This form of spectroscopy has been used to probe the absorption spectrum of strongly driven atomic systems.[27-31] In this experiment I modulate the intensity of the pump beam and study the total intensity of the laser and the intensity of the fluorescence emitted by atoms in the gain medium (the fluorescent intensity is proportional to the excited-state population). I report a phase sensitive measurement of the modulations induced in the laser and the fluorescent intensities using a lock-in amplifier. The modulation frequency is varied to obtain a spectrum of the laser's response. The results of the experiment will be quantitatively compared with the single-mode laser theory.

The response of the fluorescent intensity to a modulated optical field has been considered by Saxena and Agarwal.[32] They treat the case of a two-level atom in free space subjected to an amplitude modulated field. The calculations reveal that the fluorescence responds as a Lorentzian whose width broadens as the intensity of the laser is increased and that for large field strengths a peak occurs in the AM spectrum of the fluorescence at twice the Rabi frequency. This result is quite interesting though not closely related to the present work.

C. Theory of a laser with pump-intensity modulation

From here on I will not be concerned with a steady-state analysis but instead will be analyzing the temporal response of the laser by modulating the pump intensity $I_p(t)$ and observing the response of the laser intensity $I(t)$ and

the response of the excited-state population expectation $\rho(t)$ to the modulated pump. The pump intensity $I_p(t)$ is weakly modulated at the angular frequency $\delta\omega$ as

$$I_p(t) = \overline{I}_p + 2\delta I_p \cos(\delta\omega t). \qquad (4.9)$$

The dc or time-averaged pump intensity is represented by $\overline{I}_p$, and the amplitude of the modulation sidebands is represented by δI_p, which is considered small in this experiment. The modulation frequency $\delta\omega$ is expressed in units of radians per second.

Floquet's theorem tells us that in the stationary state, the excited-state population and the laser intensity will respond at higher harmonics of the modulation fundamental $\delta\omega$. Since we are interested in the stationary-state response, we can expand the temporal response of these variables in a harmonic series of overtones of $\delta\omega$. The excited-state population can be written as

$$\rho(t) = \sum_{n=-\infty}^{\infty} \rho_n \exp(in\delta\omega t), \qquad (4.10a)$$

and the intensity of the laser is given by

$$I(t) = \sum_{n=-\infty}^{\infty} I_n \exp(in\delta\omega t). \qquad (4.10b)$$

The nth-harmonic response of the excited-state population is ρ_n, and the nth-harmonic response of the laser intensity is I_n. When we substitute Eqs. (4.10a) and (4.10b) into Eqs. (4.1) and (4.2) and equate terms of equal time dependence, we get the following recurrence relation:

$$(1 + \overline{I}_p + in\delta\omega T_1)\rho_n$$
$$= -\sum_{m=-\infty}^{\infty} \rho_m I_{n-m} - \delta I_p(\rho_{n+1} + \rho_{n-1}) + \overline{I}_p\delta_{n,0}$$
$$+ \delta I_p(\delta_{n,1} + \delta_{n,-1}), \qquad (4.11)$$

from the excited-state population rate equation, Eq. (4.1), and

$$(1 + in\delta\omega\tau_c)I_n = g\tau_c \sum_{m=-\infty}^{\infty} \rho_m I_{n-m}, \qquad (4.12)$$

from the intensity rate equation, Eq. (4.2), where $\delta_{i,j}$ is the Kronecker delta function.

We can analyze these recurrence relations for a particular value of the subscript n to obtain the nth-harmonic response of $I(t)$ and $\rho(t)$. Since we use weak modulation in this experiment, we can truncate the harmonic expansion of the excited-state population and that of the intensity of the laser to first order ($n=1$). Likewise, we ignore all products which are of order two or higher (i.e. neglect terms such as $\delta I_p \rho_1$ and $\rho_1 I_1$). With these simplications, we get four recurrence relations: two from the excited-state population recurrence relation, Eq. (4.11) for $n = 0$ and $n = 1$; and two from the intensity recurrence relation, Eq. (4.12). For the index $n = 0$ we recover the steady-state solutions we obtained without the modulation (i.e., $\rho_0 = \rho_{ss}$ and $I_0 = I_{ss}$). This result is consistent with the perturbative approach we are using. Solving Eqs. (4.11) and (4.12) for $n = 1$, we get the first-harmonic response of the intensity of the laser,

$$I_1 = I_0 \left[\frac{1}{\rho_0} - 1 \right] \delta I_p \frac{[I_0 - (\delta\omega T_1)(\delta\omega\tau_c)] - i[(1 + \overline{I}_p + I_0)(\delta\omega\tau_c)]}{[(1 + \overline{I}_p + I_0)(\delta\omega\tau_c)]^2 + [I_0 - (\delta\omega T_1)(\delta\omega\tau_c)]^2}, \qquad (4.13)$$

The time-averaged responses of the intensity and the excited-state population are I_0 and ρ_0, respectively.

The first-harmonic response of the excited-state population can be derived in a similar manner, and the result is

$$\rho_1 = (1 - \rho_0)(\delta\omega\tau_c)\delta I_p \frac{[(1 + \overline{I}_p + I_0)(\delta\omega\tau_c)] + i[I_0 - (\delta\omega T_1)(\delta\omega\tau_c)]}{[(1 + \overline{I}_p + I_0)(\delta\omega\tau_c)]^2 + [I_0 - (\delta\omega T_1)(\delta\omega\tau_c)]^2}. \qquad (4.14)$$

To understand this phenomenon better, I plot the response of the intensity of the laser and of the excited-state population in the same plot in Figs. 4.3(a)

and 4.3(b). In these figures the population lifetime is one one-hundredth the cavity lifetime $T_1 = 0.01\tau_c$, and the laser is operating 10% above threshold, or $I_0 = 0.1$. The first thing to notice is that the in-phase first-harmonic response of the laser intensity and the first-harmonic response of the excited-state population cross each other at the half-maximum values for each. The population response is a high-pass filter for fluctuations the laser cannot follow. Furthermore, in this limit where $(\delta\omega T_1)(\delta\omega\tau_c) \ll I_0$, the response of the intensity of the laser to a modulated pump intensity is a Lorentzian whose half-width at half-maximum (HWHM) is equal to the reciprocal of the cavity lifetime $1/\tau_c$ times the "saturated" pump parameter β, which I define as

$$\beta = \frac{I_0}{1 + I_0 + \overline{I}_p}. \qquad (4.15a)$$

The bandwidth of the laser turns out to be equal to the stability exponent of the laser [see Eq. (4.8)]. By measuring the modulation bandwidth of the laser we are measuring the stability exponent of the laser! In the parameter regime of the experiment, the laser and pump intensities are nonsaturating (i.e., $I_0, \overline{I}_p \ll 1$); consequently, the pump parameter becomes

$$\beta \simeq I_0 = \frac{\overline{I}_p}{I_{p,thr}} - 1. \qquad (4.15b)$$

This "unsaturated" pump parameter is in agreement with previous definitions of the pump parameter[1] [see Eq. (4.7a)].

The response of the excited-state population displays a dip at low modulation frequency. I consider this result to be a manifestation of the effects of inversion clamping at nonzero frequencies. Another way to interpret this result is that the laser acts as a pump-intensity noise eater, keeping the inversion of the atoms constant in the presence of low frequency pump fluctuations.
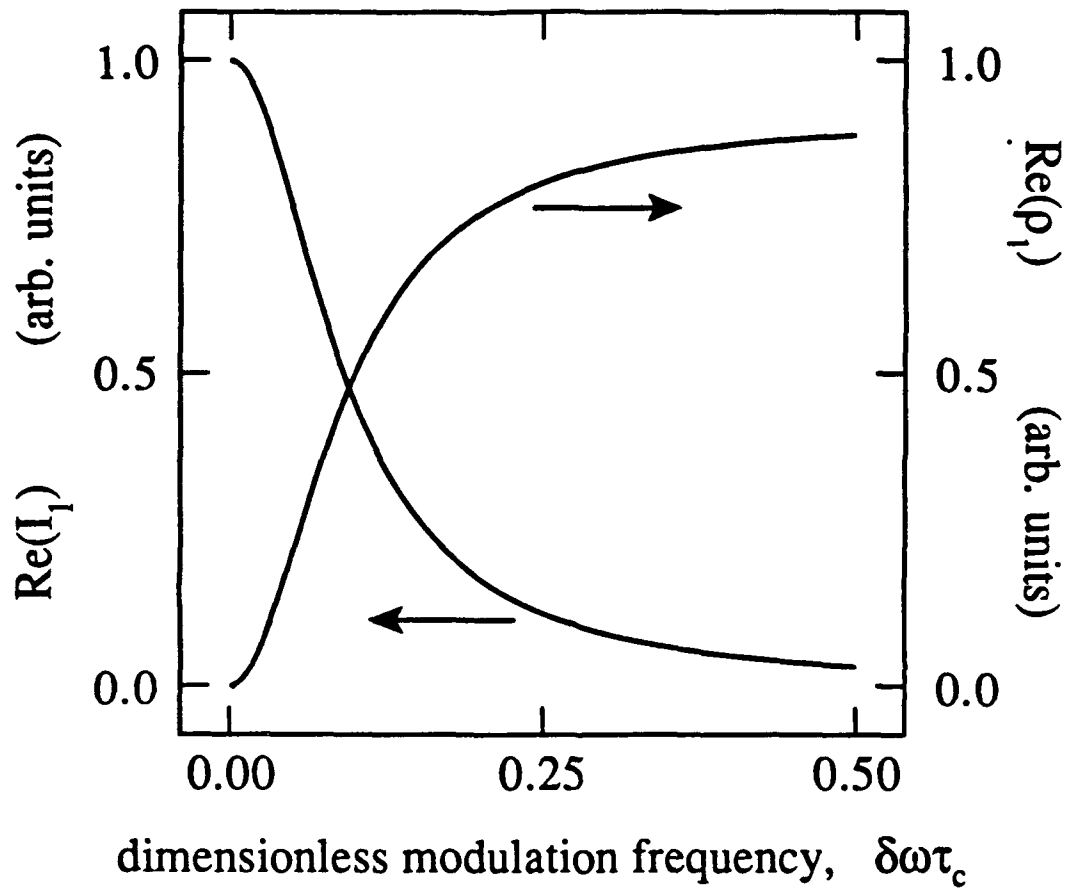
Fig. 4.3(a) The in-phase first-harmonic response of the laser intensity, $Re(I_1)$, and the in-phase first-harmonic response of the excited-state population, $Re(\rho_1)$, versus the normalized pump modulation frequency $\delta\omega\tau_c$. The parameters used in this figure are $T_1 = 0.01\tau_c$, and $I_0 = 0.1$ (ie. the laser is 10% above threshold).
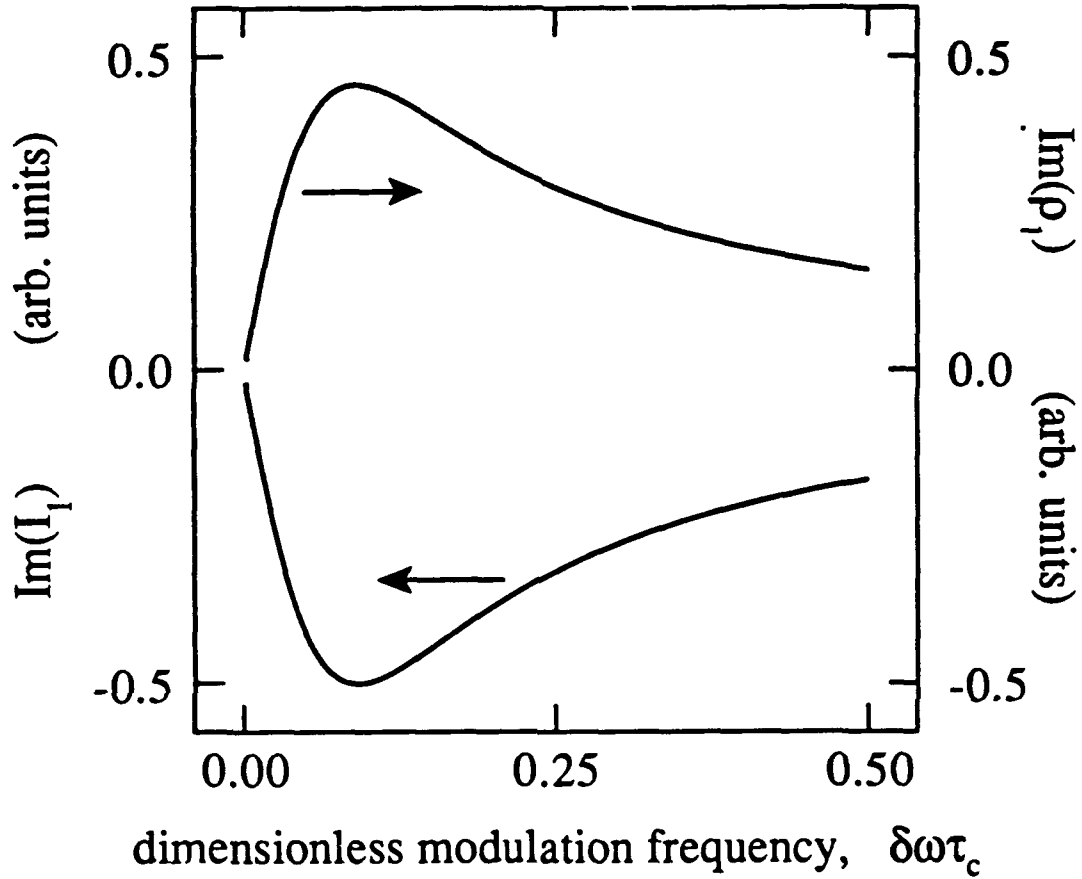
Fig. 4.3(b) The in-quadrature first-harmonic response of the laser intensity, $Im(I_1)$, and the in-quadrature first-harmonic response of the excited-state population, $Im(\rho_1)$, versus the normalized modulation frequency $\delta\omega\tau_c$. The parameters used in this figure are $T_1 = 0.01\tau_c$, and $I_0 = 0.1$ (ie. the laser is 10% above threshold).

D. Experimental Apparatus

1. The amplitude stabilization process

As I showed in the theoretical section, the temporal response depends strongly on the pump parameter or rather the amount the laser is operated in excess of threshold. In order to perform an accurate measurement of the laser response and compare it quantitatively with the theory you must be able to accurately determine the pump parameter and prevent it from varying during the modulation measurement. This is the crux of the experimental technique. The pump parameter must be constant during a modulation spectral measurement. To solve this problem we constructed a unique amplitude stabilization circuit. The circuit holds the output intensity of the laser fixed with respect to low frequency fluctuations while giving little correction at the frequencies used to modulate the pump intensity for the modulation experiment. In simpler terms, I constructed a low frequency amplitude stabilization circuit. A unique aspect of this circuit is that the output intensity of the laser is being stabilized by adjusting the intensity of the pump laser.

In order for the reader to appreciate the purposefulness of the inclusion of this circuit I will perform a brief analysis of the measurement of the pump parameter and the effect of fluctuations on this measurement. Consider a measurement of the laser intensity I_0. In general the measurement will yield a result $I_0 \pm \Delta I_0$. We can arrive at an expression for ΔI_0 by partially differentiating Eq. (4.15b)

$$\Delta I_0 = \frac{\Delta \bar{I}_p}{I_{p,thr}} - \frac{\Delta I_{p,thr}}{I_{p,thr}} \frac{\bar{I}_p}{I_{p,thr}}. \qquad (4.16)$$

The first term on the right hand side of Eq. (4.16) describes fluctuations in the output intensity of the laser arising from fluctuations in the pump amplitude. These fluctuations should be corrected by the circuit and cause no further dif-

ficulty. It is the fluctuations described by the second term on the right hand side of Eq. (4.16) which cause problems. These fluctuations arise from a change in the threshold pump power or rather a change in the amount of loss in the cavity. We cannot compensate for these losses properly by adjusting the pump power. The loss value has been changed and all we can do is compensate for this change in loss by adjusting the pump power accordingly. However, in doing this we are actually keeping the pump parameter constant which is what we want to do. However the systematic time constant depends on the product of the pump parameter and the reciprocal cavity lifetime $(1/T_1)$, or cavity loss rate. Therefore a large drift in the loss of the cavity would cause experimental error beyond our capacity to compensate.

Since the entire experiment is carried out over a small range of pump-parameters $(0 \leq 0.15)$ great care must be taken to insure accuracy in the determination of the pump parameter. In fact the steps taken in pump parameters between successive spectra is often less than 1%! If we look at Eq. (4.15) it is easy to see that a drift of one percent in either the pump intensity I_p or a comparable drift in the threshold $I_{p,thr}$ results in an error comparable to the stepsize of the data. This completely blurs the results we are after. Instead of relying on a direct measurement of these individual quantities, we measured only I_0 for each spectra and infer the value of the pump I_p from this measurement and a slope efficiency measurement made prior to each data set. That is to say that the value of I_p is obtained by dividing the laser intensity I_0 by the slope efficiency $\delta I_0/\delta I_p$.

Now that we are content with the necessity of the stabilization circuit and its application we can discuss the circuit itself. In Fig. 4.4 is a block diagram of the stabilization circuit and the lasers it acts upon. A fast photodiode is used to
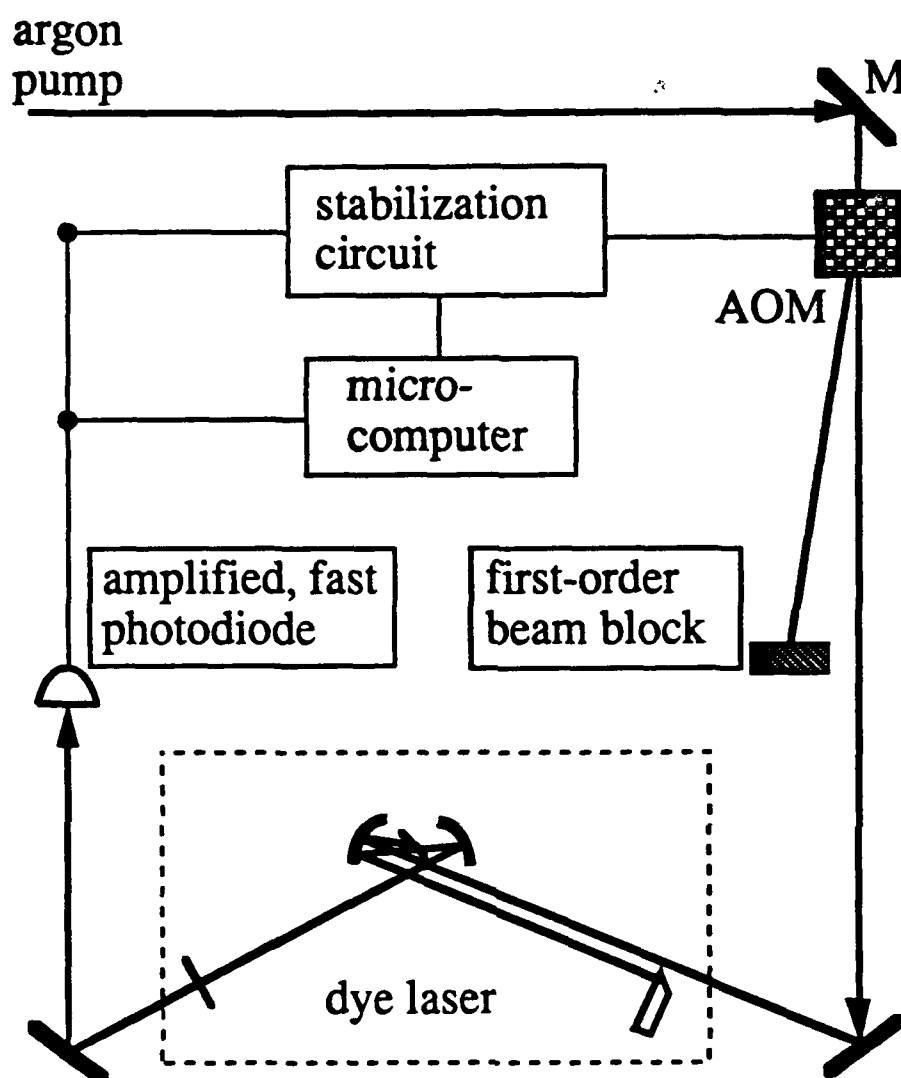
Fig. 4.4 Block diagram of the amplitude stabilization aparatus. The signal from an amplified fast photodiode is fed to the micro computer and the stabilization circuit electronics. The circuit performes a comparison with a DC voltage supplied by the computer and sends an error signal to the acousto-optic modulator (AOM). The AOM diffracts a variable amount of intensity out of the pump-laser beam to control the dye-laser intensity.

measure the output intensity of the dye laser. The signal from this detector is fed to the circuit which processes the signal and supplies a controlling voltage to the acousto-optic modulator (AOM) positioned in the path of the argon pump beam before it hits the dye laser. The AOM diffracts a variable percentage of the pump beam intensity out of its path to the dye laser. In this way the voltage from the stabilization circuit adjusts the pump intensity. Since the detection of the error signal at the photodetector occurs after the controling transducer (the AOM) this is a closed-loop stabilization process. We used the Intra Action ADM-40 acousto-optic modulator with the DE-40M VCO Deflector Driver for the closed-loop stabilization.

In Fig. 4.5 is a detailed circuit diagram of the stabilization circuit. The design is quite simple. The voltage from the photodiode is fed into the first stage amplification of 10x. After the signal is amplified the second op-amp takes a difference between the amplified signal and a DC voltage, which is set by the computer and a coarse-adjustment potentiometer. The feedback for the second op-amp is a unique design which provides a large low-frequency gain without the need for a separate woofer device. This feedback is similar in nature to the design discussed in Chapter 3 for the laser-frequency stabilization circuit. The components in this circuit were chosen to provide minimal correction and therefore little phase error at 5 kHz which is the lowest frequency used in the modulation measurement. All op-amps used in the cicuit are Motorola 356.

2. Measuring the AM spectrum of the dynamic variables

In this section I describe the experimental measurement of the frequency response of multimode ring and standing-wave dye lasers operating near threshold. A diagram of the experimental apparatus is shown in Fig. 4.6. A commercially

123

signal input from photo-diode

37μF

10k

1k

1k

20k pot.   500Ω

100k

11μF   2 k

1μF

+15V

output to AOM

5k pot.

3μF

5.5k   5.5k

56k
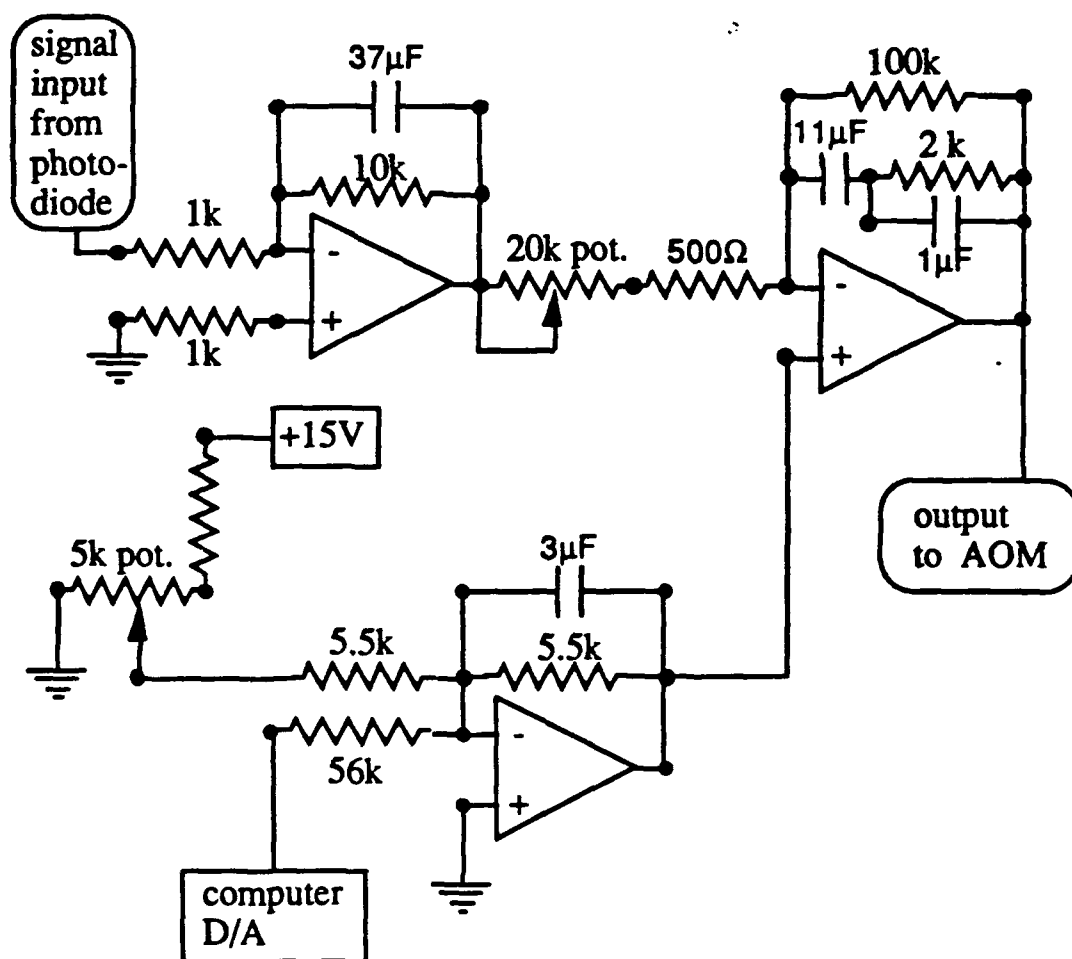
computer D/A

Fig. 4.5 Circuit diagram for the low-frequency amplitude stabilization circuit. The signal from the intensity detector is compared via a subtraction with a voltage input from the computer digital-to-analog converter. The right-most op-amp performs this subtraction and supplies the resulting voltage to the acousto-optic modulator (AOM) to adjust the pump-laser intensity as necessary. All op-amps are Motorola 356 type.

available dye jet supplied by Coherent Inc. is used in all the laser cavities discussed. The dimensions of the jet are 3 mm by 0.3 mm. The jet is run at approximately 30-35 psi. with a mixture of ethylene glycol and rhodamine 6G. The concentration of the dye is approximately 1.5 mg/liter giving a single-pass absorption of the 5145 angstrom argon line of 95%. Two 5 cm radius of curvature high-reflector focusing mirrors are employed to focus and recollimate the laser through the dye jet. One of the mirrors also serves to focus the argon pump beam into the dye jet. The interaction region is near the waste of the pump laser giving a 10-15 μ diameter interation region. A knife-edge high reflector mirror is used in all cavities to allow the argon pump beam to be brought in parallel to the cavity axis (see Fig. 4.6). In the case of the high-Q cavities, a fourth high-reflector is used; otherwise, a 5% output coupler is used. No dispersive elements are used in any of the cavities. Furthermore, the lasers operate in an extremely multimode state as was verified using a Fabry-Perot interferometer. In fact, the lasers' time-averaged spectra each consisted of hundreds of longitudinal modes at the highest pump settings used in the experiement, and at the lowest pump settings the spectra consisted of tens-of-modes.

The argon pump beam is brought in parallel to one arm of the laser cavity. The pump beam passes through both AOM1 and AOM2 before impinging upon the dye jet. The first acousto-optic modulator, AOM1, is driven by the slow amplitude noise-eater circuit to stabilize the dye-laser intensity. The second modulator, AOM2, is the Isomet 1205C modulator driven by the 232A-1 driver. The AOM2 is driven by a Wavetek model 188 Sweep/Function Generator. The Wavetek supplies a sinusoidally varying voltage to drive the AOM2. The Wavetek accepts an external voltage over the range ±1 Volt to vary the oscillator frequency remotely. The computer sweeps the frequency during the
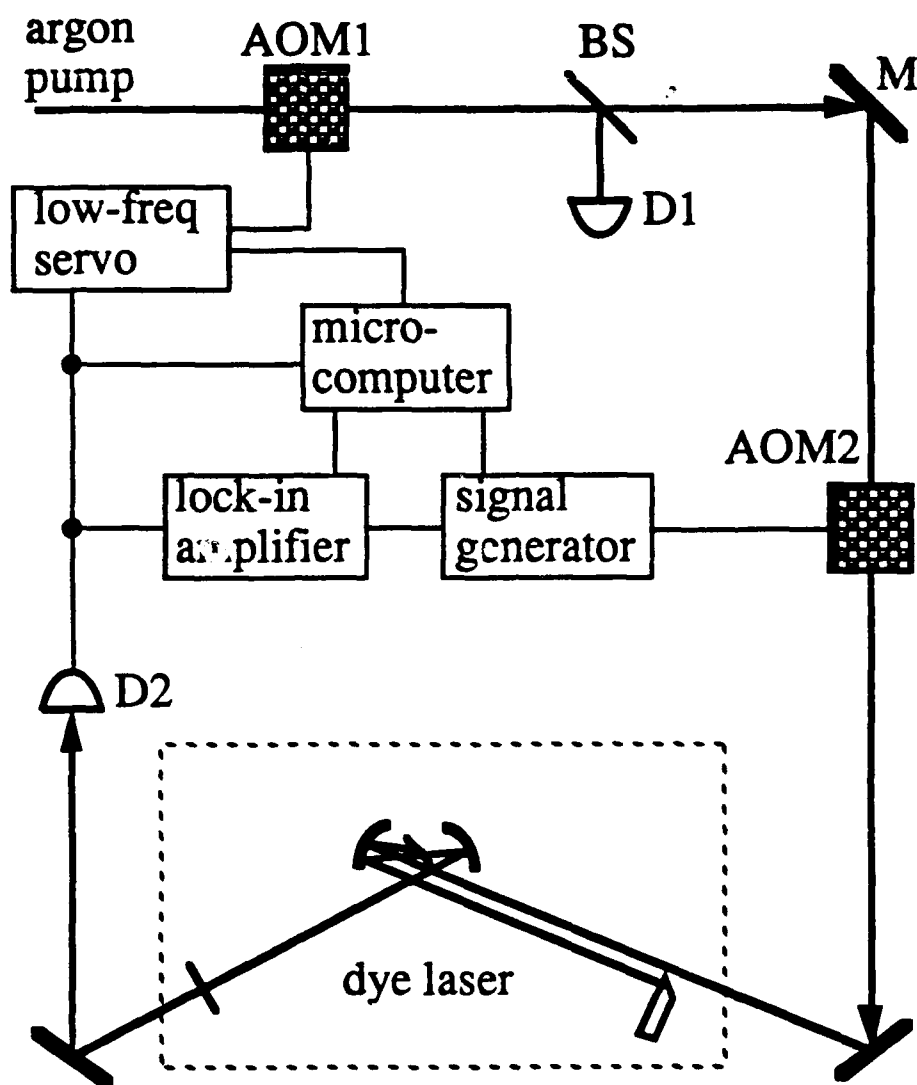
Fig. 4.6 Experimental setup. The following labeling conventions are used in this figure: AOM1- acousto-optic modulator for amplitude-stabilization servo circuit; AOM2- acousto-optic modulator for modulating the pump intensity; BS- beam splitter; M- mirror; D1- detector for measuring the argon-ion pump-beam intensity; D2- detector for measuring the dye-laser intensity.

experiment and also sets the offset voltage for the amplitude noise eater circuit. The detector D2 measures the dye-laser intensity. The signal from this detector is fed to the lock-in amplifier (EG&G PARC model 5210 dual-phase Lock-in Amplifier). The lock-in amplifier evaluates the signal at the modulation frequency by performing a phase sensitive measurement. The reference signal to the lock-in amplifier is provided by the Wavetek signal generator. The in-phase and in-quadrature signal from D1 are reported by the lock-in amplifier via an IEEE parallel interface to the PDP 11\23 microcomputer. The time-averaged dye-laser intensity is also recorded by the computer along with the time-averaged argon pump-laser intensity, as measured by detector D1. To obtain a slope-efficiency measurement we sweep the pump intensity between the threshold value and a value 20% above threshold and record the dye-laser and pump-laser intensities at each setting. The slope and intercept of this data are used in determining the value of the dimensionless intensity, I_0, of the dye laser. This measurement is crucial to fitting the data.

E. Discussion of experimental results

1. Multimode lasers and single-mode theory

In the first part of the experiment I show that single-mode traveling wave laser theory is an accurate prediction of the dynamics of the total intensity of multi-mode lasers with a fluctuating pump intensity. Sinusoidal amplitude modulation is applied to the pump intensity of these multimode dye lasers and the response of the output intensity of the laser is studied with phase sensitive detection techniques. In particular, the experiment exemplifies the critical slowing down of the temporal behavior of the total intensity of these lasers. In this section I analyze high-Q cavities in which all the mirrors are high reflectors.

The passive-cavity lifetimes of these laser cavities are maximized in each case by extending their lengths to 1 meter for the standing wave cavities and 2 meters for the ring cavities. The free spectral range of these cavities is about 150 MHz. These high-Q cavities typically have lifetimes τ_c on the order of 200-400 ns.

The first cavity I consider is the high-Q standing wave cavity. This cavity is actually unstable to single longitudinal mode oscillation due to the effects of spatial hole burning. In Fig. 4.7 I plot the dye-laser intensity as a function of time after the pump is extinguished in a heavy-side step fashion. All the data points are fit to an exponential, except for those earlier than 100 ns after the start of the decay, since these times coincide with the turn-off time of the pump intensity. This procedure insures that the lifetime obtained from the fit is truly the passive-cavity lifetime instead of an active-cavity lifetime. I assume here that the unpumped dye molecules are not absorbers at the dye laser wavelength. The solid line in Fig. 4.7 represents the best theoretical fit to the data corresponding to a cavity lifetime of 252 ± 4 ns. I will compare this directly measured cavity decay rate with the lifetime derived from fitting the amplitude modulation spectrum of the laser.

In Fig. 4.8 I plot the signal from the output of the lock-in amplifier (squares) versus the modulation frequency, $\delta\omega/2\pi$, for several different pump powers. This voltage corresponds to the in-phase first-harmonic response of the dye-laser intensity. The curves broaden as the pump parameter, β, is increased [see Eqs.(4.15a) and (4.15b)]. All modulation spectra shown in Fig. 4.8 are fit simultaneously using the time-averaged intensity I_0, which is directly measured before each modulation run, and the data points from the lock-in as constraints. The best theoretical fit using single-mode laser theory are also shown in Fig. 4.8 (solid lines). The cavity lifetime derived from fitting the data in Fig. 4.8

Fig. 4.7 Dye-laser intensity vs time for a multimode, high-Q standing-wave laser. This figure shows the decay of the dye-laser intensity after a rapid and complete turn-off of the pump beam. The solid line represents the best-fit exponential whose time constant is 245 ns.

Fig. 4.8 The in-phase first-harmonic response of the laser intensity I_1 vs the pump modulation frequency $\delta\omega/2\pi$. I plot the in-phase or x-channel output of the lock-in amplifier vs frequency for a high-Q standing-wave laser for several values of the pump parameter β given in Eq. (4.15). The curves, from left to right, correspond to $\beta=0.011$, $\beta=0.021$, $\beta=0.031$, $\beta=0.041$, $\beta=0.050$, $\beta=0.060$, and $\beta=0.070$. The solid lines represent the single-mode best-theoretical fit to all the data fit simultaneously. The cavity lifetime which gives this fit is 230 ns.

Fig. 4.9 The modulation bandwidth (HWHM) of the in-phase first-harmonic response of the intensity of the laser vs the pump parameter β. The curves shown in Fig. 4.8 were individually fit to Lorentzians and the bandwidth (HWHM) of these fits are plotted here with squares. The solid line represents the result of a linear regression performed on these points. The slope of this line is proportional to the reciprocal of the cavity lifetime $1/\tau_c$. The cavity lifetime we get from the slope is 235 ns.

is 230 ns, which agrees with the lifetime we measure directly from the data in Fig. 4.7 to within 7%. This implies that single-mode theory is quite adequate in describing the behavior of the total intensity of a multimode standing-wave laser operating near the first threshold.

Another way of analyzing the data is to separately fit the individual modulation spectra to Lorentzians and plot the HWHM of each file versus the measured pump parameter β. In Fig. 4.9 I plot the HWHM of the individual fits together with the best-fit straight line through the data. The reciprocal of the slope of this line is equal to 2π times the cavity lifetime τ_c. The value of the cavity lifetime obtained from the slope of this curve is 235 ± 3 ns, which is also in close agreement with the value obtained directly from the data shown in Fig. 4.7.

I carried out the same experiment in a high-Q bidirectional ring laser. For this case, I measured the total intensity exiting the ring cavities from one direction of propagation. The results are independent of which direction of propagation is studied. The data in Fig. 4.10 shows the exponential decay of the laser intensity. The exponential fit (solid line) corresponds to a lifetime of 329 ± 4 ns. In Fig. 4.11 I plotted the in-phase response of the total intensity exiting the laser cavity from one propagation direction of the multimode ring dye laser. The cavity lifetime which gives the best simultaneous fit to all these data using single-mode theory is 335 ns. In Fig. 4.12 I plotted the HWHM of the individual Lorentzian fits to these data versus the pump parameter β, given in Eq. (4.15a). A linear regression is performed on this data to obtain a cavity lifetime of 344 ± 2ns. This value for the lifetime is within 5% of the value obtained directly from the data shown in Fig. 4.10.

The conclusion is that single-mode laser theory accurately describes the behavior of the total intensity of multimode lasers. Experimental results with
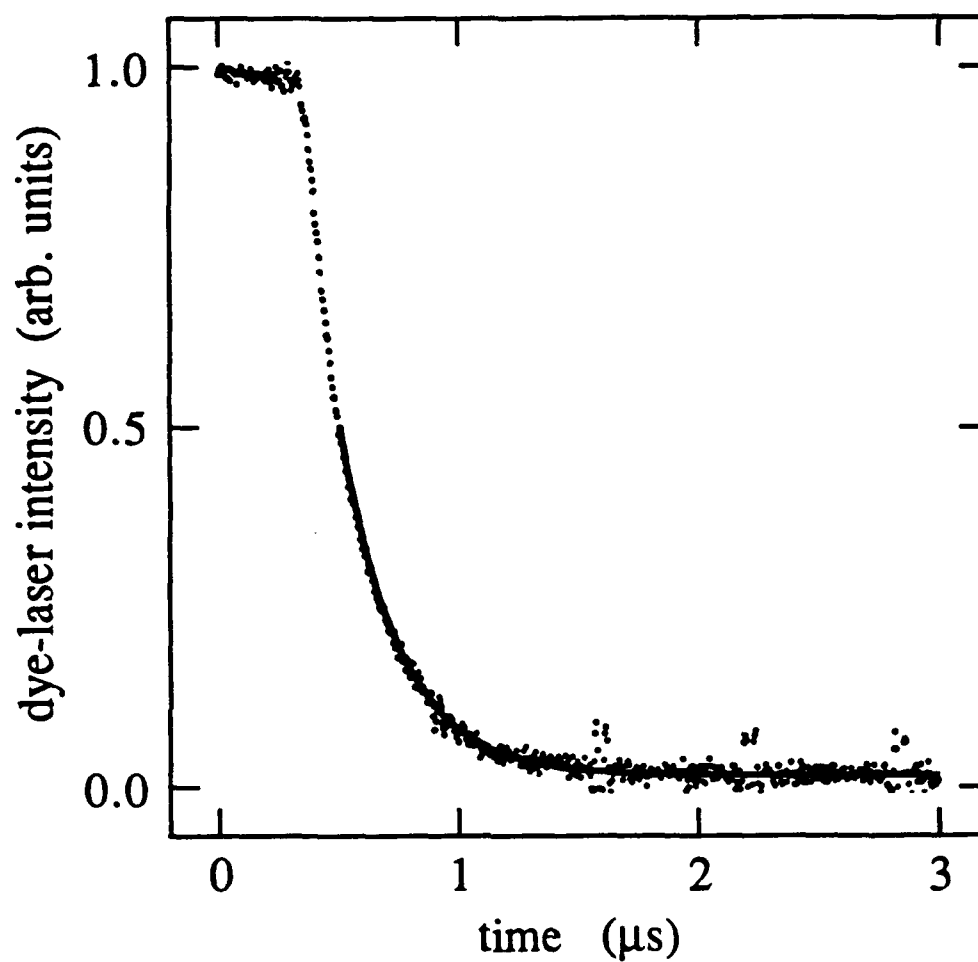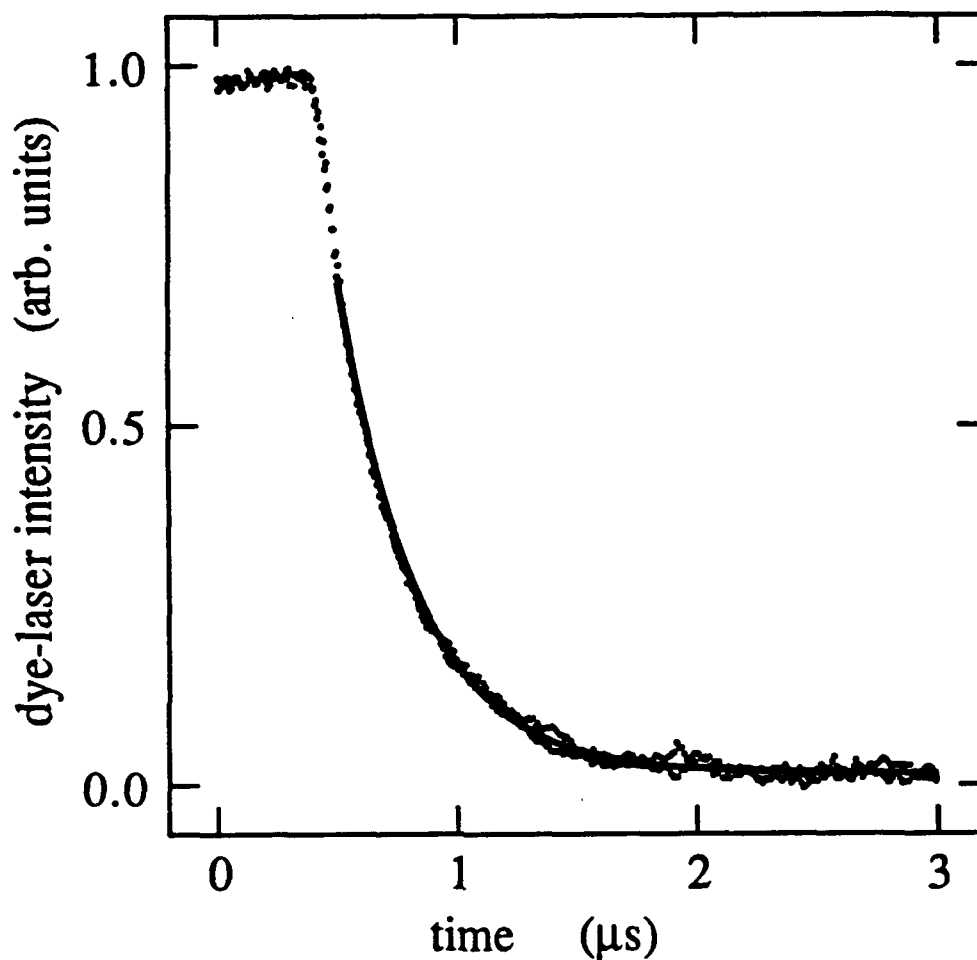
Fig. 4.10 Dye-laser intensity vs time for a multimode, high-Q bidirectional ring laser. This figure shows the decay of the dye-laser intensity propagating in one direction of the ring laser after a rapid and complete turn-off of the pump beam. The solid line represents the best-fit exponential whose time constant is 329 ns.
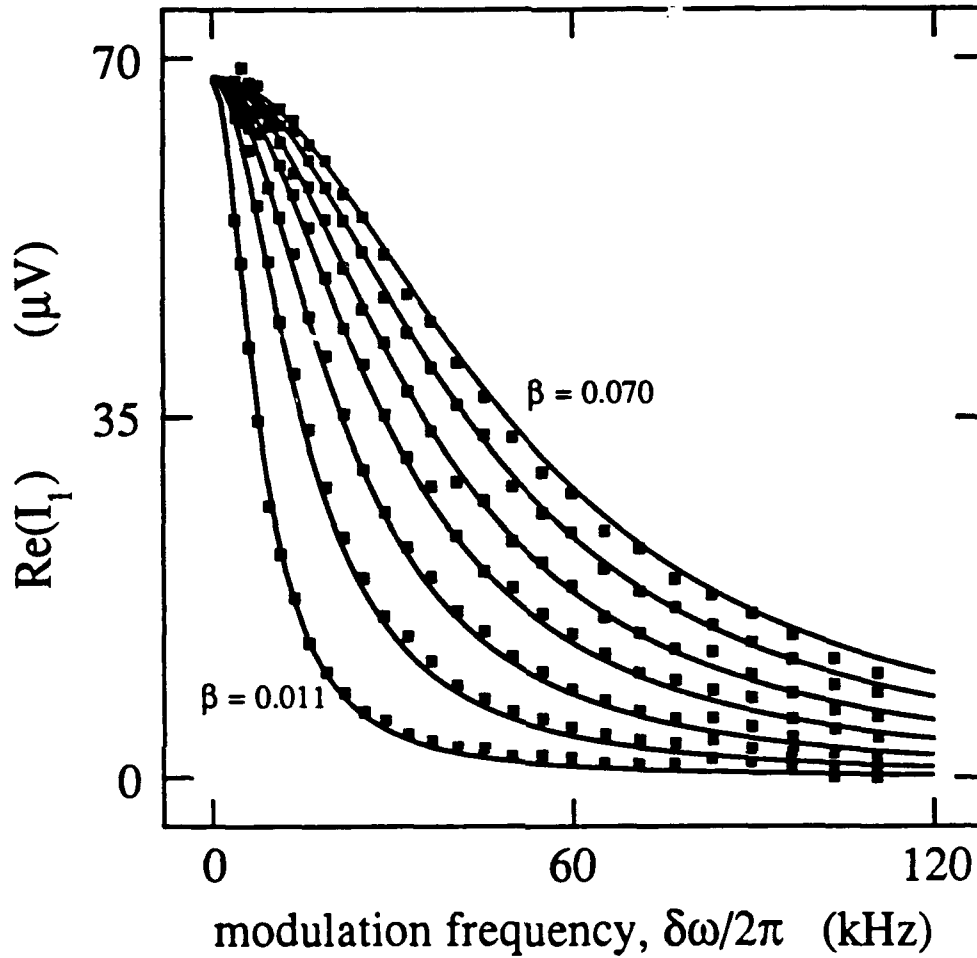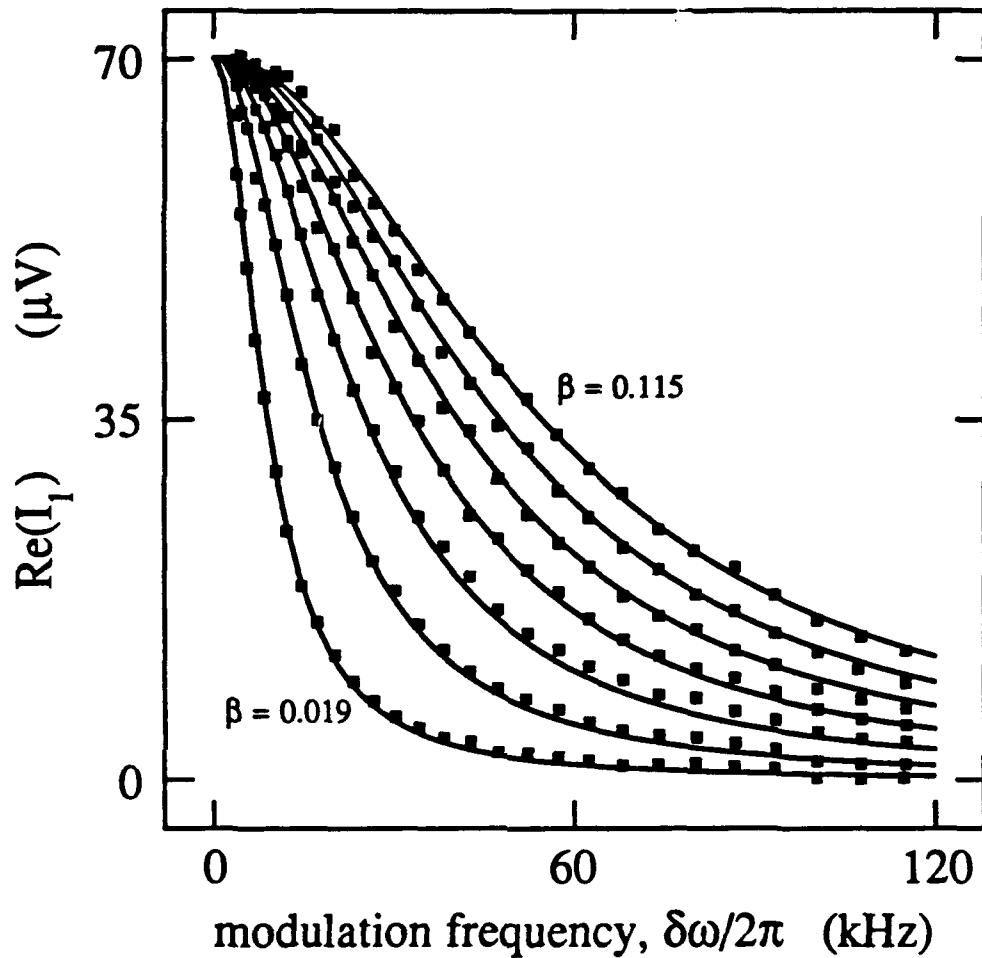
Fig. 4.11 The in-phase first-harmonic response of the laser intensity I_1 vs the pump modulation frequency $\delta\omega/2\pi$. I plot the in-phase or x-channel output of the lock-in amplifier vs frequency for a high-Q bidirectional ring laser for several values of the pump parameter β given in Eq. (4.15). The curves, from left to right, correspond to $\beta=0.019$, $\beta=0.036$, $\beta=0.053$, $\beta=0.070$, $\beta=0.085$, $\beta=0.100$, and $\beta=0.115$. The solid lines represent the single-mode best-theoretical fit to all the data fit simultaneously. The cavity lifetime which gives us this fit is 335 ns.
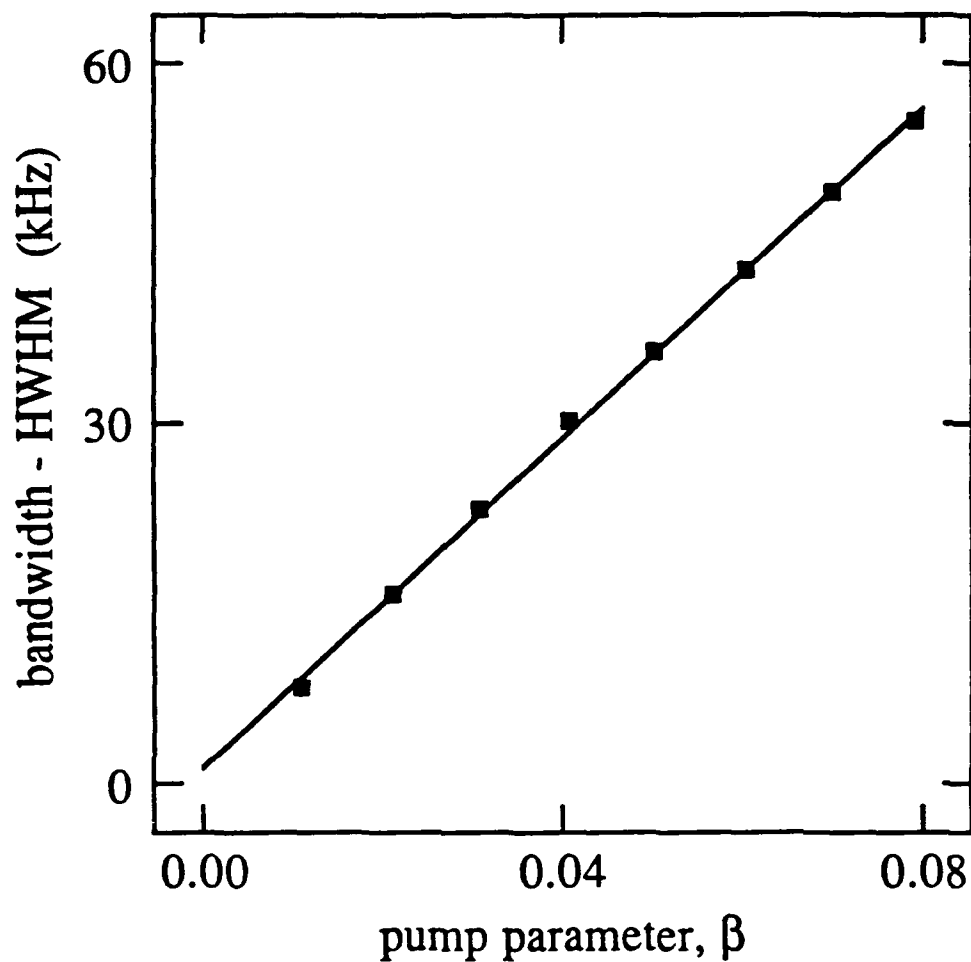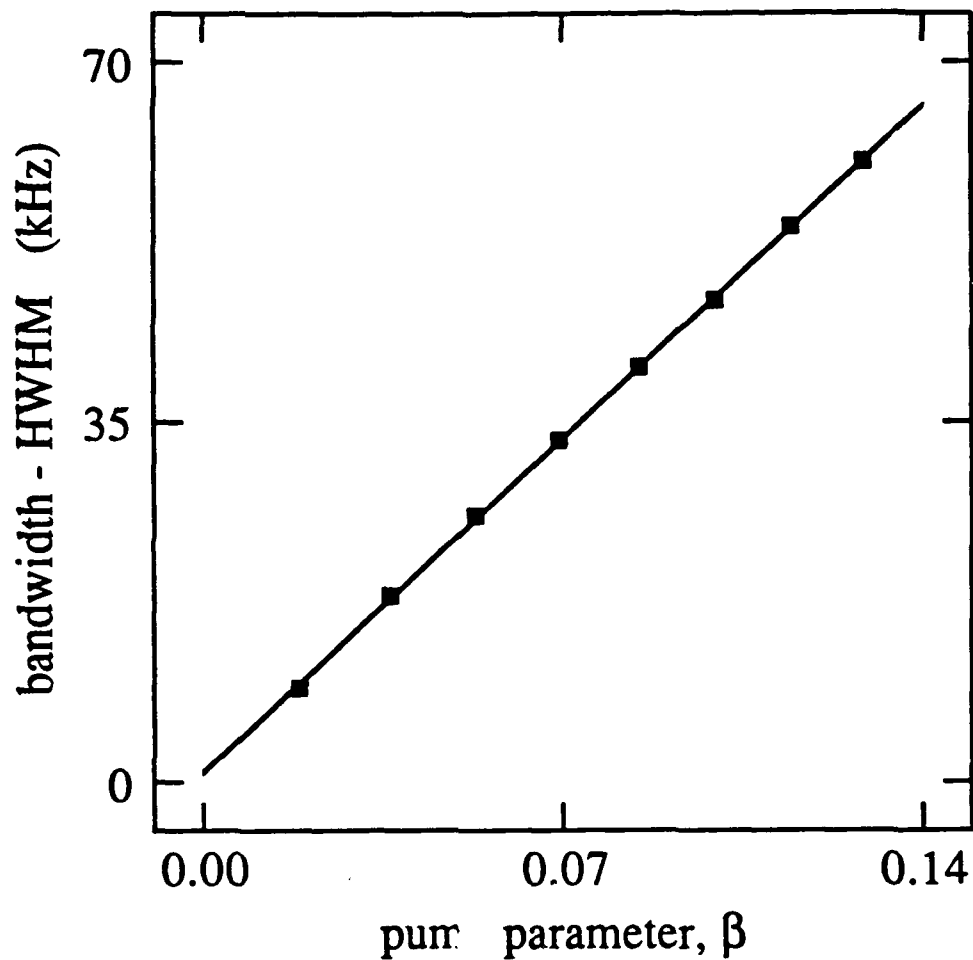
Fig. 4.12   The modulation bandwidth HWHM of the in-phase first-harmonic response of the intensity of the laser vs the pump parameter β. The curves shown in Fig. 4.11 were individually fit to Lorentzians and the bandwidth (HWHM) of these fits are plotted here with squares. The solid line represents a linear regression performed on these points. The slope of this line is proportional to the reciprocal of the cavity lifetime $1/\tau_c$. The cavity lifetime we get from the slope is 344 ns.

ring and standing-wave laser cavity configurations confirm this conclusion.

2. Laser and fluorescent intensity AM spectra

To connect the effects of critical slowing down in the laser intensity with the effects observed in the fluorescent intensity, I have characterized both quantities for the same cavity configurations. Another detector is used to measure the intensity of the fluorescence emitted off-axis by atoms in the interaction region. A lens is used to collect the fluorescence emitted over a large solid angle of roughly 0.2 steradians. Care was taken to slightly overfill the detector to insure that the light collected was from atoms in the center of the pump region (these atoms are more likely to be within the mode volume of the laser as well as the pump beam).

In this section I will discuss the first-harmonic response of the intensity of the laser and the intensity of the fluorescence from the interaction region in the gain medium for a multimode standing-wave laser with a 5% output coupler. In Fig 4.13 the in-phase first-harmonic response of the fluorescent intensity is plotted. To fit the fluorescence data I assume that the detector measures some fluorescence from atoms that are pumped by the argon pump laser but are not in the interaction region of the dye laser. A small dc offset is added to the theory to simulate this experimental complication. The solid lines correspond to a single-mode theoretical fit using a value of τ_c=87 ns for the cavity lifetime. In Fig. 4.14 I plot the response of the laser intensity to the modulated pump for the same laser cavity. The single mode fit to the data was obtained using the value τ_c=86 ns for the cavity lifetime. This cavity lifetime corresponds quite well with that used to fit the spectral response of the fluorescence. We can conclude that the intensity of the fluorescence from the interaction region of this laser

also behaves as the single mode theory predicts.

To better appreciate the relation between the response of the fluorescent intensity and the response of the laser intensity, I plot both responses versus the modulation fequency $\delta\omega/2\pi$ for the same pump parameter β, in Figs. 4.15(a) and 4.15(b). In Fig. 4.15(a) the in-phase first-harmonic response of the fluorescent intensity is plotted together with the in-phase first-harmonic response of the laser intensity versus the modulation frequency $\delta\omega/2\pi$. In Fig. 4.15(b) I plot the in-quadrature response of the intensity of the fluorescence and that of the intensity of the laser versus modulation frequency. This curve shows that the phase lag of the laser response produces a phase lead in the fluorescent response. The interpretation of these two figures [Figs. 4.15(a) and 4.15(b)] is that when the dye laser can follow the modulations of the pump the atomic inversion is constant in time (AC gain clamping). I consider this effect to be a manifestation of AC gain clamping. Just as the DC response of the excited-state population is clamped to the threshold value, the AC response is clamped to zero as long as the laser intensity can follow the pump fluctuations. However, at higher modulation frequencies the laser cannot respond to the fluctuations of the pump. The AC response of the inversion becomes unclamped at these higher frequencies and the atoms begin to respond to the modulations or fluctuations of the pump intensity.

To better connect the AM spectral behavior of the fluorescent and laser intensities I have plotted both the bandwidth of the laser's response (squares) and the bandwidth of the hole in the response of the fluorescence (triangles) versus the pump parameter β on the same graph in Fig. 4.16. Notice that both these data lie on the same line for the same cavity. This fit indicates a lifetime τ_c=90 ns. The solid line is the result of a linear regression analysis performed on all the data shown in the figure.
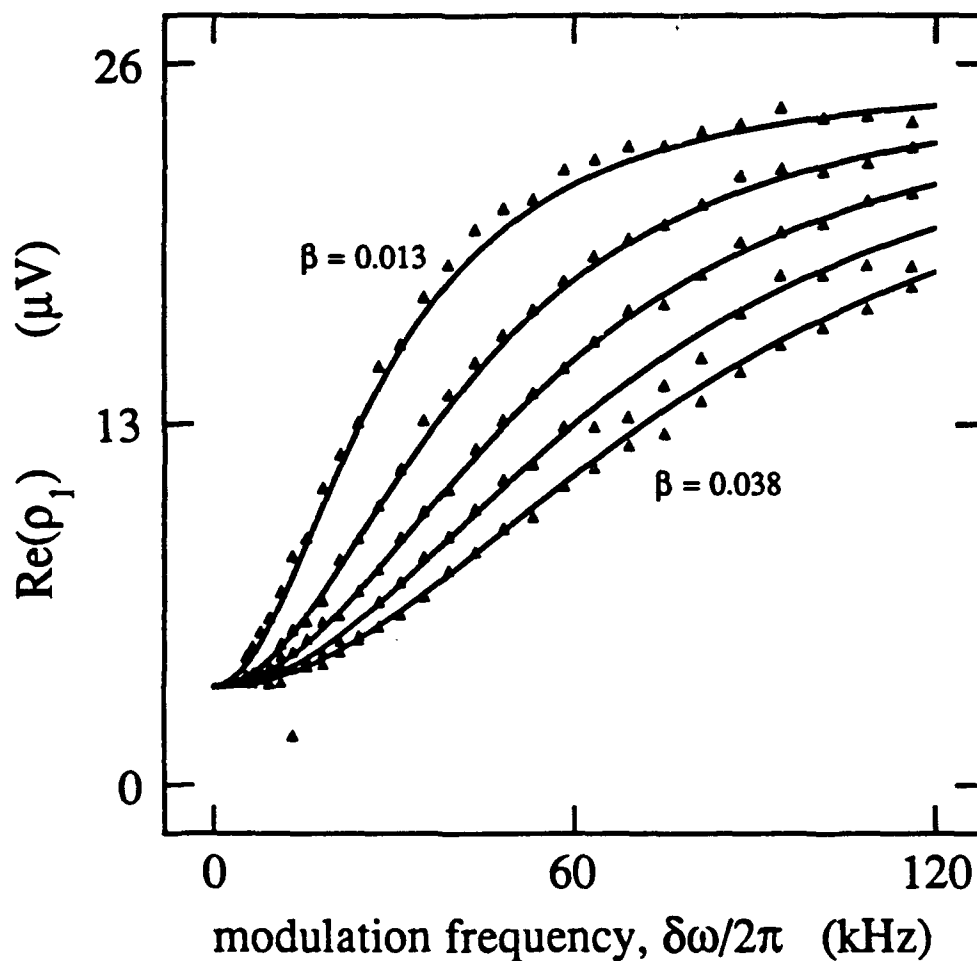
137

Fig. 4.13   The in-phase first-harmonic response of the intensity of the fluorescence emitted from atoms in the interaction region of the gain medium vs the pump modulation frequency $\delta\omega/2\pi$. I plot the in-phase or x-channel output of the lock-in amplifier vs frequency for a standing-wave laser with a 5% output coupler for several values of the pump parameter β given in Eq. (4.15). The curves, from left to right, correspond to $\beta=0.013$, $\beta=0.019$, $\beta=0.026$, $\beta=0.033$, and $\beta=0.038$. The solid lines represent the single-mode best-theoretical fit to all the data fit simultaneously. The cavity lifetime which gives us this fit is 87 ns.
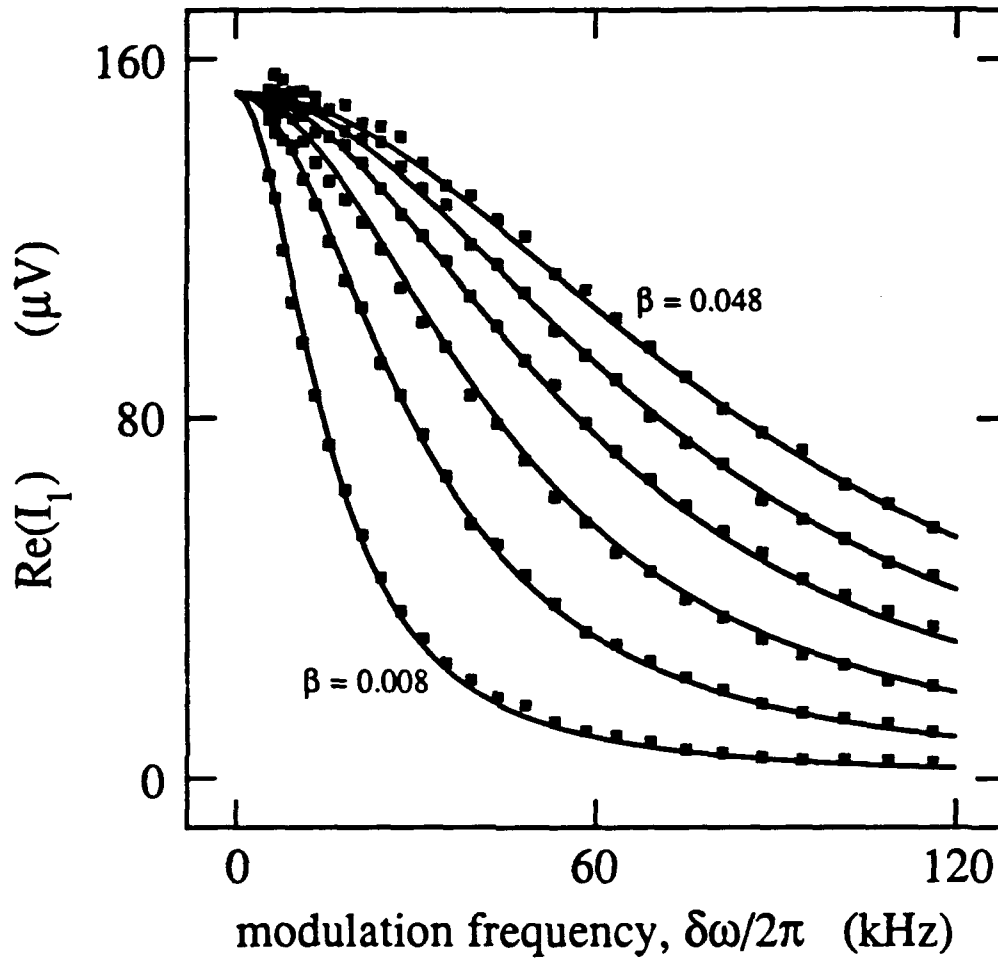
Fig. 4.14 The in-phase first-harmonic response of the laser intensity I_1 vs the pump modulation frequency $\delta\omega/2\pi$. I plot the in-phase or x-channel output of the lock-in amplifier vs frequency for a standing-wave laser with a 5% output coupler for several values of the pump parameter β given in Eq. (4.15). The curves, from left to right, correspond to $\beta=0.0.008$, $\beta=0.017$, $\beta=0.025$, $\beta=0.033$, $\beta=0.041$, and $\beta=0.048$. The solid lines represent the single-mode best-theoretical fit to all the data fit simultaneously. The cavity lifetime which gives us this fit is 86 ns.
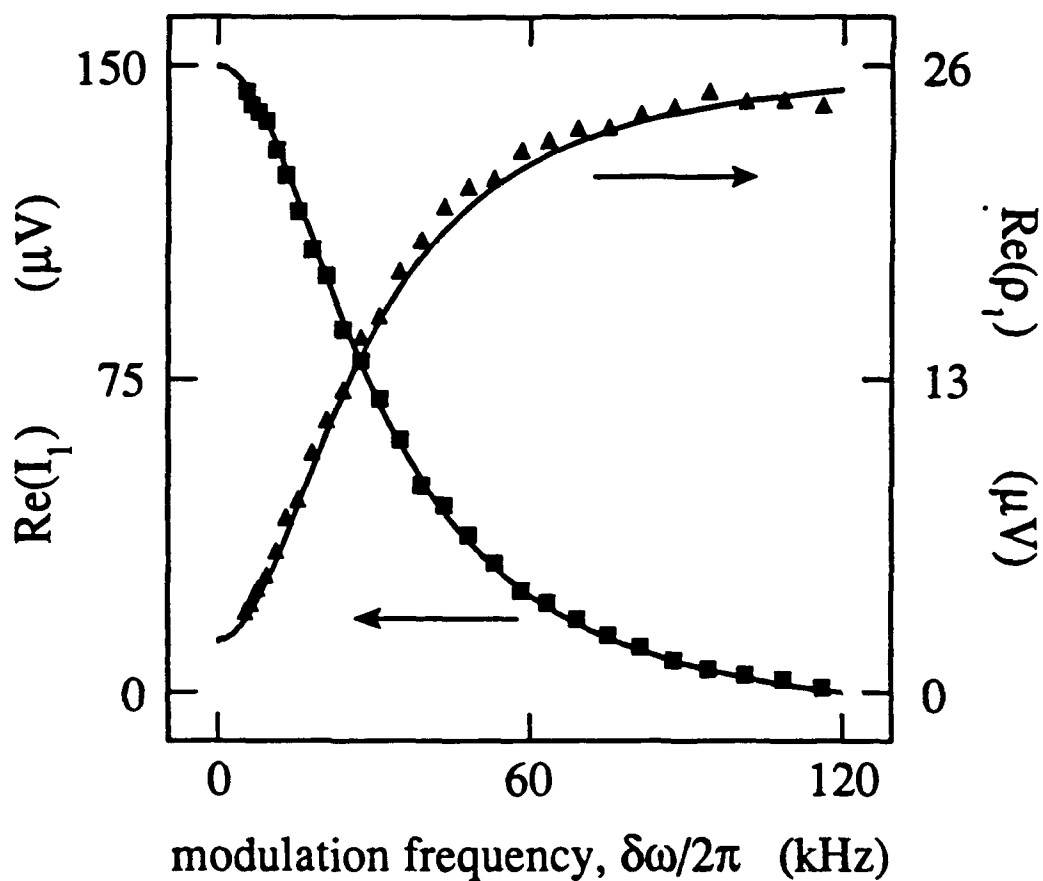
Fig. 4.15(a) The in-phase first-harmonic response of the fluorescent intensity and the in-phase first-harmonic response of the laser intensity vs the modulation frequency $\delta\omega/2\pi$. I plot the in-phase first-harmonic response of the fluorescent intensity, triangles, and the in-phase first-harmonic response of the laser intensity, squares, for approximately the same p. ⁻ ̦p parameter $\beta \approx 0.018$. The solid lines represent the single-mode best theoretical fit to the data.
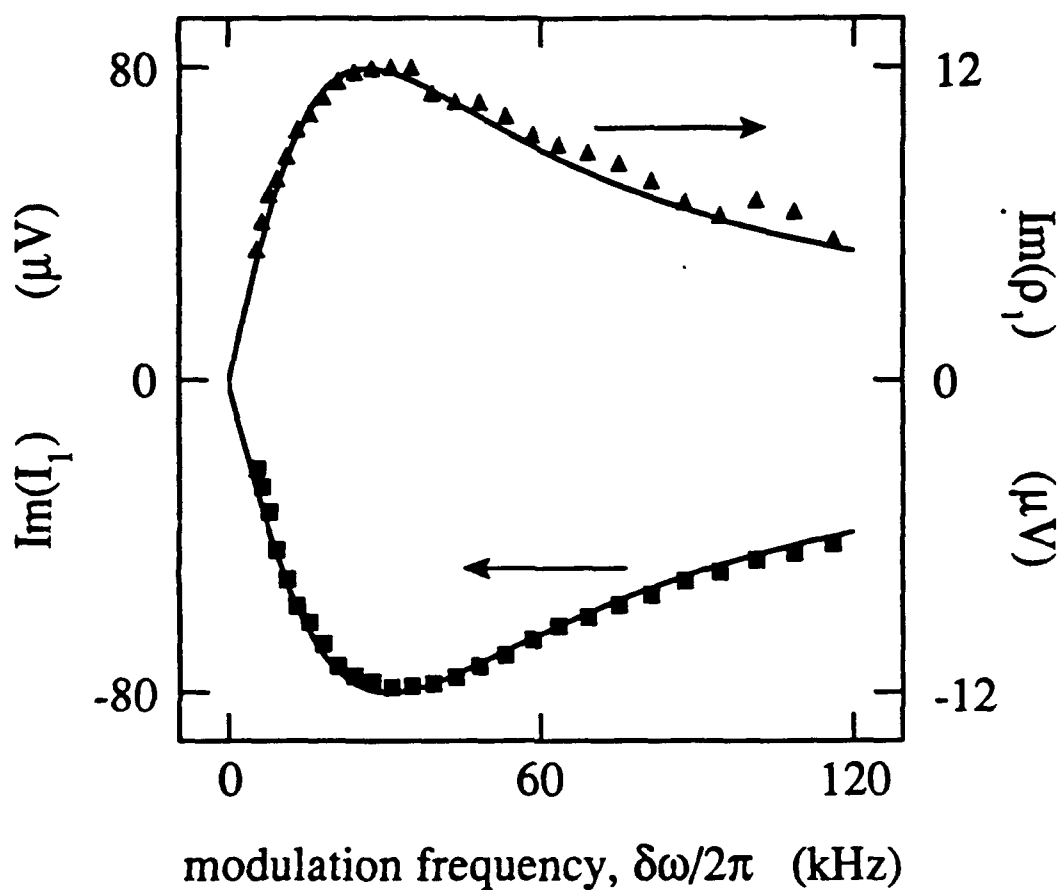
Fig. 4.15(b) The in-quadrature first-harmonic response of the fluorescent intensity and the in-quadrature first-harmonic response of the laser intensity vs the modulation frequency δω/2π. I plot the in-quadrature first-harmonic response of the fluorescent intensity, triangles, and the in-quadrature first-harmonic response of the laser intensity, squares, for approximately the same pump parameter β≈0.018. The solid lines represent the single-mode best-theoretical fit to the data.

Fig. 4.16 The modulation bandwidth (HWHM) of the in-phase first-harmonic response of the fluorescent intensity and that of the in-phase first-harmonic response of the laser intensity vs the pump parameter, β. The HWHM values of the data shown in Figs. 4.13 and 4.14 are plotted. The HWHM values of the fluorescence curves are plotted using triangles; and the HWHM of the laser intensity curves are plotted using squares. The solid line represents the result of a linear regression performed on all the points shown. The slope of the line corresponds to a cavity lifetime of 90 ns.

To demonstrate the universality of these results (at least in dye laser systems) I have repeated these experiments for multimode ring and standing-wave laser cavities for both high-Q cavities and cavities with a single 5% output coupler. In Fig. 4.17 I plot the HWHM of the in-phase first-harmonic response of the fluorescent intensity and that of the laser intensity for three of the cavities studied. The HWHM data for the high-Q standing wave and the high-Q ring cavities are labeled (b) and (c) respectively in the figure. The lifetimes associated with these cavities are τ_c=246 ns for the standing-wave cavity and τ_c=344 ns for the ring cavity. In the case of the high-Q cavities the dominant loss mechanism is probably the imperfect Brewster-angle reflection from the surfaces of the dye jet. In the standing-wave laser the modes encounter the dye jet twice per round trip while in the case of the the ring cavities the dye jet is encountered only once per round trip; consequently the ring cavity has less loss per round trip and therefore a longer cavity lifetime. The cavities with output couplers have approximately the same lifetime of 90 ns regardless of the cavity configuration (ring or standing-wave). The dominant loss mechanism in this case is undoubtedly the output coupler which is encountered once per round trip for both standing-wave and ring laser cavities. The data labeled (a) in Fig. 4.17 are for a unidirectional ring laser with a 5% output coupler (τ_c=85 ns). The laser is forced to oscillate in one direction by retroreflecting the output from one propagation direction back into the cavity. Retroreflection of one cavity direction is effective in providing unidirectional operation with a contrast ratio of at least 100:1 in these multimode lasers.

3. Hole burning in the absorption of pump modulations

In the previous section we saw that the laser carries away the modulation

143
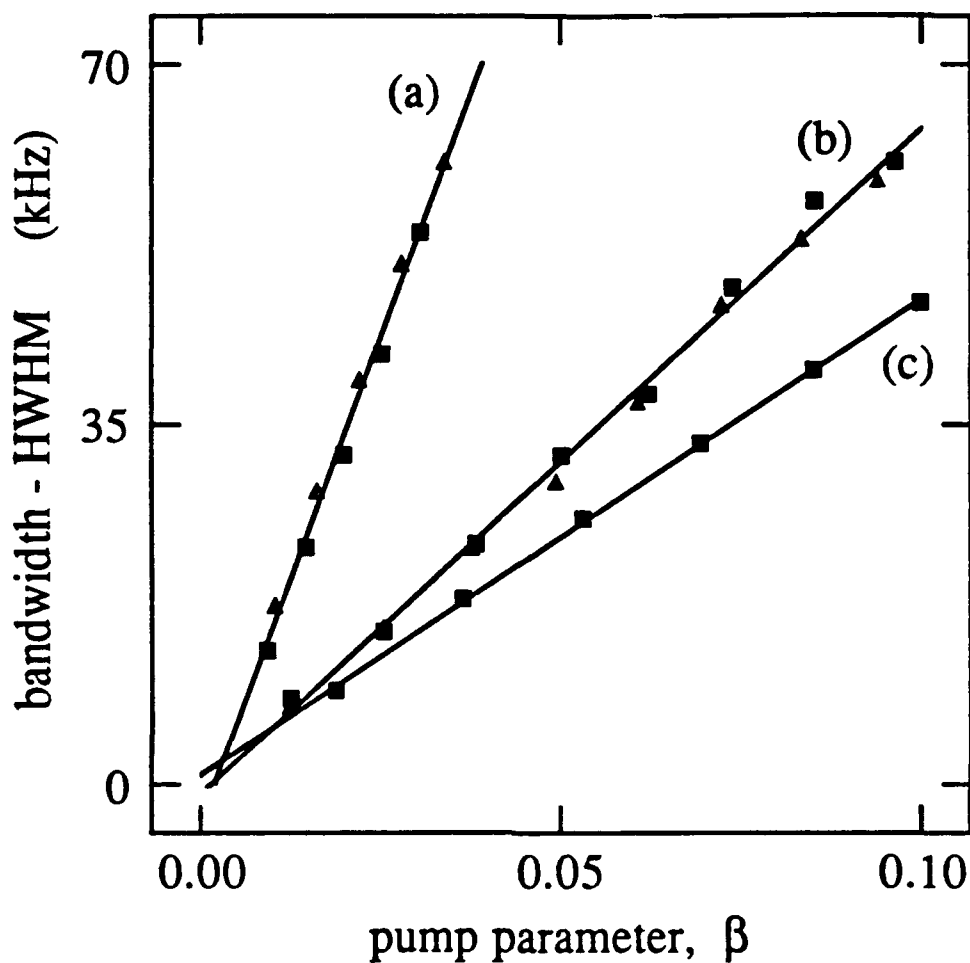
Fig. 4.17 The modulation bandwidth (HWHM) of the in-phase first-harmonic response of the fluorescent intensity and the laser intensity vs the pump parameter, β. Plotted are the bandwidths of the responses for three different cavity configurations. The squares represent the dye-laser intensity response, the triangles represent the fluorescent intensity response, and the solid lines result from a linear regression analysis of these data. The cavities shown are (a) a unidirectional ring cavity with a 5% output coupler (τ_c=85 ns), (b) a high-Q standing wave cavity (τ_c=246 ns), and (c) a high-Q bidirectional ring cavity (τ_c=344 ns).

energy for small modulation frequencies, while the fluorescence carries away the modulation energy at higher modulation frequencies. If the absorption of the modulation energy from the pump intensity were constant with respect to modulation frequency the amount of modulation in the laser intensity at low frequency would equal the amount of modulation in the fluorescent intensity at higher frequencies. Even when we scale the modulation signal in the fluorescent intensity by the appropriate factor to account for the incomplete collection angle, the signal in the fluorescent intensity at high frequencies is less than the signal in the laser intensity at low frequencies. The pump modulation energy is not absorbed as efficiently at the higher frequencies. This decreased absorption of pump modulations is due to the change in the response of the population to the pump modulations. When a system follows a modulation, the absorption of the modulation is affected. This effect has previously been observed in modulation experiments carried out in passive absorbers.[28-31]

To demonstrate the origin of the detail in the absorption spectrum of the pump modulation I write the equation for the spatial attenuation of the pump intensity in a rate equation formalism:

$$\frac{d}{dz} I_p(t, z) = -\alpha I_p(t, z) \rho_g(t, z), \qquad (4.17)$$

where α is the inverse Beer's absorption length and ρ_g is the ground-state population. As I assumed in Eqs. (4.10a) the response of the ground-state population is expressed in a harmonic series

$$\rho_g(t, z) = \sum_{n=-\infty}^{\infty} \rho_{g,n}(z) \exp(in\delta\omega t), \qquad (4.18)$$

where $\rho_{g,n}(z)$ is the nth harmonic response of the ground state at the position z in the material. Once the expression for $I_p(t)$ given in Eq. (4.9) is substituted

into Eq. (4.17) I can equate terms of equal time dependence to get an expression for the spatial dependence of the sideband intensity of the pump, δI_p,

$$\frac{d}{dz}\delta I_p(z) = -\alpha\{\delta\overline{I}_p(z)\rho_{g,0}(z) + I_p(z)Re[\rho_{g,1}(z)]\}. \qquad (4.19)$$

The first term on the right hand side of Eq. (4.19) is the product of the AC field component, δI_p, and the DC absorption, $\alpha\rho_{g,0}$. The second term on the right is the DC pump intensity, $\overline{I}_p$, times the AC absorption, $\alpha Re[\rho_{g,1}]$. It is this second term which gives rise to the spectral variation in the absorption of the modulation energy. The population conservation equation

$$1 = \sum_{n=-\infty}^{\infty} \rho_{g,n}\exp(in\delta\omega t) + \sum_{n=-\infty}^{\infty} \rho_n\exp(in\delta\omega t), \qquad (4.20)$$

can be employed to rewrite Eq. (4.19) in terms of the excited-state population harmonic components, ρ_n. The absorption equation takes the form

$$\frac{d}{dz}\delta I_p(z) = -\alpha\{\delta I_p(z)(1-\rho_0) - \overline{I}_p(z)Re[\rho_1(z)]. \qquad (4.21)\}$$

This expression indicates that a change in the response of the excited-state population to the modulation as a function of frequency induces a change in the absorption of the modulation itself. Since the last term in Eq. (4.21) is negative, the decreased fluorescent reponse at low modulation frequencies contributes to an increase in the absorption of the modulation. The laser system is a more efficient absorber of modulations when the atomic population can not follow the modulations.

In order to perform the energy balance of the system the two outlet ports for the modulation energy (the laser intensity and the fluorescent intensity) as well as the inlet port (the absorption) must be considered in detail. In this section I will describe the measurement we performed to verify that the absorption of

the modulation is increased when the laser can follow the modulation and the fluorescent intensity is clamped to a constant.

The same apparatus is used in this part of the experiment as was used for the previous two measurements except that another detector is employed to measure the transmitted intensity of the argon pump beam. The transmitted argon is collected with a curved mirror and the collimated beam is then focused onto a fast detector. A notch filter is used to pass only light at the frequency of the argon laser (5145 angstroms) to filter out the fluorescence from the dye jet. This insures that the spectral behavior of the fluorescent intensity will not affect the measurement. The increased absorption does not cause the transmitted modulation intensity to go to zero at low frequency since complete attenuation is impossible. Consequently, this measurement is intrinsically noisier than the previous two involving the laser and fluorescent intensities.

I study the intensity of the argon pump beam transmitted through the dye jet for a standing-wave laser cavity with a 5% output coupler. The cavity with an output coupler experiences this increased absorption to a greater extent than the high-Q cavities. The reason for this is that the cavity with the output coupler has a higher threshold and the atoms are more saturated at threshold. The depth of the hole is related to the amount of saturation. After all, this increase in the absorption is actually a tip within the $1/T_1$ hole for a collisionally broadened system.[28-31] This total effect is shown in the theoretical plot in Fig. 4.18(a) and 4.18(b). The response of the excited state population is plotted in Fig. 4.18(a). The hole in the low frequency response can be seen together with the entire $1/T_1$ response. In Fig. 4.18(b) I have plotted the absorption spectrum of the pump modulations by the laser gain medium as given by Eq. (4.21). These curves in Fig. 4.18(b) directly mirror the effects seen in Fig. 4.18(a). It should
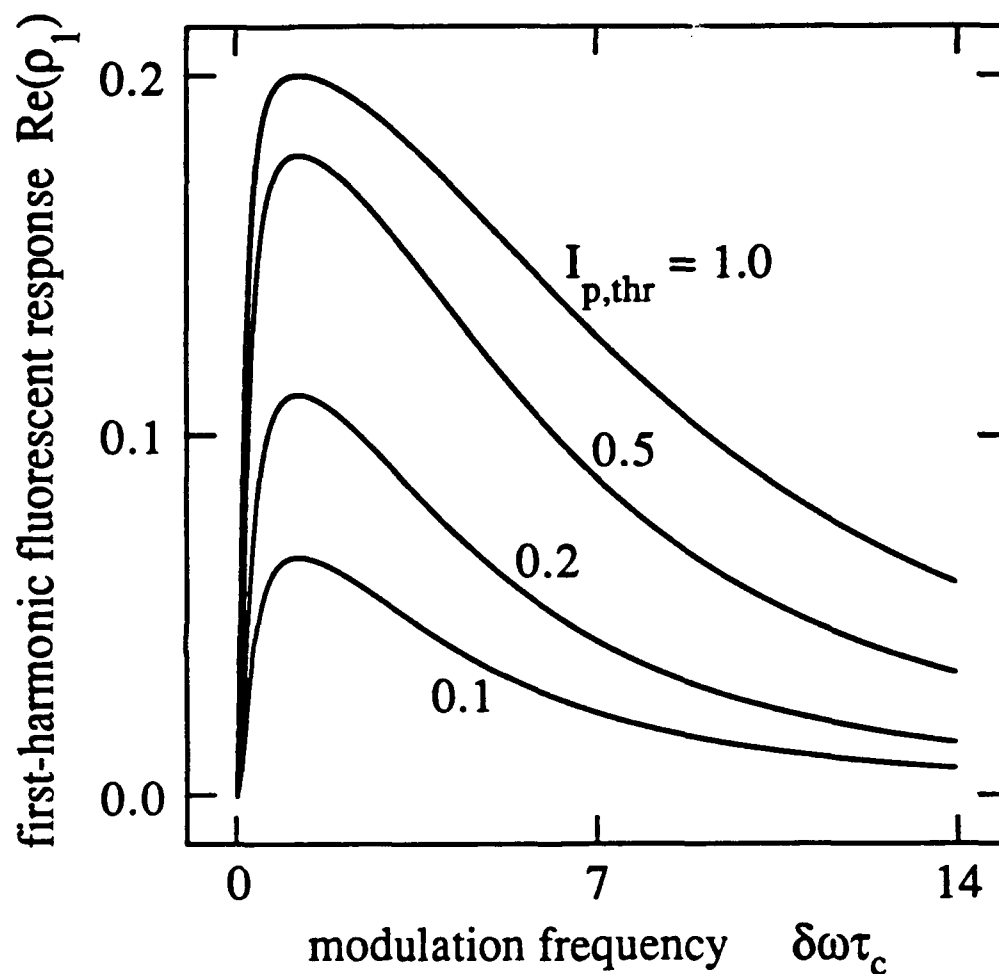
Fig. 4.18(a) Spectrum of the first-harmonic response of the excited-state population (fluorescent intensity). The spectrum of the first-harmonic response of the excited-state population is plotted for frequencies large compared with $1/T_1$. This data is generated for $T_1 = 0.33\tau_c$, $I_0 = 0.5$, and four different threshold pump intensities: $I_{p,thr} = 1.0, 0.5, 0.2$, and 0.1. The hole in the fluorescent response is a hole within a Lorentzian of width $1/T_1(1+I_p+I_0)$.
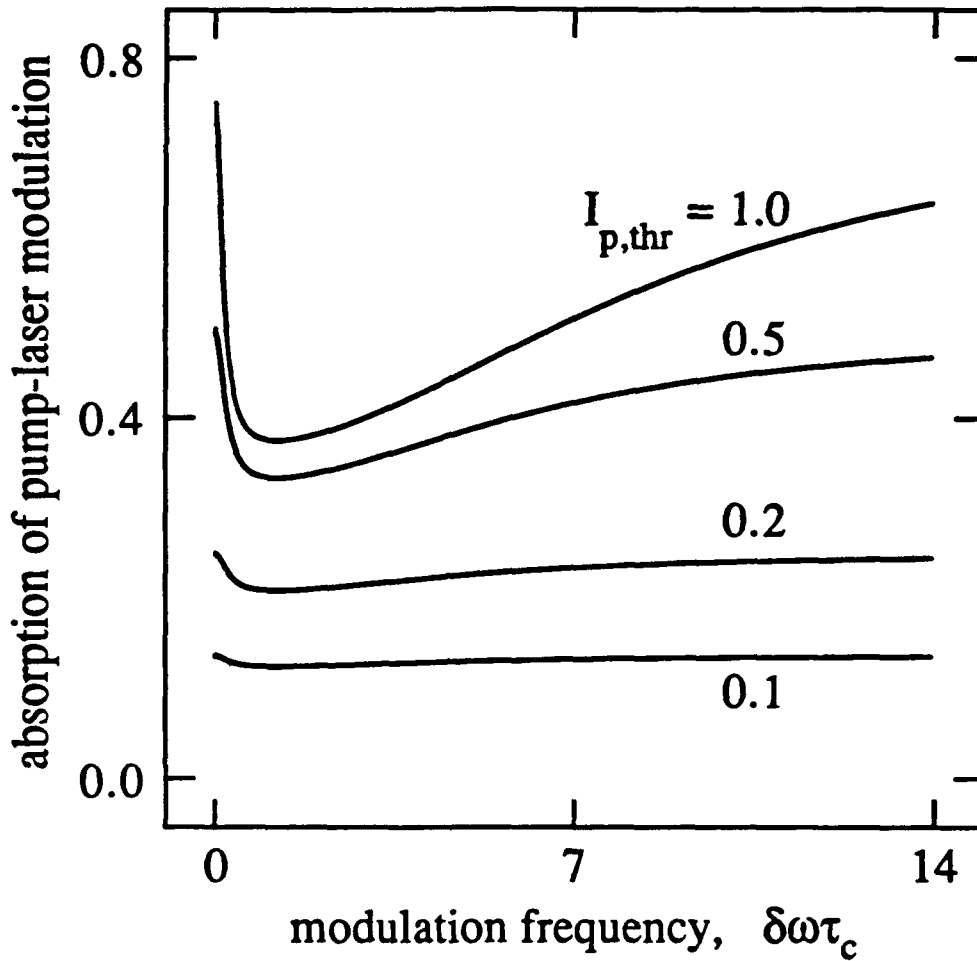
Fig. 4.18(b)   Spectrum of the absorption of modulation in the intensity of the pump laser. The absorption coefficient in Eq. (4.21) is normalized with respect to α and then plotted as a function of modulation frequencies which are large compared with $1/T_1$. The data are generated for $T_1 = 0.33\tau_c$, $I_0 = 0.5$, and four different threshold pump-laser intensities: $I_{p,thr} = 1.0, 0.5, 0.2$, and 0.1. These data correspond to the same parameters used to obtain the plots in Fig. 4.18(a). The "tip" in the absorption spectrum of the pump modulations is within a "dip" of width $1/T_1(1+I_{p,thr}+I_0)$.

be apparant to the reader what I mean by the tip within the hole.

In Fig. 4.19 I have plotted the transmitted modulation spectrum of the argon pump beam. Shown are the AM spectra for four different pump values ranging from 0.9% above threshold to 1.9% above threshold. The solid line curves represent the best theoretical fit to all the data fit simultaneously. This data is intrinsically noiser than the laser spectra and the fluorescent intensity spectra since this measurement is background limitted. The data shows increased transmittance of modulation at higher frequencies. This increased transmittance is due to the decreased absorption of pump modulations when the atomic population is capable of responding at the modulation frequency.

F. Conclusion

I have employed AM spectroscopic techniques to study the behavior of lasers operating near the first threshold. In particular, this chapter has focused on the comparison of single-mode four-level laser rate equations with the behavior of multimode dye lasers. I find that the total intensity of these multimode dye lasers responds to weak amplitude modulation of the pump intensity the same way that the intensity of a single mode laser does. This agreement is a good example of the synergetic behavior of the multiple modes in the multimode laser.[33] The many modes cooperate to maintain a total intensity which behaves according to single-mode laser theory, even though the underlying behavior of the individual modes may be much more complicated. McMackin et al.[34] and Atmanspacher et al.[35] show that the individual modes in a multimode laser can undergo full scale chaotic fluctuations even when the total intensity is quite calm.

In the theoretical section of this chapter I derive a theory based on four-
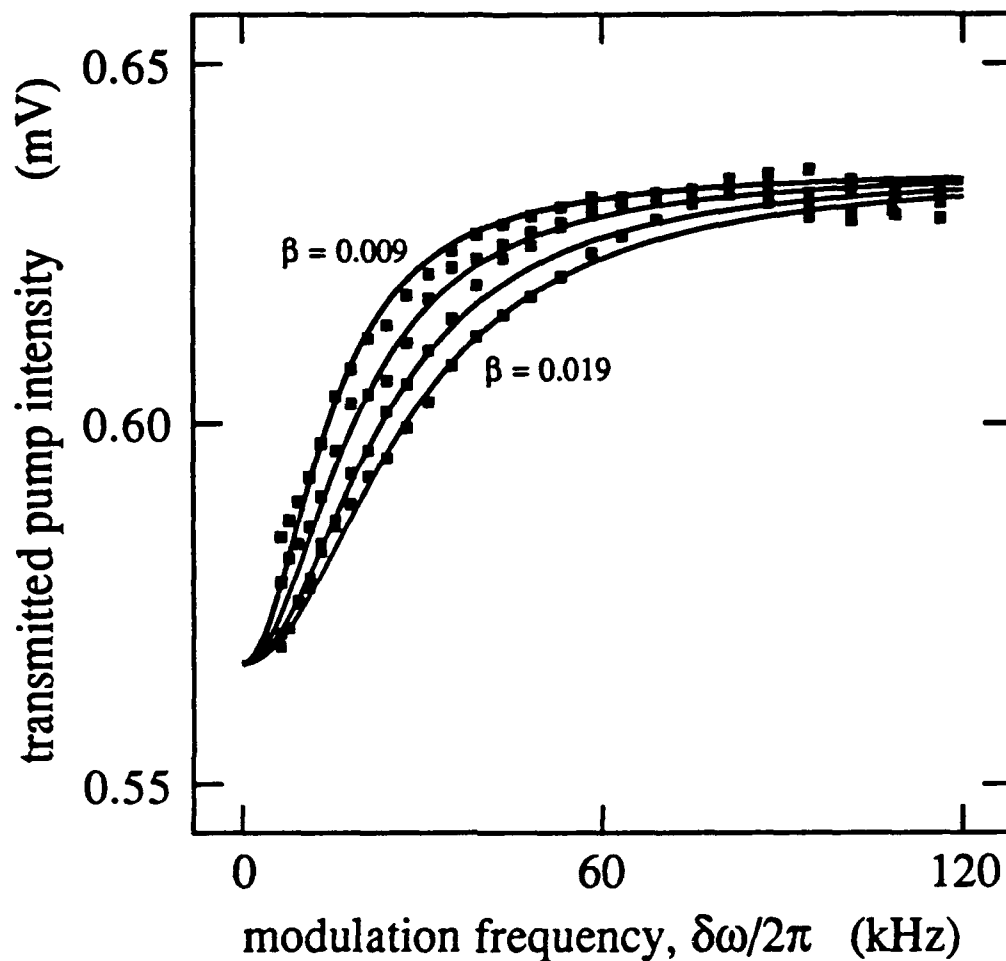
Fig. 4.19 Transmission of modulated argon pump intensity vs pump modulation frequency $\delta\omega/2\pi$. I plot the in-phase first-harmonic of the intensity of the argon pump beam after it has passed through the interaction region of the gain medium. The curves, from left to right, correspond to β=0.009, β=0.014, β=0.017, and β=0.019.

level rate equations for the behavior of the laser intensity and the excited-state population of the atoms in the gain medium in response to a weak amplitude modulation of the pump intensity. The theory demonstrated that the laser behaved as a low-pass amplifier of pump fluctuations. Furthermore, the bandwidth of response of the laser to these fluctuations is equal to the product of the pump parameter, β, and the reciprocal of the passive-cavity lifetime, τ_c. I also showed that this bandwidth, β/τ_c, is equal in magnitude to the stability exponent for the on-solution of the laser rate equations above threshold. I propose AM spectroscopy in lasers as an accurate method for determining the stability exponent of the laser equation! Furthermore, if you can accurately measure the stability exponent and determine the pump parameter then the cavity lifetime, τ_c, can be determined as well.

In the first experimental section of this chapter I reported experiments carried out with high-Q standing-wave and bidirectional-ring dye lasers. For each of these cavity comfigurations I directly measure the passive cavity decay rates, $1/\tau_c$, and compare these measurements with the cavity decay rates for these lasers determined with a modulation measurement. The agreement between these two measurement techniques demonstrates that the single mode laser theory is accurate in describing the behavior of the total intensity of these multimode lasers subjected to weakly modulated pump intensities. I also employ these AM techniques to measure the passive-cavity devay rates, $1/\tau_c$, of some cavities with output couplers. These cavities typically have lifetimes less than 1 μs. The AM techniques has been used to measure a cavity decay rate which is outside the bandwidth capabilities of our detectors. This is simply accomplished by operating the laser near threshold where its reponse is slowed by a factor of β. Then, the rapid cavity decay rate can be inferred by scaling the resulting

time constant by $1/\beta$.

The other prediction of the four-level rate equation theory is that the AM spectrum of excited-state population of the gain medium displays a hole at zero modulation frequency. That is to say that the excited-state population remains immune to modulations which the laser intensity can follow. I consider this behavior to be evidence of dynamic inversion clamping. Up until now inversion clamping has been interpreted as an adiabatic phenomenon.[26] In the presence of low-frequency pump fluctuation the excited-state population remains constant while the system dissipates absorbed modulation in the form of a fluctuating laser intensity. The laser intensity cannot follow high frequency pump-modulations; consequently the population does not remain constant in the presence of these rapid fluctuations. The laser seems to act as a pump-intensity noise eater keeping the population constant with respect to fluctuations which the laser intensity can follow.

In the experimental section of this chapter I measure the response of the fluorescence emitted from atoms in the interaction region of the dye laser systems. The total fluorescence is a measure of the excited-state population for a four-level laser. I demonstrate that the width of the hole at DC in the AM spectrum of the fluorescent intensity corresponds quantitatively to the Lorentzian low-frequency response of the laser intensity. These measurements are carried out in both high-Q lasers and lasers with output couplers in ring and standing-wave configurations. The dynamic inversion clamping phenomenon which the theory predicts has been experimentally verified.

At this point I perform an energy balance of the modulation energy in and out of the system. To do this, I consider both input and output ports of modulation energy into and out of the laser system. The two exiting ports are

the laser intensity and the fluorescent intensity. However, consideration of only these two ports does not lead to conservation of modulation energy. I have to include the fact that the absorption of modulation energy into the system is not constant over frequency. The behavior in the response of the population induces changes in the absorption spectrum of modulation energy from the pump. In the final sections of this chapter I report a measurement of the modulation in the intensity of the argon pump beam after it has passed through the dye jet. The spectrum of the transmitted pump intensity reveals that less modulation energy is absorbed by the gain medium at high modulation frequency where the population reponds to the modulations. The population absorbs modulations less efficiently when it it can repond to the modulation. This effect has also been observed in the dynamics of passive absorbers.[28-31]

I am compelled to qualify the interpretation of these results. The lasers I have reported on were all extremely broadband. The time-averaged spectra of these lasers consisted of hundreds of longitudinal modes at even the lowest of pump settings. When the number of modes is not very large, the modes may couple to produce deterministic oscillations of the total intensity of the laser in addition to responding to the multiplicative fluctuations of the pump intensity.[36] Another restriction which should apply to the interpretation of these results is that the modulation frequency was always much less than the frequency separation between adjacent longitudinal cavity modes. When the modulation frequency is comparable to the modal frequency separation and the modulation amplitude is large, the modes may couple to produce mode locking or deterministically chaotic fluctuations of the total intensity.[16] Furthermore, the gain medium in the dye-jet dye lasers used in these experiments are extremely thin (ie. 100 μm). A thin gain medium allows modes which differ substantially in

frequency to maintain a constant phase difference throughout the gain medium. This allows many possible combinations of laser modes to uniformly saturate the gain medium. The laser cannot distinguish between the uniform saturation of many simultaneously lasing modes and that of a single traveling-wave mode. Therefore the multimode standing-wave lasers studied are not less efficient due to spatial hole burning effects.

I have analyzed theoretically and experimentally the flow of modulation through the input port (the absorption from the pump intensity) and both output ports (the laser intensity and the fluorescent intensity) of various laser systems. Modulation spectroscopy has lent itself to a quantitatively exact study of critical slowing down in the behavior of dye lasers operating near threshold. AM techniques have been used to measure the stability exponent of lasers with several different cavity configurations. A hole in the response of the fluorescent intensity to pump modulations has been observed. This spectral hole is a manifestation of dynamic inversion clamping. Furthermore, the spectral response of the atomic population induces a change in the ability of the atoms in the interaction region of the gain medium to absorb pump modulations. All three ports of modulation energy in a laser display interesting spectral behavior.

References

1. K. Kaminishi, R. Roy, R. Short, and L. Mandel, "Investigation of photon statistics and correlations of a dye laser," Phys. Rev. A **24**, 370-378 (1981). The pump parameter is defined in this work such that the scaled intensity is equal to the pump parameter as I have done in chapter 4. The only difference is that Kaminishi *et al.* scale the intensity to be equal to the photon occupation number, wheras I use the dimensionless intensity in this thesis.

155

2. R. Graham, M. Höhnerbach, and A. Schenzle, "Statistical properties of light from a dye laser," Phys. Rev. Lett. **48**, 1396-1399 (1982).

3. R. Short, L.Mandel, and R. Roy, "Correlation functions of a dye laser: Comparison between theory and experiment," Phys. Rev. Lett. **49**, 647-650 (1982).

4. S.N. Dixit and P.S. Sahni, "Nonlinear stochastic processes driven by colored noise: Application to dye-laser statistics," Phys. Rev. Lett. **50**, 1273-1276 (1983).

5. S. Schenzle and R. Graham, "Photon statistics of dye lasers, a non-Marcovian analytical model," Phys. Lett. **98A**, 319-323 (1983).

6. R.F. Fox, G.E. James, and R. Roy, "Laser with a fluctuating pump: Intensity correlations of a dye laser," Phys. Rev. Lett. **52**, 1778-1781 (1984).

7. R. Roy and L. Mandel, "Optical bistability and first-order phase transition in a ring dye laser," Opt. Commun. **34**, 133-136 (1980).

8. P. Jung and H. Risken, "Distribution function for a nonlinear laser model with multiplicative colored noise," Phys. Lett. **103A**, 38-40 (1984).

9. P. Lett, E.C. Gage, and T.H. Chyba, "Colored-noise-induced first-order phase transition in a single-mode dye laser," Phys. Rev. **A 35** 746-751 (1987).

10. M.R. Young and S. Singh, "Statistical properties of a laser with multiplicative noise," Opt. Lett. **13** 21-23 (1988).

11. M.R. Young and S. Singh, "Effects of multiplicative white noise on laser light fluctuations," Phys. Rev. **A 38** 238-244.

11. R. Roy, A.W. Yu, amd S. Zhu, "Quantum fluctuations, pump noise, and the growth of laser radiation," Phys. Rev. Lett. **55**, 2794-2797 (1985).

12. R.J. Fox, "Laser-noise analysis by first-passage-time techniques," Phys. Rev. **A 34**, 3405-3408 (1986).

13. S. Zhu, A.W. Yu, and R. Roy, "Statistical fluctuations in laser transients," Phys. Rev. **A 34**, 4333-4347 (1986).

14. P. Lett, "Investigation of first-passage-time problems in the two-mode dye laser," Phys. Rev. **A 34**, 2044-2057 (1986).

15. H. Fu and H. Haken, "Semiclassical theory of dye lasers: the single frequency

and multifrequency steady states of operation," J. Opt. Soc. Am. B **5**, 899-906 (1988).

H. Fu and H. Haken, "Multichromatic operations in cw dye lasers," Phys. Rev. Lett. **60**, 2614-2617 (1988).

16. T. Ogawa and E. Hanamura, "Dynamical properties of the multi-mode laser with modulated inversion," Opt. Commun. **61**, 49-54 (1987).
T. Ogawa and E. Hanamura, "Numerical analysis of multi-mode laser with modulated inversion," Appl. Phys. B **43**, 139-153 (1987).
T. Ogawa, "Quasiperiodic instability and chaos in the bad-cavity laser with modulated inversion: Numerical analysis of a Toda oscillator system," Phys. Rev. A **37**, 4286-4302 (1988).

17. P. Mandel and T. Erneux, "Laser Lorenz equations with a time-dependent parameter," Phys. Rev. Lett. **53**, 1818-1820 (1984).
P. Mandel and T. Erneux, "Nonlinear control in optical bistability," IEEE J. Quantum Electron. **QE-21**, 1352-1355 (1985).

18. G. Broggi, A. Colombo, L.A. Lugiato, and P. Mandel, "Influence of white noise on delayed bifurcations," Phys. Rev. A **33**, 3635-3637 (1986).

19. M. San Miguel and M.C. Torrent, "First passage time distribution for delayed laser threshold instability," J. Phys. (Paris) **49**, 149-151 (1988).

20. M.C. Torrent and M. San Miguel, "Stochastic-dynamics characterization of delayed laser threshold instability with swept control parameter," Phys. Rev. A **38**, 245-251 (1988).

21. W. Scharpf, M. Squicciarini, D. Bromley, C. Green, J.R. Tredicce, and L.M. Narducci, "Experimental observation of a delayed bifurcation at the threshold of an argon laser," Opt. Commun. **63**, 344-348 (1987).

22. F. Papoff, D. Dangoisse, E. Poite-Hanoteau, and P. Glorieux, "Chaotic transients in CO_2/sub 2/ laser with modulated parameters: critical slowing-down and crisis-induced intermittency," Opt. Commun. **67**, 358-362 (1988).

23. E.C. Gage, and L.Mandel, "Hysteresis effects in the two-mode dye ring laser," J. Opt. Soc. Am. B, **6**, 287-291 (1989).

24. A.W. Yu, G.P. Agrawal, and R. Roy, "Noise propagation from pump to secondary lasers," Opt. Lett. **12**, 806-808 (1987).

25. G.P. Agrawal and R. Roy, "Effect of injection-current fluctuations on the spectral linewidth of semiconductor lasers," Phys. Rev. A **37**, 2495-2501 (1988).

26. A.E. Siegman, *Lasers* (University Science Books, California, 1986), Chapt. 13.

27. F.T. Wu, S. Ezekiel, M. Dulcoy, and B.R. Mollow, Phys. Rev. Lett. **38**, 1077 (1977).

28. L.W. Hillman, R.W. Boyd, J. Krasinski, and C.R. Stroud, Jr., "Observation of a spectral hole due to population oscillations in a homogeneously-broadened optical absorption line," Opt. Commun. **45**, 416-419 (1983).

29. M.S. Malcuit, R.W. Boyd, L.W. Hillman, J. Krasinski, and C.R. Stroud, Jr., "Saturation and inverse-saturation absorption line shapes in alexandrite," J. Opt. Soc. Am. B **1**, 73-75 (1984).

30. M.A. Kramer, R.W. Boyd, L.W. Hillman, and C.R. Stroud, Jr., "Propagation of modulated optical fields through saturable absorbing media: a general theory of modulation spectroscopy," J. Opt. Soc. Am. B **2**, 1444-1455 (1985).

31. S.H. Chakmakjian, K. Koch, S. Papademetriou, and C.R. Stroud, Jr., "Effects of pump modulation on a four-level laser amplifier," J. Opt. Soc. Am. B, **6**, 1746-1751 (1989).

32. R. Saxena and G.S. Agarwal, "AC Stark effect and fluorescence using modulated laser beams I. Effect of laser fluctuations and arbitrary relaxation parameters," J. Phys. B **12**, 1939-1951 (1979).

33. H Haken, *Synergetics* (Springer-Verlag, New York, 1983).

34. I. McMackin, C. Radzewicz, M. Beck, and M.G. Raymer, "Instabilities and chaos in a multimode, standing-wave, cw dye laser," Phys. Rev. A **38**, 820-832 (1988).

35. H. Atmanspacher, H. Scheingraber, and C.R. Vidal, "Mode-correlation times and dynamical instabilities in a multimode cw dye laser," Phys. Rev. A **33**, 1052-1059 (1986).

36. S. Chakmakjian, L.W. Hillman, K. Koch, and C.R. Stroud, Jr., *Optical Bistability III* (Springer-Verlag, New York, 1986).

SUMMARY

The goal of this thesis was to provide an explanation of modulation interactions in various optical systems. I have presented an account of experimental work performed in a variety of systems: two-level atom; a multi-level laser amplifier; and a dye-laser system. In each of these systems modulation interactions are used to perform a frequency-domain measurement of some systematic time-constant or parametric interaction.

In chapter 2, the interaction of a 100% AM field with an ensemble of two-level atoms was studied. The interaction revealed the existence of several parametric resonances between the Rabi frequency and the modulation frequency of the bichromatic field. The absorption of the modulated field is increased whenever the Rabi frequency is equal to the modulation frequency or a higher harmonic of the modulation frequency. When the Rabi frequency and the modulation frequency are large compared with the natural linewidth of the transition, the nonlinearity of the interaction produces harmonic overtones of the modulation frequency in the response of the atomic variables. These overtones can lead to parametric resonances when they coincide with the Rabi frequency of the atomic medium. Since the field is modulated the system is always in a sort of

158

transient regime in which the Rabi oscillations are constantly being reinitiated.

In chapter 3 I treated the case of a collisionally-broadened four-level laser amplifier interacting with a weakly modulated pump field (the pump laser was tuned to the pump transition of the amplifier) and a probe field tuned to the inverted transition of the amplifier. The spectrum of the transfer of modulation from the pump-laser intensity to the probe-laser intensity was studied. Although the lasers do not interact with a common atomic level, modulation energy is transferred from the pump-laser intensity to the probe-laser intensity via population oscillations. The modulation bandwidth of the laser amplifier is equal to the sum of the spontaneous decay rate of the inverted transition and the stimulated rates induced by the pump and probe lasers. Since the modulation transfer rate is actually the rate at which population oscillations cycle through the entire circuit of energy levels, I conclude that modulation spectroscopy can be used to isolate any hidden slow decay rates which would diminish this modulation transfer rate.

The data collected in chapter 3 was first compared with a simple four-level rate equation model and then with a more complicated and accurate model based on what is known about the energy levels of alexandrite. In this second model I included the thermal pump rate which takes population from the storage level to the upper vibronic level. This thermal equilibration process is central to the operation of an alexandrite laser and gives rise to increased lasing efficiency at higher temperatures. I used this thermal-pump theory to arrive at the temperature increase coefficient per unit pump intensity. The temperature increase occurs since the pump photons are not completely converted into laser or fluorescence photons. This coefficient is a relevant parameter to understanding the operation of an argon-pumped or a flash-lamp-pumped alexandrite laser.

In chapter 4 I examined the near-threshold behavior of multimode dye lasers with a weakly amplitude-modulated pump intensity. Standing-wave and ring lasers with and without output couplers were studied. The predictions of single-mode laser theory were compared with the behavior of multimode lasers in this chapter, and the total intensity of multimode lasers were found to behave according to the predictions of single-mode laser theory. This phenomenon is an example of synergetic, or cooperative, behavior in a nonlinear system with several degrees of freedom. Although the individual modes may, themselves, undergo full scale intensity fluctuations, the total intensity follows the modulated gain in a manner identical to a single-mode laser.

I demonstrated that modulation spectroscopy can be used to measure rapid laser-cavity decay rates. The modulation bandwidth of a laser is the product of the pump parameter (the percent above threshold) times the passive-cavity decay rate. The cavity decay rate of two high-Q cavites were directly measured by monitoring the exponential decay of laser intensity from the cavity after the pump intensity was extinguished. This direct measurement of the cavity decay rate τ_c was compared with the decay rate derived from fitting the modulation data. The agreement between these two methods of determining τ_c was within a 5% margin of error. I also used the modulation measurement to determine the decay rate of some laser cavities which included an output coupler. The lifetime of the laser field in these cavities was less than the response time of any of the equipment we have available in the laboratory. However, we were able to accurately determine these decay rates using the AM measurement. By operating the laser near threshold, the dynamics are critically-slowed enough so that our equipment could accurately measure the systematic time constant. The systematic time constant is then scaled by the pump parameter to arrive at

a value for the passive-cavity decay rate of these cavities with output couplers.

Another consequence of this research is that the concept of inversion clamping can now be interpreted as a non-adiabatic phenomenon. I show that just as the steady-state inversion (the inversion of a four-level laser is equal to the excited-state population) of a laser is clamped at the threshold value once the lasing threshold is reached, the ac response of the excited-state population is zero, within the modulation bandwidth of the laser. Over a small bandwidth, the laser acts as a pump-intensity noise eater, keeping the excited-state population constant, and dissipating pump fluctuations in the form of laser intensity. At higher rates the laser cannot follow the pump fluctuations, and the population begins to follow the modulations of the pump laser intensity emitting the modulation energy in the form of a fluctuating fluorescent intensity.

A further consequence of these dynamics is that the absorption of the pump modulations is affected by the response of the population. The absorption of the modulations is diminished whenever the population itself can follow the them. This phenomenon is a manifestation of the physics I reported in chapter 3; population oscillations affect the transfer of modulation through an optical system and also affects the absorption of the modulation by the system.

I have extended the application and usefulness of modulation spectroscopy in this thesis. However I believe that there is more work to be done in this area. It seems that more questions are raised than are answered. For instance, what is the response of multilevel radiatively-broadened atomic systems to the strong modulation interaction studied in chapter 2. Also, in chapter 4 I studied the response of dye lasers which are strongly collisionally broadened. What is the response of a laser system which can only be adequately described by keeping the equations for the atomic polarization, the atomic inversion, and the field

equation?

In closing, I have some advice. If all else fails, try modulation techniques, and use a lock-in amplifier.

Bibliography

J.A. Abate, "Preparation of atomic sodium as a two-level atom," Opt. Commun. **10**, 269-272 (1974).

G.S. Agarwal, "Generation of squeezed states of radiation at submultiple Rabi resonances," J. Opt. Soc. Am. B **5**, 180-183 (1988).

G.S. Agarwal, "Subharmonic Raman effect in nonlinear mixing," J. Opt. Soc. Am. **13**, 482-484 (1988).

G.S. Agarwal, and N. Nayak, "Multiphoton processes in two-level atoms in two intense pump beams," J. Opt. Soc. Am. B **1**, 164-169 (1984).

G.P. Agrawal and R. Roy, "Effect of injection-current fluctuations on the spectral linewidth of semiconductor lasers," Phys. Rev. A **37**, 2495-2501 (1988).

H. Atmanspacher, H. Scheingraber, and C.R. Vidal, "Mode-correlation times and dynamical instabilities in a multimode cw dye laser," Phys. Rev. A **33**, 1052-1059 (1986).

A.M. Bonch-Breuvich, T.A. Vartanyan, and N.A. Chigir, "Subradiative structure in the absorption spectrum of a two-level system in a biharmonic radiation field," Sov. Phys. JETP **50**, 901-906 (1979).

R.W. Boyd, "Spectral holes due to population oscillations in a homogeneously broadened media," in *Coherence and Quantum Optics V*, L. Mandel and E. Wolf, eds. (Plenum, New York, 1984).

R.W. Boyd and S. Mukamel, "Origin of spectral holes in pump-probe studies of homogeneously broadened lines," Phys. Rev. A **29**, 1973-1983 (1984).

R.W. Boyd, M.G. Raymer, P. Narum, and D.J. Harter, "Four-wave parametric interactions in a strongly driven two-level system," Phys. Rev. A **24**, 411-423 (1981).

G. Broggi, A. Colombo, L.A. Lugiato, and P. Mandel, "Influence of white noise on delayed bifurcations," Phys. Rev. A **33**, 3635-3637 (1986).

S. Chakmakjian, L.W. Hillman, K. Koch, and C.R. Stroud, Jr., "Multimode instabilities of homogeneously-broadened lasers," *Optical Bistability III* (Springer-Verlag, New York, 1986).

S.H. Chakmakjian, K. Koch, S. Papademetriou, and C.R. Stroud, Jr., "Effects of pump modulation on a four-level laser amplifier," J. Opt. Soc. Am. B, **6**, 1746-1751 (1989).

163

M. Citron "Study of a two-level system in sodium using laser optical pumping," University of Rochester, Ph.D. Thesis (1977).

S.N. Dixit and P.S. Sahni, "Nonlinear stochastic processes driven by colored noise: Application to dye-laser statistics," Phys. Rev. Lett. **50**, 1273-1276 (1983).

J.H. Eberly and V.D. Popov, "Phase-dependent pump-probe line-shape formulas," Phys. Rev. A **37**, 2012-2016 (1988).

B.J. Feldman and M.S. Feld, "Theory of high-intensity gas laser," Phys. Rev. A **1**, 1375-1396 (1970).

R.J. Fox, "Laser-noise analysis by first-passage-time techniques," Phys. Rev. A **34**, 3405-3408 (1986).

R.F. Fox, G.E. James, and R. Roy, "Laser with a fluctuating pump: Intensity correlations of a dye laser," Phys. Rev. Lett. **52**, 1778-1781 (1984).

H. Fu and H. Haken, "Semiclassical theory of dye lasers: the single frequency and multifrequency steady states of operation," J. Opt. Soc. Am. B **5**, 899-906 (1988).

H. Fu and H. Haken, "Multichromatic operations in cw dye lasers," Phys. Rev. Lett. **60**, 2614-2617 (1988).

E.C. Gage and L. Mandel, "Hysteresis effects in the two-mode dye ring laser," J. Opt. Soc. Am. B, **6**, 287-291 (1989).

J.E.M. Goldsmith and R.L. Farrow, "Spatially resolved optical stark-modulation spectroscopy in flames," Opt. Lett. **7**, 215-217 (1982).

R. Graham, M. Höhnerbach, and A. Schenzle, "Statistical properties of light from a dye laser," Phys. Rev. Lett. **48**, 1396-1399 (1982).

M.T. Gruneisen, K.R. MacDonald, and R.W. Boyd, "Induced gain and modified absorption of a weak probe beam," J. Opt. Soc. Am. B **5**, 123-129 (1988).

S. Guch, Jr., and C.E. Jones, "Alexandrite laser performance at high-temperature," Opt. Lett. **7**, 608-610 (1982).

H. Haken, *Synergetics* (Springer-Verlag, New York, 1983).

R.G. Harrison, J.V. Moloney, J.S. Uppal, and W. Forysiak, "Analysis of instability and chaos in optically pumped three level lasers," **Instabilities and Chaos in Quantum Optics II**, (Plenum Press, New York, 1988).

D.J. Harter and R.W. Boyd, "Four-wave mixing enhanced by ac-Stark-split levels in self-trapped filaments of light," Phys. Rev. A **29**, 739-748 (1984).

165

165

D.J. Harter, P. Narum, M.G. Raymer, and R.W. Boyd, "Four-wave parameteric amplification of Rabi sidebands in sodium," Phys. Rev. Lett. **46**, 1192-1195 (1981).

S. Haroche and F. Hartmann, "Theory of saturated absorption line shapes," Phys. Rev. A **6**, 1280-1300 (1972).

M.Hercher "The spherical mirror Fabry-Perot interferometer," Appl. Opt. **7**, 951-966 (1968).

L.W. Hillman, "Interaction of modulated optical fields with saturable media and its applcation to laser instability," University of Rochester, Ph.D. Thesis (1984).

L.W. Hillman, R.W. Boyd, J. Krasinski, and C.R. Stroud, Jr., "Observation of a spectral hole due to population oscillations in a homogeneously broadened optical absorption line," Opt. Commun. **45**, 416-419 (1983).

L.W. Hillman, R.W. Boyd, and C.R. Stroud, Jr., "Natural modes for the analysis of optical bistability and laser instability," Opt. Lett. **7**, 426-428 (1982).

L.W. Hillman, J. Krasinski, R.W. Boyd, and C.R. Stroud, Jr., "Observation of higher order dynamical states of a homogeneously broadened laser," Phys. Rev. Lett. **52**, 1605-1608 (1984).

L.W. Hillman, J. Krasinski, K. Koch, and C.R. Stroud, Jr., "Dynamics of homogeneously broadened lasers: higher-order bichromatic states," J. Opt. Soc. Am. B **2**, 211-217 (1985).

P. Jung and H. Risken, "Distribution function for a nonlinear laser model with multiplicative colored noise," Phys. Lett. **103A**, 38-40 (1984).

K. Kaminishi, R. Roy, R. Short, and L. Mandel, "Investigation of photon statistics and correlations of a dye laser," Phys. Rev. A **24**, 370-378 (1981).

K.W. Koch III, "Dynamics and instabilities in homogeneously broadened lasers," University of Rochester, Ph.D. Thesis (1989).

M.A. Kramer, R.W. Boyd, L.W. Hillman, and C.R. Stroud, Jr., "Propagation of modulated optical fields through saturable-absorbing media: a general theory of modulation spectroscopy," J. Opt. Soc. Am. B **2**, 1444-1455 (1985).

M.A. Kramer, "Nonlinear Optical Properties of Impurity-Doped Solids," University of Rochester, Ph.D. Thesis (1985).

P. Lett, "Investigation of first-passage-time problems in the two-mode dye laser," Phys. Rev. A **34**, 2044-2057 (1986).

P. Lett, E.C. Gage, and T.H. Chyba, "Colored-noise-induced first-order phase transition in a single-mode dye laser," Phys. Rev. A **35** 746-751 (1987).

M.S. Malcuit, R.W. Boyd, L.W. Hillman, J. Krasinski, and C.R. Stroud, Jr., "Saturation and inverse-saturation absorption line shapes in alexandrite," J. Opt. Soc. Am. B **1**, 73-75 (1984).

A.A. Mak, S.G. Przhibel'skii, and N.A. Chigir, "Nonlinear resonance phenomena in bichromatic fields," Ser. Fiz. **47**, 1976-1983 (1983).

P. Mandel and T. Erneux, "Laser Lorenz equations with a time-dependent parameter," Phys. Rev. Lett. **53**, 1818-1820 (1984).

P. Mandel and T. Erneux, "Nonlinear control in optical bistability," IEEE J. Quantum Electron. **QE-21**, 1352-1355 (1985).

I. McMackin, C. Radzewicz, M. Beck, and M.G. Raymer, "Instabilities and chaos in a multimode, standing-wave, cw dye laser," Phys. Rev. A **38**, 820-832 (1988).

B.R. Mollow, "Stimulated emission and absorption near resonance for driven systems," Phys. Rev. A **5**, 2217-2222 (1972).

T.W. Mossberg and M.L. Lewenstein, Department of Physics, University of Oregon, Eugene, Oregon 97403 (personal communication).

T.W. Mossberg and M. Lewenstein, "Transient dynamics of a two-level atom in the presence of a bichromatic excitation field,"

T. Ogawa, "Quasiperiodic instability and chaos in the bad-cavity laser with modulated inversion: numerical analysis of a Toda oscillator system," Phys. Rev. A **37**, 4286-4302 (1988).

T. Ogawa and E. Hanamura, "Dynamical properties of the multi-mode laser with modulated inversion," Opt. Commun. **61**, 49-54 (1987).

T.Ogawa and E. Hanamura, "Numerical analysis of multimode laser with modulated inversion," Appl. Phys. B **43**, 139-153 (1987).

F. Papoff, D. Dangoisse, E. Poite-Hanoteau, and P. Glorieux, "Chaotic transients in CO_2/sub 2/ laser with modulated parameters: critical slowing-down and crisis-induced intermittency," Opt. Commun. **67**, 358-362 (1988).

H. Risken and K. Nummedal, "Instability of off resonance modes in lasers," Phys. Lett. **26A**, 275-276 (1968).

H. Risken and K. Nummedal, "Self pulsing in laser," J.Appl Phys. **39**, 4662-4672 (1969).

R. Roy and L. Mandel, "Optical bistability and first-order phase transition in a ring dye laser," Opt. Commun. **34**, 133-136 (1980).

R. Roy, A.W. Yu, amd S. Zhu, "Quantum fluctuations, pump noise, and the growth of laser radiation," Phys. Rev. Lett. **55**, 2794-2797 (1985).

W.M. Ruyten, "Harmonic behavior of the multiple quantum resonances of a two-level atom driven by a fully-amplitude-modulated field," Phys. Rev. A, **40**, 1447-1455, (1989).

W.H. Ruyten, "Subharmonic resonances in terms of multiphoton processes and generalized Bloch-Siegert shifts," J. Opt. Soc. Am. B, **6**, 1796-1802 (1989).

S.E. Schwartz and T.Y. Tan, "Wave interactions in saturable absorbers," Appl. Phys. Lett. **10**, 4-6 (1967).

M. San Miguel and M.C. Torrent, "First passage time distribution for delayed laser threshold instability," J. Phys. (Paris) **49**, 149-151 (1988).

M. Sargent III, M.O. Scully, and W.E. Lamb, Jr., *Laser Physics*, (Addison-Wesley, Reading, Mass., 1974).

M. Sargent III and P.E. Toschek, "Unidirectional saturation spectroscopy, II, general lifetimes, interpretations and analogies," Appl. Phys. **11**, 107-120 (1976).

M. Sargent III, P.E. Toschek, and H.G. Danielmeyer, "Unidirectional saturation spectroscopy. I, Theory and short dipole lifetime limit," Appl. Phys. **11**, 55-62 (1976).

R. Saxena and G.S. Agarwal, "AC Stark effect and fluorescence using modulated laser beams I. Effect of laser fluctuations and arbitrary relaxation parameters," J. Phys. B **12**, 1939-1951 (1979).

W. Scharpf, M. Squicciarini, D. Bromley, C. Green, J.R. Tredicce, and L.M. Narducci, "Experimental observation of a delayed bifurcation at the threshold of an argon laser," Opt. Commun. **63**, 344-348 (1987).

S. Schenzle and R. Graham, "Photon statistics of dye lasers, a non-Marco-vian analytical model," Phys. Lett. **98A**, 319-323 (1983).

R. Short, L.Mandel, and R. Roy, "Correlation functions of a dye laser: Comparison between theory and experiment," Phys. Rev. Lett. **49**, 647-650 (1982).

A.E. Siegman, *Lasers* (University Science Books, California, 1986), Chapt. 13.

R.E. Silverans, G. Borghs, P. De Bisschop, and M. Van Hove, "Phase effects in bichromatic field interactions with two-level atom," Phys. Rev. Lett. **55**, 1070-1073 (1985).

M.C. Torrent and M. San Miguel, "Stochastic-dynamics characterization of delayed laser threshold instability with swept control parameter," Phys. Rev. A

38, 245-251 (1988).

P. Thomann, "Optical resonances in strong modulated laser beam," J. Phys. B **13**, 1111-1124 (1980).

P. Thomann, "Optical parametric resonances," J. Phys. B **9**, 2411-2419 (1976).

G.I. Toptygina and E.E. Fradkin, "Theory of subradiative absorption in the interaction between two intense waves in a nonlinear medium," Sov. Phys. JETP **55**, 246-251 (1982).

N. Tsukada and T. Nakayama, "Modulation of optical bistability by an additional laser beam," Phys. Rev. A, **25**, 964-977 (1982).

J.C. Walling, O.G. Peterson, H.P. Jenssen, R.C. Morris, and E.W. O'Dell, "Tunable alexandrite lasers," IEEE J. Quantum Electron. **QE-16**, 1302-1314 (1980).

J.C. Walling, D.J. Heller, H. Samuelson, D.J. Harter, J.A. Pete, and R.C. Morris,"xmod Tunable alexandrite lasers: development and performance," IEEE J. Quantum Electron. **QE-21**, 1568-1581 (1985).

F.Y. Wu, S. Ezekiel, M. Ducloy, and B.R. Mollow, "Observation of amplification in a strongly driven two-level atomic system at optical frequencies," Phys. Rev. Lett. **38**, 1077-1080 (1977).

M.R. Young and S. Singh, "Statistical properties of a laser with multiplicative noise," Opt. Lett. **13** 21-23 (1988).

M.R. Young and S. Singh, "Effects of multiplicative white noise on laser light fluctuations," Phys. Rev. A **38** 238-244 (1988).

A.W. Yu, G.P Agrawal, and R. Roy, "Noise propagation from pump to secondary lasers," Opt. Lett. **12**, 806-808 (1987).

S. Zhu, A.W. Yu, and R. Roy, "Statistical fluctuations in laser transients," Phys. Rev. A **34**, 4333-4347 (1986).

Appendix A

BLACKBODY PHONON IRRADIANCE

In this appendix I evaluate an expression for the total blackbody flux capable of pumping population out of the storage level in the alexandrite crystal and into the upper vibronic level. This expression is evaluated as a function of temperature. The storage level is separated from the upper vibronic level by 800 cm^{-1}. I evaluate the total blackbody flux of energy 800 cm^{-1} and above since only these phonons are energetic enough to pump population into the vibronic transitions. I start this calculation with the expression for the blackbody irradiance per unit frequency

$$L_\nu = \left(\frac{8\pi h}{c^3}\right) \frac{\nu^3}{\exp(h\nu/kT) - 1},\qquad (A1)$$

where C is a constant, ν is the frequency of the radiation, h is Planck's constant, k is Boltzmann's constant, and T is the absolute temperature. Since we are interested in evaluating this integral over frequencies $\nu \geq 800 cm^{-1}$, and at temperatures $T \approx 300°K$ the exponential in the denominator of Eq. (A1) is

169

much larger than unity so the irradiance can be rewritten

$$L_\nu \approx \left(\frac{8\pi h}{c^3}\right) \nu^3 \exp(-\frac{h\nu}{kT}). \tag{A2}$$

Now I integrate the expression given in Eq. (A2) from the minimum frequency ν_0 (the frequency ν_0 corresponds to 800 cm^{-1}) to infinity

$$\int\limits_{\nu_0}^{+\infty} \nu^3 \exp(\phi\nu) = \exp(\phi\nu_0) \sum_{n=0}^{3} (-1)^n \frac{3!\nu_0^{3-n}}{(3-n)!\phi^{n+1}}, \tag{A3}$$

where $\phi = -h/kT$. In the limitting case that the integration limit ν_0 goes to zero frequency this integral takes on the familiar Wien's law T^4 dependence. This integral will be used to give the temperature dependence of the blackbody radiation within the alexandrite crystal as described in chapter 3 of this thesis

$$L_{\nu_0} \approx \left(\frac{8\pi h}{c^3}\right) \exp(\phi\nu_0) \sum_{n=0}^{3} (-1)^n \frac{3!\nu_0^{3-n}}{(3-n)!\phi^{n+1}}. \tag{A4}$$

Appendix B

MODULATION OF THE PHONON IRRADIANCE
IN ALEXANDRITE

In this appendix I use the expression from appendix A given in Eq. (A4) for L_{ν_0} (the integrated phonon irradiance cabable of inducing a population transfer from the storage level to the upper vibronic level) to derive an expression for the modulated phonon irradiance due to heat absorption from the pump laser. To do this I first derive an expression for the heat absorption in the interaction region in the crystal. Next, the temperature is related to the heat absorption by invoking simple thermodynamic arguments. The temperature is assumed to depend linearly on the rate of heat absorption (this assumption is consistent with the fact that the sample is convectively cooled). Finally I apply the modulated temperature to the expression for the irradiance and linearize this expression to yield the modulated phonon irradiance capable of pumping population into the vibronic laser levels. This expression will be applied to Eq. (3.19) in chapter 3. We begin with the expression for the integrated irradiance as a function of

temperature

$$L_{\nu_0} \approx \left(\frac{8\pi h}{c^3}\right) \exp[\phi(t)\nu_0] \sum_{n=0}^{3} (-1)^n \frac{3!\nu_0^{3-n}}{(3-n)!\phi(t)^{n+1}}, \qquad (B1)$$

where $\phi(t) = -h/kT(t)$. Since we are interested in the temperature dependence of this expression I rewrite Eq. (B1) as

$$L_{\nu_0} \approx \left(\frac{8\pi h}{c^3}\right) \exp\left(\frac{h\nu}{kT(t)}\right) \left(AT(t) + 3BT(t)^2 + 6CT(t)^3 + 6DT(t)^4\right), \quad (B2)$$

where

$$A = \nu_0^3 \left(\frac{k}{h}\right), \qquad (B3a)$$

$$B = \nu_0^2 \left(\frac{k}{h}\right)^2, \qquad (B3b)$$

$$C = \nu_0 \left(\frac{k}{h}\right)^3, \qquad (B3c)$$

and

$$D = \left(\frac{k}{h}\right)^4. \qquad (B3d)$$

Now, it is necessary to derive an expression for the temperature of the interaction region in the crystal including heating due to the pump laser. The interaction region is heated by the absorption of photons from the pump laser. Pump absorption takes place from the ground state and from the excited state. Part of the energy absorbed by the atoms from the ground state is dissipated as fluorescence, while all the energy absorbed by the atoms in the excited state is dissipated as heat. The energy released in the form of fluorescent emission can be represented by including a quantum efficiency multiplier. The heat due to pump absorbtion can be represented as

$$Q_p \propto \alpha \epsilon I_\lambda(t)\rho_g(t) + \beta I_\lambda(t)\rho_3(t), \qquad (B4)$$

where α is the unsaturated ground state absorption coefficient, ϵ is the quantum efficiency of the heat generation (eg. the fraction of each quanta of pump photon converted into heat) when the pump photon is absorbed from the gound state, and the factor β represents the *unsaturated excited state absorption coefficient.* The first term in Eq. (B4) is the heat generated due to ground state absorption and the second term is the heat generated due to excited state absorption. I only consider the population in level 3 for excited state absorption since very little population resides in the excited vibronic state whose decay rate is so rapid. These three coefficients, α, β, and ϵ are known quantities (see references 18-23 in chapter 3).

At this point it is helpful to consider the energy balance of heat transfer in and out of the crystal. In general, heat is absorbed by the sample from the pump (actually light quanta are absorbed and converted into heat) and then the heat is removed from the interaction region via conduction into other parts of the alexandrite crystal and by convection into the air. In fact, all the heat absorbed from the pump laser is eventually removed from the crystal via convection (radiation is ignored since it is inefficient at these low temperatures). The rate of convective removal of heat is merely proportional to the difference between the temperature of the heated object and the temperature of the surrounding fluid at large distances from the object. Therefore, in the stationary state the increase in the temperature of the crystal over room temperature is proportional to the rate heat is absorbed by the crystal. The temperature of the crystal can be written as

$$T(t) = T_{room} + \psi I_\lambda(t)[\alpha\epsilon\rho_g(t) + \beta\rho_3(t)], \qquad (B5)$$

where the factor ψ relates the rate of heat transfer into the interaction region to

the temperature increase. This factor depends on the geometry of the sample, the bulk conduction coefficient and the convection coefficient. In practice I will determine the coefficient, ψ by fitting the data. The value of this treatment is in the evaluation of this coefficient which relates the pump intensity to the temperature in the interaction region.

Since the response of the population in the ground state and the excited states (levels 2 and 3) contain both DC and harmonic terms it is convenient at this point to rewrite Eq. (B5) as

$$T(t) = T_0 + [\delta T \exp(i\delta\omega t) + C.C.], \qquad (B6)$$

where T_0 is the DC temperature

$$T_0 = T_{room} + \sigma I_\lambda(\alpha\epsilon\rho_{g,0} + \beta\rho_{3,0}), \qquad (B7)$$

and δT is the modulated component of the temperature

$$\delta T = [\alpha\epsilon(\rho_{g,0}\delta I_\lambda + \rho_{g,1}I_\lambda) + \beta(\rho_{3,0}\delta I_\lambda + \rho_{3,1}I_\lambda)]. \qquad (B8)$$

The C.C. in Eq. (C6) represents the complex conjugate.

The expression for the temperature $T(t)$ given in Eq. (B5) is substituted into the expression for the phonon irradiance given in Eq. (B1). When this is done and the expression is linearized with respect to the modulated component of the temperature δT the result is

$$L_{\nu_0}(t) = \left(\frac{8\pi h}{c^3}\right) \exp\left(\frac{-h\nu_0}{kT_0}\right) \left\{ (AT_0 + 3BT_0^2 + 6CT_0^3 + 6DT_0^4) \right. \qquad (B9)$$

$$\left. + \left[\delta T\left(A\frac{h\nu_0}{kT_0} + 4A + 12BT_0 + 24CT_0^2 + 24DT_0^3\right)\exp(i\delta\omega t) + C.C.\right] \right\}.$$

This expression for the time-dependent irradiance is used in chapter 3 to evaluate the time-dependent thermal pump rate $R_T(t)$.

Appendix C

STABILITY ANALYSIS OF THE
FOUR-LEVEL LASER RATE EQUATIONS

In this appendix I will review the stability analysis of the four-level laser
rate equations. The stability analysis will be carried out for both the above-
threshold and the below-threshold solutions to these equations. We start with
the rate equations for the excited-state population of the laser transition ρ,

$$\frac{d}{dt}\rho = -\frac{1}{T_1}(1 + I + I_p)\rho + \frac{1}{T_1}I_p, \qquad (C.1)$$

and the equation for the intracavity dimensionless intensity of the laser I,

$$\frac{d}{dt}I = \left(g\rho - \frac{1}{\tau_c}\right)I. \qquad (C.2)$$

These equations are discussed in detail in Chapter 4. The steady-state solutions
of these equations which were found in Chapter 4 will be referred to as I_{ss} for the
laser intensity and ρ_{ss} for the atomic population. If we imagine that the system
is prepared in the steady-state save for a small time-dependent perturbation of
the variables we can write these solutions as

$$I(t) = I_{ss} + \delta I(t), \qquad (C.3a)$$

for the laser intensity, and

$$\rho(t) = \rho_{ss} + \delta\rho(t), \qquad (C.3b)$$

for the atomic population. The time-dependent perturbations are considered small in order to linearize the equations. Upon substituting the expressions given in Eqs.(C.3a) and (C.3b) into the population rate equation, Eq.(C.1), we get

$$\frac{d}{dt}[\rho_{ss} + \delta\rho(t)] = -\frac{1}{T_1}[\rho_{ss} + \delta\rho(t)]\{1 + [I_{ss} + \delta I(t)] + I_p\} + \frac{1}{T_1}I_p, \qquad (C.4)$$

which can be rewritten as

$$\begin{aligned}
\frac{d}{dt}\rho_{ss} + \frac{d}{dt}[\delta\rho(t)] = & -\frac{1}{T_1}(1 + I_{ss} + I_p)\rho_{ss} + \frac{1}{T_1}I_p \\
& -\frac{1}{T_1}\rho_{ss}\delta I(t) - \frac{1}{T_1}(1 + I_{ss} + I_p)\delta\rho(t) \\
& -\frac{1}{T_1}\delta\rho(t)\delta I(t).
\end{aligned} \qquad (C.5)$$

The first term on the left hand side of Eq. (C.5) is zero since the steady-state solutions are constant. The first line on the right hand side of Eq. (C.5) is equal to zero for both sets of steady-state solutions. The third line of the Eq. (C.5) is neglected since it is of second order in the perturbative quantities. The remaining terms represent the linearized equation for the perturbed atomic population,

$$\frac{d}{dt}[\delta\rho(t)] = -\frac{1}{T_1}\rho_{ss}\delta I(t) - \frac{1}{T_1}(1 + I_{ss} + I_p)\delta\rho(t). \qquad (C.6)$$

In a similar manner Eq. (C.2) can be solved to obtain a linearized equation of motion for the perturbed intensity

$$\frac{d}{dt}[\delta I(t)] = gI_{ss}\delta\rho(t) + \left(g\rho_{ss} - \frac{1}{\tau_c}\right)\delta I(t). \qquad (C.7)$$

These linearized equations can be solved by assuming a time dependence of the perturbation of the form:

$$\delta\rho(t) = \delta\rho \exp(\lambda t), \qquad\qquad (C.8a)$$

and

$$\delta I(t) = \delta I \exp(\lambda t), \qquad\qquad (C.8b)$$

for the population and the intensity respectively. When we substitute these expressions into the linearized equations [Eqs. (C.6) and (C.7)] the following two eigenvalue equations result:

$$\begin{bmatrix} -\frac{1}{T_1}(1 + I_{ss} + I_p) - \lambda & -\frac{1}{T_1}\rho_{ss} \\ gI_{ss} & g\rho_{ss} - \frac{1}{\tau_c} - \lambda \end{bmatrix} \begin{pmatrix} \delta\rho \\ \delta I_{ss} \end{pmatrix} = 0. \qquad (C.9)$$

For a non-trivial solution of this set of equations the determinant must be equal to zero. Solving for the determinant and setting it equal to zero yields a quadratic equation for the eigenvalue λ,

$$\lambda^2 + \lambda\left[\frac{1}{T_1}(1 + I_{ss} + I_p) + \frac{1}{\tau_c} - g\rho_{ss}\right]$$
$$+ \frac{1}{T_1\tau_c}(1 + I_{ss} + I_p) - \frac{g\rho_{ss}}{T_1}(1 + I_p) = 0. \qquad (C.10)$$

The eigenvalues can be evaluated for both sets of steady-state solutions to Eqs. (C.1) and (C.2). The steady-state solutions are found by setting the time-derivatives in the rate equations to zero. The two solutions are for the laser-on state and the laser-off state. First I evaluate the eigenvalues for the laser-off solution for which

$$I_{ss} = 0, \qquad\qquad (C.11a)$$

and

$$\rho_{ss} = \frac{I_p}{1 + I_p}. \qquad\qquad (C.11b)$$

For this solution we obtain two eigenvalues:

$$\lambda_1 = -\frac{1}{T_1}(1 + I_p), \qquad (C.12a)$$

and

$$\lambda_2 = g\frac{I_p}{1 + I_p} - \frac{1}{\tau_c}. \qquad (C.12b)$$

The eigenvalue labeled λ_1 is always negative and therefore leads to no instability. It is the second eigenvalue, λ_2, which gives rise to an instability for values of the pump intensity which are greater than the threshold value. The off solution becomes unstable for

$$I_p \geq I_{p,thr} = \frac{1}{g\tau_c - 1}. \qquad (C.13)$$

The interpretation of this is that the laser stays off if the pump intensity is kept below the threshold value. Conversly the laser is not in a stable state if it is off when pump intensity is above the threshold value.

Next we can examine the stability of the laser-on steady-state solutions to Eqs. (C.1) and (C.2). The steady-state solutions are

$$I_{ss} = \frac{I_p}{I_{p,thr}} - 1, \qquad (C.14a)$$

for the laser intensity and

$$\rho_{ss} = \frac{1}{g\tau_c}, \qquad (C.14b)$$

for the excited-state population. When these relations are substituted into the eigenvalue equation, Eq. (C.10), the result is

$$\lambda^2 + \lambda\frac{1}{T_1}\left(\frac{I_p}{I_{p,thr}} + I_p\right) + \frac{1}{T_1\tau_c}\left(\frac{I_p}{I_{p,thr}} - 1\right) = 0. \qquad (C.15)$$

This quadratic equation has two solutions:

$$\lambda = -\frac{1}{2T_1}\left(\frac{I_p}{I_{p,thr}} + I_p\right)$$

$$\pm \sqrt{\left(\frac{1}{2T_1}\right)^2\left(\frac{I_p}{I_{p,thr}} + I_p\right)^2 - \frac{1}{T_1\tau_c}\left(\frac{I_p}{I_{p,thr}} - 1\right)}. \qquad (C.16)$$

The solution with the minus sign is always negative and leads to no instability for this steady-state solution. It is the solution with the plus sign which has the propensity to go positive and indicate an instability. Before proceeding further, it is helpful to recognize that the last term inside the square-root bracket contains the pump parameter given by:

$$\beta = \frac{I_p}{I_{p,thr}} - 1, \qquad (C.17)$$

which is small when the laser is close to threshold. Furthermore, dye lasers operate in the good cavity limit (eg. $\tau_c \gg T_1, T_2$). Therefore, the last term in the radical in Eq. (C.16) is small. To make use of the fact that this term is small, the expression inside the radical can be rewritten as:

$$\sqrt{} = \frac{1}{2T_1}\left(\frac{I_p}{I_{p,thr}} + I_p\right)\sqrt{1 - \frac{4T_1\beta}{\tau_c}\left(\frac{I_p}{I_{p,thr}} + I_p\right)^{-2}}. \qquad (C.18)$$

This expression is now of the form $\sqrt{1-x}$, which for small x is

$$\sqrt{1-x} = 1 - \frac{x}{2} + \ldots. \qquad (C.19)$$

This small argument expansion may now be applied to the radical expression in Eq. (C.18) and the results substituted into the eigenvalue expression in Eq. (C.16). The eigenvalue becomes

$$\lambda = -\left(\frac{1}{\tau_c}\right)\frac{I_{ss}}{\left(\frac{I_p}{I_{p,thr}}\right) + I_p} = -\left(\frac{1}{\tau_c}\right)\frac{I_{ss}}{1 + I_{ss} + I_p} \qquad (C.19)$$

In the limit of nonsaturating pump and laser intensities this eigenvalue is equal to the product of the laser intensity and the cavity decay rate. The characteristic passage time of the system is slowed as the laser intensity goes to zero. If the system is perturbed away from the steady-state solution very close to threshold, it takes a long time to return to the steady-state. This behavior is called critical slowing down.